Charité / Berlin-Brandenburg Center for Regenerative Therapies

Analysis of the derivation phase of human adipose tissue-derived multipotent mesenchymal stromal cells

Von der Fakultät III - Prozesswissenschaften

der Technischen Universität Berlin

zur Erlangung des akademischen Grades

Doktor der Naturwissenschaften

– Dr. rer. nat. –

genehmigte Dissertation

vorgelegt von

Dipl.-Biol. Julian Braun

Promotionsausschuss:

1. Gutachter: Prof. Dr. rer. nat. Leif-Andreas Garbe
2. Gutachter: Prof. Dr. rer. nat. Andreas Kurtz

Vorsitzender: Prof. Dr. Rer. nat. Peter Neubauer

Tag der wissenschaftlichen Aussprache: 21. Juni 2013

Berlin 2013

D 83

Content

Abbreviations

AdSC	Adventitial Stromal Cells
ALCAM	Activated Leukocyte CAM, CD166
APC	Allophycocyanin
ARC	Adventitial Reticular Cells
AT	adipose tissue
AURKA	Aurora Kinase A
BM	bone marrow
BMP	Bone Morphogenetic Proteins
BSA	Bovine Serum Albumin
CAM	Cell Adhesion Molecules
CCL19	macrophage inflammatory protein-3-beta; MIP-3-beta
CCL2	monocyte chemotactic protein-1,MCP-1;
CCN	Cyclin
CD105	Endoglin, ENG
CD14	LPS receptor
CD146	Melanocyte Cell Adhesion Molecule, MCAM, MUC18
CD271	low affinity Nerve Growth Factor Receptor, NGFR, p75
CD31	PECAM, Platelet Endothelial CAM
CD34	hematopoietic progenitor cell antigen
CD45	Protein Tyrosine Phosphatase Receptor type C, PTPRC
CD73	Ecto-5'-Nucleotidase, NT5E
CD90	THY1
CDC	Cell Division Cycle
CDH1	E-Cadherin
CDH2	N-Cadherin
CDK	Cyclin-Dependent Kinase
CDKN	Cyclin-Dependent Kinase Inhibitors
cDNA	complementary DNA
CHEK1	Checkpoint Kinase 1
CLDN	Claudin
COL	Collagen
C_T	Cycle Threshold
CTV	Cell Tracker Violet
CXC3L1	Fractalkine
CXCL12	Stromal cell-derived Factor-1, SDF1
CXCL14	BRAK, breast and kidney-expressed chemokine
CXCL9	Monokine induced by gamma interferon, MIG
dH_2O	demineralized water
DMEM	Dulbecco's Modified Eagle's Medium
Dkk1	Dickkopf-1
dsDNA	Double stranded DNA
EBM	Endothelial Basal Medium
EC	Endothelial Cells
ECcult	Endothelial Cell culture condition
ECM	Extracellular Matrix
EDTA	Ethylenediaminetetraacetic acid
EGF	Epidermal Growth Factor
EGM-2	Endothelial Growth Medium-2
Egr1	Early growth response 1
EL	Erythrocyte Lysis
EMT	Epithelial-to-Mesenchymal Transition
ES	Enrichment score
ES cells	Embryonic Stem Cells
FACS	fluorescence-activated cell sorting
FBLN1	Fibulin-1
FBS	Fetal Bovine Serum
fDC	follicular dendritic cells
FGF	Fibroblast Growth Factor
FGF-1	Fibroblast Growth Factor acidic
FGF-2	Fibroblast Growth Factor basic
FGFR	FGF receptor
FN1	Fibronectin-1
FSP1	Fibroblast-specific Protein 1
FZD	Frizzled
GAS	Growth Arrest-Specific
GDF	Growth and Differentiation Factor
GM	Growth Medium
GREM	Gremlin
GSEA	Gene Set Enrichment Analysis
GSK-3β	Glycogen Synthase Kinase-3β
HBSS	Hank's Buffered Saline Solution
HLA	Human Leukocyte Antigen
HLA	Human Leukocyte Antigen
HMMR	hyaluronan-mediated motility receptor
HPRT	hypoxanthine phosphoribosyltransferase
HSC	Hematopoietic Stem Cells
IGF-1	Insulin-like Growth Factor-1
IL13A1	Interleukin IL13 receptor α1
iMFI	Integrated Mean Fluorescence Intensity
ISCT	International Society for Cellular Therapy
JAK	Janus Kinase
KRT	Cytokeratin
LAM	Laminin
LRP	Low density lipoprotein Receptor-related Protein
LUM	Lumican
MACS	magnetic cell separation
MAPK	Mitogen-Activated Protein Kinase
MELK	Maternal/Embryonic Leucine Zipper Kinase
MFI	Mean Fluorescence Intensity
MHC	major histocompatibility complex
MHC	Major Histocompatibility Complex
MMP	Matrix metalloproteinase
MSC	multipotent mesenchymal stromal cells
MScult	MSC culture condition
MXI1	MAX-inhibitor 1
MYO10	Myosin X
NGF	Nerve Growth Factor
PBS	Phosphate-buffered Saline
PC	Pericytes
PCR	Polymerase Chain Reaction
PDGF	Platelet-Derived Growth Factor
PDGFR	PDGF receptor
PI3K	Phosphoinositol-3-Kinase
PLEK2	pleckstrin-2
PLK1	Polo-Like Kinase 1
PODXL	Podocalyxin
qPCR	Quantitative PCR
REX1	Reduced Expression 1
RTK	Receptor Tyrosine Kinase
SMAD	SMA/mothers Against Decapentaplegic
SMTN	Smoothelin
SNAI1	Snail
SNAI2	Slug
SPRY	Sprouty
STAT	Signal Transducer and Activator of Transcription
SVF	Stromal Vascular Fraction
TCPS	tissue culture polystyrene
TGFBR	TGF-β receptor
TGF-β	Transforming Growth Factor β
TNFSF13B	B-cell activating factor, BAFF; CD257
TNXB	Tenascin XB
TPM1	Tropomyosin-1
VCAM1	Vascular CAM, CD106
VEGF	Vascular Endothelial Growth Factor
WNT	Wingless-type MMTV integration site family
ZFP42	Zinc Finger Protein 42
αSMA	α-Smooth Muscle Actin, ACTA2

1. Abstract

Mesenchymal stromal cells (MSC) are characterized *in vitro* by plastic-adherent proliferation, a specific immunophenotype and multipotency. The *in vivo* cell types giving rise to MSC, referred to as MSC progenitors, have been recently described as perivascular cells. However, further characterization of these MSC progenitors is necessary and it remains to be elucidated whether the *in vitro* characteristics of MSC are intrinsic to MSC progenitors *in vivo* or are acquired upon *in vitro* culture. We addressed this question by analyzing morphology, proliferation, immunophenotype and transcriptome of human MSC progenitors during the early *in vitro* culture phase, the "MSC derivation phase".

To identify potential human adipose tissue-derived MSC (AT-MSC) progenitors, stromal vascular cell subsets were characterized by multi-parametric flow cytometry using diverse MSC progenitor markers, such as CD34, CD105, CD146 and CD271. Further, MSC progenitor subsets were monitored during early culture in tight kinetic analyses to determine changes in morphology, proliferation, and immunophenotype. We identified two AT-MSC progenitor subsets: $CD34^{+}CD146^{-}CD271^{+/-}$ adventitial stromal cells (AdSC) and $CD34^{-}CD146^{+}CD271^{+/-}$ pericytes (PC). During early *in vitro* culture, AdSC exhibited high proliferative capacity, also under MSC culture conditions, whereas proliferation of PC was restricted to endothelial culture conditions. The kinetic analysis revealed that MSC progenitors became fibroblastoid as early as day 4 and upregulated CD105, CD146 and CD271. Accompanying this phenotypic transition, AdSC commenced proliferation and downregulated CD34.

Comparing transcriptomes of *ex vivo* sorted and 14-days-cultured AdSC by microarray and Gene Set Enrichment Analysis revealed that *ex vivo* AdSC were quiescent and that activation was induced *in vitro* probably by early inflammatory responses triggered by cell isolation and that proliferation was regulated by PDGF and FGF signaling and, most importantly, inhibition of WNT signaling by Dickkopf-1.

In this study, we provide the first detailed analyses of early culture-mediated changes in the properties of human MSC progenitors. Comparing AdSC and PC during early *in vitro* culture demonstrated not only that MSC derivation from different progenitor subsets is culture-dependent, but also that AdSC are the most clonogenic AT-MSC progenitors. Moreover, we identified a highly reproducible sequence of phenotypic changes during the MSC derivation process which is associated with inflammation-induced activation and proliferation and is necessary for AdSC to acquire the typical MSC phenotype.

Zusammenfassung

Mesenchymale Stromazellen (MSC) sind *in vitro* gekennzeichnet durch plastik-adhärente Proliferation, einen spezifischen Immunphänotyp und Multipotenz. Die *in vivo* Zelltypen, die zu MSC werden (MSC-Vorläufer), wurden kürzlich als perivaskuläre Zellen beschrieben. Allerdings müssen diese MSC-Vorläufer besser charakterisiert und geklärt werden, ob die MSC-Vorläufer bereits *in vivo* die *in vitro*-Eigenschaften von MSC aufweisen, oder diese erst während der *in vitro* Kultur annehmen. Um diese Frage zu beantworten, haben wir Morphologie, Proliferation und Immunphänotyp sowie Trankriptom von humanen MSC-Vorläufern während der frühen *in-vitro*-Kultur Phase, der "MSC-Ableitungsphase" analysiert.

Potenzielle human MSC-Vorläufer aus dem Fettgewebe (AT-MSC) wurden mittels multi-parametrischer Durchflusszytometrie charakterisiert, unter Verwendung diverser MSC-Vorläufer-Marker, z.B. CD34, CD105, CD146 und CD271. Die MSC-Vorläufer wurden in engen Kinetiken während der frühen Kultur überwacht. Zwei AT-MSC-Vorläufertypen wurden identifiziert: $CD34^{+}$ $CD146^{-}$ $CD271^{+/-}$ adventitielle Stromazellen (AdSC) und $CD34^{-}$ $CD146^{+}$ $CD271^{+/-}$ Perizyten (PC). AdSC proliferierten schneller, auch unter MSC-Kulturbedingungen, während die *ex-vivo*-Expansion von PC auf Endothelzell-typische Kulturbedingungen beschränkt war. Am Tag 4 der frühen *In-vitro*-Kultur wurden MSC-Vorläufer fibroblastoid und regulierten CD105, CD146 und CD271 hoch. Gleichzeitig begannen die AdSC zu proliferieren und CD34 herunterzuregulieren.

Der Vergleich der Transkriptome von *ex vivo* sortierten und 14-Tage-kultivierten AdSC mittels Microarray und „Gene Set Enrichment Analysis“ ergab, dass *ex vivo* AdSC quieszent waren, und dass die Aktivierung *in vitro* wahrscheinlich durch frühe Entzündungsreaktionen, ausgelöst durch Zellisolation, induziert und durch PDGF und FGF-Signale und, vorallem durch Dickkopf-1-vermittelte Hemmung des Wnt-Signalwegs reguliert wurden.

Diese Studie stellt die erste detaillierte Analyse der Veränderungen in den Eigenschaften der MSC-Vorläufer während der frühen Kultur dar. Der Vergleich von AdSC und PC ergab nicht nur, dass MSC-Ableitung aus unterschiedlichen Vorläufern kulturabhängig ist, sondern auch, dass AdSC die klonogensten AT-MSC-Vorläufer sind. Desweiteren haben wir eine reproduzierbare Abfolge phänotypischer Veränderungen während des MSC-Ableitungsprozesses entdeckt, die mit inflammationsbedingter Aktivierung und Proliferation korreliert und für den Erwerb des MSC-typischen Phänotyps durch AdSC essentiell ist.

2. Introduction

There currently exists high interest in stem cell research, which is highlighted by the Nobel Prize 2012 being awarded to Shinya Yamanaka and John Gurdon who demonstrated that somatic cells can be reprogrammed to a stem cell-like, pluripotent state by nuclear transfer or even by mere transfection with four stem cell-specific transcription factors **(Gurdon, 1962; Takahashi, 2006)**.

In the last decades, multipotent mesenchymal stromal cells (MSC) have been intensively investigated as well, with the main focus on potential therapeutic applications in regenerative medicine, e.g. in cell therapy or tissue engineering. Yet, the characterization of their *in vivo* stem cell properties is incomplete.

2.1. Stem Cells

Stem cells are defined by self-renewal capacity and the potential to differentiate into different cell lineages **(Lanza, 2006)**. Stem cells elicit pivotal functions in the life of a metazoan organism, not only during embryogenesis and organogenesis but also for the maintenance of organ integrity and for tissue regeneration. In the following, a brief overview about different stem cell types will be given.

Mammalian embryogenesis starts with the zygote, which has the unique potential to develop into a complete organism and is therefore classified as “totipotent” (“capable of everything”) (Fig. 1) **(Gilbert, 2010)**. In the course of development, the zygote undergoes cleavages and the first eight daughter cells, called blastomeres, are still totipotent. After further cleavages and compaction, the morula and subsequently the blastocyst are formed and cells commit to the embryonic or extra-embryonic lineage. The inner cell mass contains the foundational cells for the embryo proper, embryonic stem cells (ES cells). ES cells are “pluripotent” (“capable of many”), i.e. they can give rise to all cell types present in the entire organism but are no longer capable of embryonic organization and tissue development.

After gastrulation, the inner cell mass develops into the three germ layers, endoderm, ectoderm and mesoderm. Stem cells committed to one germ layer are referred to as multipotent stem cells, since they are limited in their differentiation potential. Endoderm-derived cells will form organs of the digestive tract, and ectoderm will develop into skin and neurons. The mesoderm, from an evolutionary perspective the newest germ layer,

contributes to extraembryonic structures, and more importantly, will develop into bone and cartilage, muscles, blood and other internal organs like liver and pancreas.

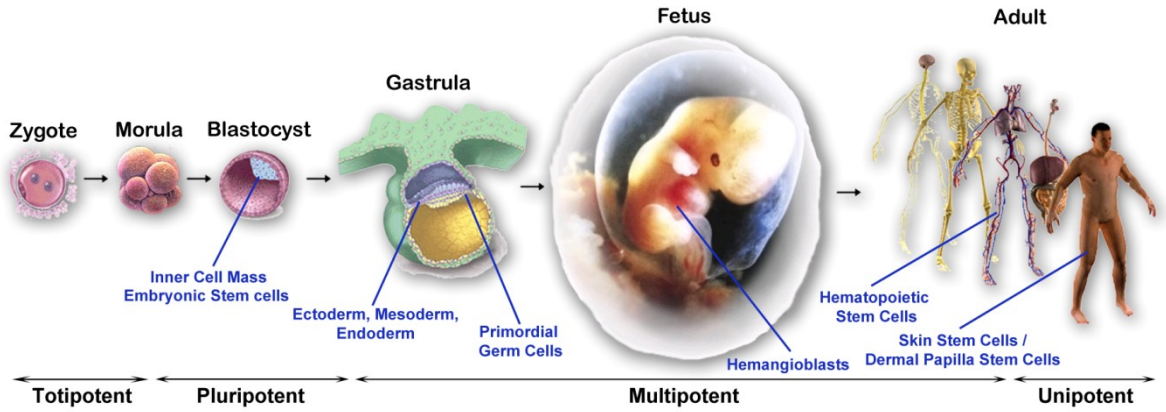

Figure 1: Embryogenesis, potency and different stem cell types.
(Modified from NCBI; www.contenidos.educarex.es; www.baby2see.com; www.cgcreators.jp)

In the adult organism multipotent stem cells are active throughout life and maintain tissue homeostasis and are involved in regenerative processes. Adult stem cells can be traced back to a fetal ancestor **(Gilbert, 2010; Lanza, 2006)**. The best investigated example is the hematopoietic stem cell (HSC), which during embryogenesis arise in the aorta-gonad mesonephros area from hemangioblasts. Later, HSCs migrate to the liver and finally to the bone marrow (BM) **(Costa, 2012; de Bruijn, 2000)**. Also the skin is permanently renewed by skin progenitor cells derived from dermal papilla stem cells which develop either from neural crest cells or from somatic or lateral plate dermomyotome **(Driskell, 2011)**. These examples illustrate that many adult stem cells can well be traced back to early embryonic precursor cells. However, the ontogenetic background of MSC remains so far elusive.

2.2. Stem cell niche

Stem cells reside in a micro-environment called the “stem cell niche” that regulates cell proliferation and differentiation **(Lander, 2012)**. In their niche, stem cells receive extracellular signals to maintain self-renewal capacity and potency (Fig. 2). Thus, daughter cells leaving the niche after cell division undergo commitment and differentiation due to missing niche-related environmental cues.

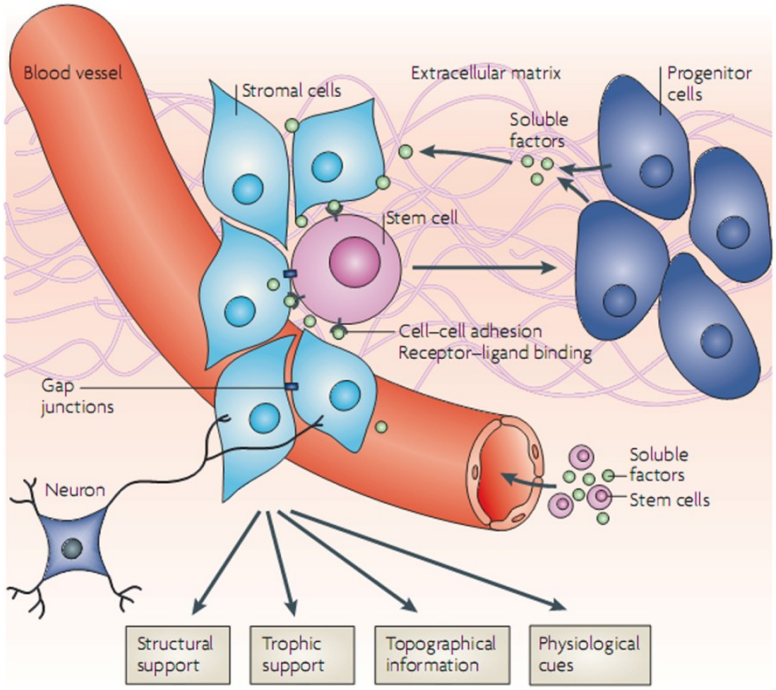

Figure 2: Schematic representation of the stem cell niche.
Taken from **(Jones, 2008)**

Stem cell niches are well described for germ cells in ovary and testis, for adult HSC, dermal papilla stem cells, crypt stem cells in the gut epithelium and neural stem cells in the adult brain **(Lander, 2012)**. In these niches, stemness and commitment are regulated by different signals. Besides physiological conditions (e.g. oxygen tension, nutrient supply), neighboring cells provide cell-cell interactions (by cell adhesion molecules), cell contact-dependent signaling (like Notch or Sonic Hedgehog) and paracrine growth factor signaling (often WNT and BMP signaling). In addition, cell-matrix-interactions (mediated by Integrins) play a pivotal role in stem cell niches **(Kolf, 2007; Lander, 2012)**. Next, these different niche components are described in detail.

Cell adhesion molecules

Cell adhesion molecules (CAM) are transmembrane receptors involved in cell-cell contacts. The cytoplasmic domain binds to the cytoskeleton and the extracellular domain interacts with other CAMs or with the extracellular matrix **(Alberts, 2002)**.

Members of the Immunoglobulin Superfamily of CAMs interact homo- and heterophilic. Vascular Cell Adhesion Molecule 1 (VCAM1, CD106) and Activated Leukocyte CAM (ALCAM, CD166, CD6L) are expressed by osteoblastic cells in the endosteal niche of HSC **(Lo Celso,**

2011). Platelet Endothelial CAM (PECAM, CD31) is a marker for endothelial cells, which was also proposed as a regulator of progenitor cell homeostasis in the HSC niche **(Ross, 2008)**.
Cadherins are calcium-dependent adhesion molecules and mediate cell-cell interactions mainly by homophilic binding. N-Cadherin (CHD2) and E-Cadherin (CDH1) are involved in stem cell niches of neural stem cells and skin stem cells **(Jones, 2008)**.
Another important CAM in the HSC niche is CD34, a member of the Sialomucin family **(Furness, 2006)**, which is the typical marker of HSC, and mediates their binding to the extracellular matrix or to stromal cells.

Extracellular matrix

Extracellular matrix (ECM) is a complex and dynamic network of proteins and polysaccharide macromolecules that fills the intercellular space in tissues **(Alberts, 2002)**. Major components of ECM are glycosaminoglycans like hyaluronan and proteoglycans like aggrecan and syndecan. Protein constituents in the ECM are Collagens, Elastin, Fibronectin. The basal lamina, a specialized ECM for epithelial tissues, further consists of Laminins, Nidogen and heparan sulfate proteoglycans.
In the stem cell niche, the ECM serves as a reservoir for growth factors and morphogens, provides contact sites for stem cells and niche cells **(Brizzi, 2012)**, and transmits biomechanical forces via Integrins to the cells, which also influences stem cell activity by cross-talk with other signaling pathways **(Kopf, 2012)**.

Soluble factors

Functions in niche regulation have been implicated for platelet-derived growth factor (PDGF), fibroblast growth factors (FGF), among others. FGF and PDGF play pivotal roles in regulating proliferation and differentiation during wound healing, angiogenesis and embryogenesis **(Alberts, 2002)**. These growth factors signal via transmembrane receptor tyrosine kinases (RTK). RTKs dimerize upon ligand binding which leads to autophosphorylation and activation of different downstream targets, such as the mitogen-activated protein (MAPK) pathway and the phosphoinositol-3-kinase (PI3K) pathway **(Alberts, 2002)**. Signaling can also be mediated by crosstalk with the JAK/STAT pathway **(Sachsenmaier, 1999)**. Signal Transducer and Activator of Transcription (STAT) proteins are

activated by Janus Kinase (JAK) and subsequently enter the nucleus to act as transcription factors and change cellular behavior.

Growth factor signaling will lead to migration, proliferation or differentiation depending on expressed receptors and individual cellular interior. For example, FGF signaling and its intracellular inhibitor Sprouty-1 (SPRY1) were recently shown to mediate satellite stem cell quiescence in the muscle **(Chakkalakal, 2012)**.

The family of transforming growth factor β (TGF-β) proteins represents a large superfamily of growth factors, including TGF-β, Activin and Inhibin, bone morphogenetic proteins (BMP) and growth and differentiation factors (GDF) **(Alberts, 2002)**. These growth factors also signal via RTKs, however, their signals are intracellularly transduced by SMAD proteins (SMA/mothers against decapentaplegic). SMAD proteins act as trimeric complex, with two receptor-activated SMADs binding a co-SMAD to enter the nucleus and regulate transcription **(Shi, 2003)**. BMPs promote quiescence of stem cells in the niche **(Lander, 2012)**, while ambivalent functions in stem cell maintenance have been assigned to TGF-β. On the one hand, TGF-β may control HSC hibernation, i.e. quiescence, in the BM **(Yamazaki, 2009)**. On the other hand, TGF-β signaling, for example, may lead to stem cell activation **(Oshimori, 2012)**.

Another important signaling cascade associated with stemness is WNT (Wingless-type MMTV integration site family) signaling which is based on proteolytic cleavage **(Alberts, 2002)**. In the absence of WNT, a protein complex around the protein Adenomatous Polyposis Coli activates glycogen synthase kinase-3β (GSK-3β) leading to phosphorylation and degradation of β-Catenin. Upon WNT binding to its receptors Frizzled (FZD) and Low density lipoprotein receptor-related protein (LRP), intracellular Dishevelled is activated, which results in inactivation of GSK-3β and stabilization of β-Catenin that can then enter the nucleus and serve as co-factor for TCF and LEF transcription factors **(Alberts, 2002)**. WNT signaling was demonstrated to be important for maintenance of intestinal crypt stem cells and HSC **(Reya, 2005)**. WNT signaling regulates the stem cell pool by inhibiting proliferation and differentiation.

The in vivo as well as in vitro niche of MSC still await in depth characterization **(Kolf, 2007)**. Moreover changes in the niche composition due to cell culture may have effects on cellular properties.

2.3. Multipotent mesenchymal stromal cells

Following the discovery of HSC in adult BM, Friedenstein and colleagues in the 1960s identified a subset of non-hematopoietic bone marrow stem cells with plastic-adherent proliferative capacity and osteogenic potential **(Friedenstein, 1966)**. In the early 1990s, Caplan termed these cells "mesenchymal stem cells", also referred to as "multipotent mesenchymal stromal cells" **(Caplan, 1991; Nombela-Arrieta, 2011)**.

MSC lack a unique surface marker and are morphologically very similar to fibroblasts. To standardize the definition of MSC, the International Society for Cellular Therapy (ISCT) summarized MSC properties **(Dominici, 2006)**. According to this set of minimal criteria, MSC are 1) plastic-adherently proliferating cells with spindle-shaped morphology; 2) multipotent and differentiate towards adipocytes, osteoblasts and chondrocytes; 3) express CD73, CD90 and CD105 and are devoid of CD14, CD34 and CD45. In addition, MSC do not express co-stimulatory molecules like CD80, CD86 and CD40.

Since the 1990s, MSC research has been focused on therapeutic applications of MSC. This medical emphasis is related to some characteristics of MSC, which make them interesting therapeutic targets.

Distribution in several adult tissues

MSC-like cells can be derived from a variety of source tissues, such as bone marrow (BM-MSC), umbilical cord blood, placenta and adipose tissue (AT-MSC) **(Fukuchi, 2004; Pittenger, 1999; Wang, 2004; Zuk, 2002)**. Thus, MSC are easily available cell types for autologous interventions.

Multipotency

MSC can differentiate into mesodermal lineages like osteoblasts, adipocytes and chondrocytes **(Mackay, 1998; Pittenger, 1999; Sekiya, 2004)** (Fig. 3). Based on such findings, Caplan postulated that MSC replenish tissue cells in the homeostatic and injury situation, following a process called "mesengenesis" **(Caplan, 1994)**.

Differentiation was also reported into cardiomyocytes as well as neuronal, pancreatic, hepatic cell types **(Anghileri, 2008; Antonitsis, 2008; Banas, 2009; Lee, 2008)**. However, these differentiation results of MSC are still debatable. For example, except for osteogenesis by BM-MSC, the differentiation into none of these lineages has been formally demonstrated

by *in vivo* experiments **(Augello, 2010; Bianco, 2008)**. However, especially multipotency has rendered MSC an attractive cell type for orthopedic therapies, ranging from cartilage replacement and bone healing improvement to tendon regeneration **(Frisbie, 2009; Ouyang, 2006; Wilke, 2007)**.

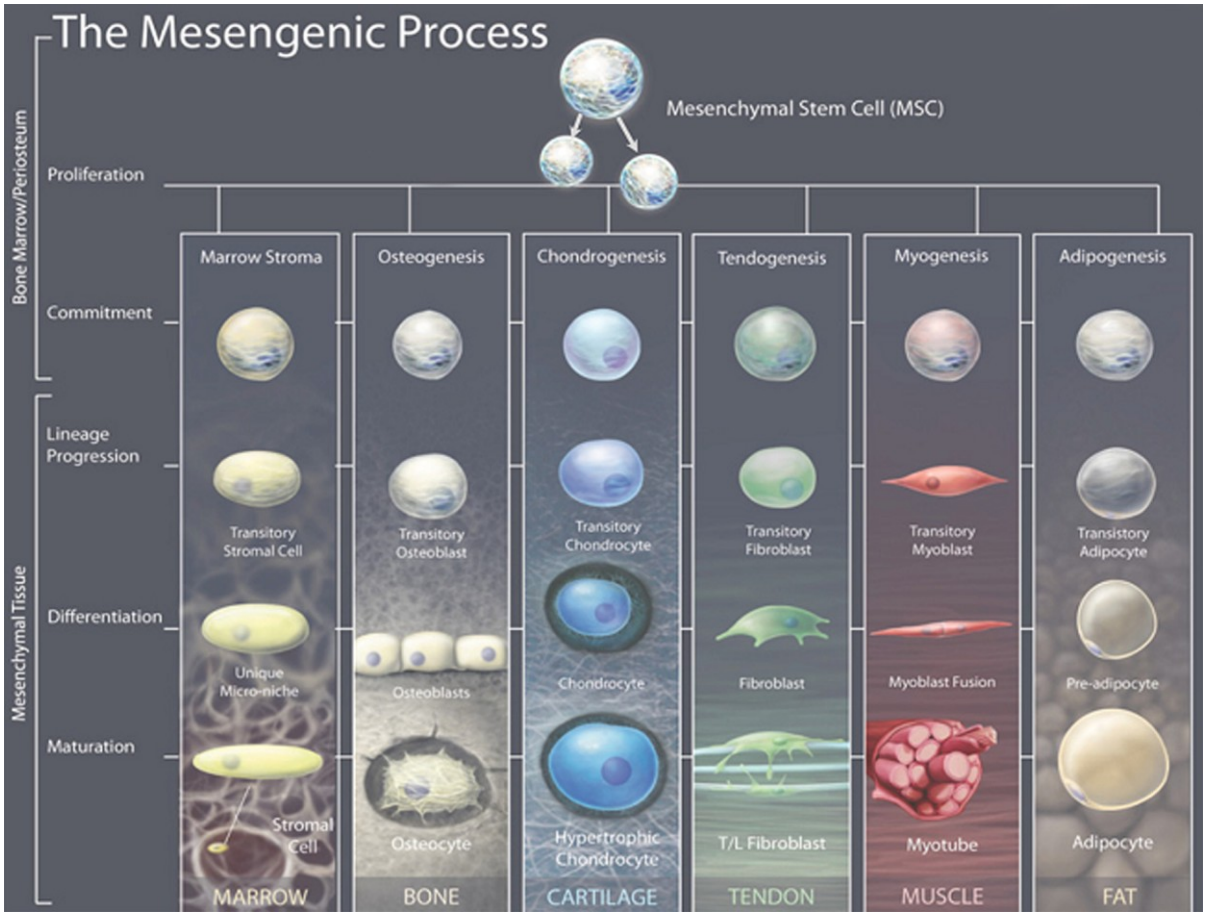

Figure 3: The Mesengenic Process.
Taken from **(Caplan, 2011a)**.

Immunomodulation

MSC are only weakly immunogenic despite expression of MHC (major histocompatibility complex) type we molecules **(Le Blanc, 2003)** and additionally seem to modulate immunological reactions **(Nauta, 2007)**, (Fig. 4). MSC are reported to modulate the response of immune cells, to inhibit maturation and differentiation of monocytes into DC and to reduce T cell proliferation in mixed lymphocyte reactions **(Li, 2005; Zhang, 2004)**; **(Di Nicola, 2002; Ramasamy, 2008; Rasmusson, 2007)**. This inhibition of proliferation is accompanied by a shift from pro-inflammatory to anti-inflammatory T cell responses **(Bai, 2009)**. Immunomodulatory properties of MSC seem to depend on cell-to-cell contact as well as on

soluble factors such as Interleukin-6, and -10, Indoleamine-2,3-dioxygenase and Prostaglandin E2 **(Nauta, 2007)**.

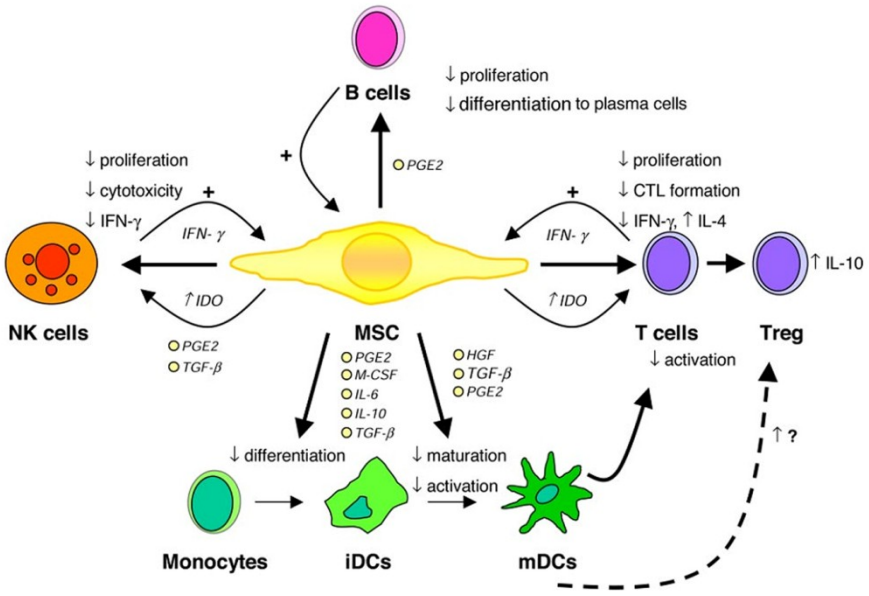

Figure 4: Immunomodulatory effects of MSC and mediating cytokines.
Taken from **(Nauta, 2007)**.

Therapeutic potentials and applications of MSC

Together, good accessibility, multipotency and low immunogenicity make MSC an ideal candidate for cell-based therapies, as auto- and allograft. Several studies with different animal models showed therapeutic and regenerative benefit provided by MSC, e.g. in muscle repair **(Dezawa, 2005; Winkler, 2008)** or treatment of critical limb ischemia **(Prather, 2009)**. But beneficial regenerative effects of MSC seemed to be mediated rather by trophic or paracrine effects than by differentiation. Thus, Caplan recently proposed "medicinal signaling cells" as a more appropriate terminology **(Caplan, 2009)**. Autologous and allogeneic MSC facilitate engraftment of HSC transplants **(Koc, 2002; Koc, 2000)** and help in treatment of graft-versus-host disease **(Bartholomew, 2002; Le Blanc, 2004)**. MSC also exert beneficial effects on angiogenesis by supporting tube formation of endothelial cells **(Huang, 2009; Kasper, 2007)**. Clinical trials have been conducted and are ongoing to investigate their effect in several diseases, such as peripheral artery disease, osteoarthritis and myocardial infarction (www.clinicaltrials.gov).

2.4. MSC progenitors

The exact identity of cells giving rise to MSC remained unknown, until in 2007, Sacchetti et al. have described perivascular, $CD146^+$ Adventitial Reticular Cells (ARC) in the BM as MSC progenitors. These ARC were not only capable of bone formation *in vivo*, but also self-renewal after secondary transplantation **(Sacchetti, 2007)**. This suggested the identification of "skeletal stem cells" as MSC progenitors. In older studies, $CD271^+$ cells were denoted as BM-MSC progenitors, yet less stringently characterized **(Quirici, 2002)**. Until recently, Tormin et al. described two $CD271^+$ BM-MSC progenitors that differed in micro-anatomical localization and CD146 expression and were also capable of bone formation *in vivo* **(Tormin, 2011)**. These in part conflicting reports imply that MSC progenitors can be identified either by CD146 or CD271 expression. Nevertheless, these previous works have opened new routes for defining MSC progenitors also in other tissues. Already in 2008, CD146 was used to identify perivascular cells as MSC progenitors in almost all adult human tissues **(Covas, 2008; Crisan, 2008)**. Moreover, CD271 was also used to identify MSC progenitors in adipose tissue **(Quirici, 2010)**. Collectively, these studies demonstrated that MSC from any vascularized adult tissue can be derived from perivascular MSC progenitors defined by CD146 or CD271 expression.

2.5. *In vivo* origin of MSC

MSC-like cells can be derived from perivascular cells of various tissues, as described above, but they differ in proliferative capacity, differentiation potential and gene expression **(Im, 2005; Kern, 2006)**. Different hypotheses exist to explain these differences.

Tissue-specific stem/progenitor cells

According to one paradigm, MSC may stem from tissue-specific progenitor cells, which also reside in perivascular niches, for example, astrocyte stem cells in the subventricular zone **(Tavazoie, 2008)**; HSC in a perivascular niche **(Doan, 2012)**; pre-adipocytes residing in blood vessel walls of adipose tissue **(Tang, 2008)**. Hence, the differences between MSC derived from different tissues may be determined by the source tissue **(Bianco, 2008)**. This hypothesis is in accordance with most experimental observations.

De-differentiation / Trans-differentiation

According to another hypothesis, MSC may be the result of de-differentiation or trans-differentiation **(Raff, 2003; Roobrouck, 2011)**. By removing cells from their normal environment, cells are deprived of the signals required to keep them in their differentiated state. Growth factors and cytokines provided by the serum further contribute to initiation of de-differentiation **(Entenmann, 1996)**. Differentiated cells can also trans-differentiate into other terminally differentiated cells without intermittent de-differentiation into a common progenitor cell **(Song, 2004)**.

MSC progenitors isolated from any given tissue may also undergo de-differentiation *in vitro* which will endow these cells with greater potency. In this regard, it remains to be understood how *ex vivo* cells that develop into MSC adapt to the artificial *in vitro* environment.

2.6. MSC derivation phase – MSC isolation and conditions of early culture

We assume that MSC progenitors adapt to the *in vitro* situation during the first days of early culture, here referred to as "MSC derivation phase", and this may represent the moment of de-differentiation. Previous reports suggested that changes in surface marker expression occur during the early culture phase, representing cellular adaptations to the *in vitro* situation. For instance, CD34 was downregulated in progenitors of AT-MSC and BM-MSC within the first two passages **(Quirici, 2010; Quirici, 2002; Suga, 2009)**. In addition, a recent report described upregulation of CD146 by BM-MSC during the early culture phase **(Tormin, 2011)**. Based on these preliminary insights, a comprehensive study of the MSC derivation phase has to be conducted, also focusing on immunophenotypical changes.

MSC isolation and subsequent culture according to the standard protocol comprises three steps: (1) isolation from the source tissue (often using enzyme digestion), (2) seeding on tissue-culture plastic and functional enrichment by plastic adherence, and (3) expansion until a spindle-shaped, fibroblastoid cell type has emerged and the cells proliferate actively.

For MSC derivation, the conventional culture condition for MSC (here referred to as MScult) employs uncoated tissue-culture plastic and Dulbecco's Modified Eagle's Medium (DMEM) supplemented with fetal calf serum **(Friedenstein, 1974)**. However, comparison of different recent publications revealed that different culture conditions were utilized for early MSC culture (Table 1). Although, most commonly, MScult was used, supplements like heparin,

FGF-1 (acidic fibroblast growth factor) or dexamethasone were often added. These compounds are known to increase proliferation rates.

Table 1: Literature summary of conditions for *ex vivo* culture of MSC progenitors.

Publication	**Crisan, 2008**	**Suga, 2009**	**Zimmerlin, 2010**	**Corselli, 2011**	**Maumus, 2011**	**Tormin, 2011**	**Traktuev, 2008**
Condition	**ECcult**	**MScult**	**MScult**	**ECcult**	**MScult**	**MScult**	**ECcult**
Medium	EGM-2	Medium 199	DMEM + DMEM/F12	EGM-2	alpha-MEM	NH expansion medium	EBM or EGM2-MV
FCS	2% FBS	10% FBS	10% FCS	2% FBS	2%/10% FCS	10% FCS	2/5% FBS
Coating	0.2% Gelatine	-	-	+ 0.2% Gelatine	-	-	-
Supplements	hEGF, Hydrocortisone, VEGF, hFGF-B, R3-IGF-1, Ascorbic Acid, Heparin	heparin, Fibroblast Growth Factor-1	Dexamthasone	hEGF, Hydrocortisone, VEGF, hFGF-B, R3-IGF-1, Ascorbic Acid, Heparin	-	-	Bovine Bone Extract, hEGF, Hydrocortisone
Antibiotics	GA-1000 (Gentamicin, Amphotericin-B)	Penicillin, Streptomycin	Penicillin, Gentamycin-sulfate	GA-1000	na	1% P/S	GA-1000
Seeding density [cells/sqcm]	$2x10^4$	$6x10^3$	$1,0\text{-}2,5x10^4$	$2x10^4$	$4x10^3$	20-50	$3x10^3$

Another culture method was also frequently utilized, which was originally designed for culturing endothelial cells (ECcult). In ECcult, cells are grown in Endothelial Growth Medium-2 (EGM2) and seeded on gelatin-coated culture flasks. The EGM2 medium is supplemented with 2% FBS (fetal bovine serum), hydrocortisone, ascorbic acid, and heparin, and the growth factors FGF-2 (basic FGF), VEGF (Vascular Endothelial Growth Factor), IGF-1 (Insulin-like Growth Factor-1) and EGF (Epidermal Growth Factor). These factors are supplemented to induce proliferation of endothelial cells. Interestingly, Crisan et al. have ultilized this condition for characterization of $CD146^+$ pericytes as MSC progenitors **(Crisan, 2008)**.

Different culture conditions in MSC research, especially during early culture, may affect cellular behavior and/or selection of different cell subsets. A comprehensive comparison of the effects of culture condition on MSC derivation has not yet been performed.

2.7. Aim of the study

It has been clarified that perivascular cells from various adult human tissues give rise to MSC during early *in vitro* culture. However, an uncertainty remains concerning phenotyping of these MSC progenitors using CD146 or CD271. Moreover, it remains to be elucidated whether and how MSC progenitors acquire the properties typical for MSC *in vitro*.

Hence, this study aimed at

1) improving characterization of MSC progenitors
2) performing comprehensive kinetic analysis of the MSC derivation phase
3) deciphering signaling cascades and transcriptional programs regulating MSC derivation

No previous study has so far analyzed the MSC derivation phase in detail. Thus, we undertook a comprehensive screening of the early culture phase in tight kinetics focusing on proliferation, morphology and immunophenotype. For these extensive kinetic analyses of MSC progenitors, high initial numbers of MSC progenitors were required. These were obtained from the densely vascularized white adipose tissue (AT), the stromal vascular fraction (SVF) of which harbors high amounts of MSC progenitors **(da Silva Meirelles, 2009; Zuk, 2002)**.

SVF cell subsets were characterized by multi-parametric flow cytometry and enriched by fluorescence-activated cell sorting (FACS) or magnetic cell separation (MACS). Characterization of MSC progenitors *ex vivo* was improved by including the following surface markers:

- CD73 (Ecto-5'-Nucleotidase, NT5E)
- CD90 (THY1)
- CD105 (Endoglin, ENG)
- CD146 (Melanocyte Cell Adhesion Molecule, MCAM, MUC18)
- CD271 (low affinity Nerve Growth Factor Receptor, NGFR, p75)
- CD34 (hematopoietic progenitor cell antigen)
- CD14 (LPS receptor)
- CD45 (Protein Tyrosine Phosphatase Receptor type C, PTPRC)
- CD31 (Platelet Endothelial Cell Adhesion Molecule, PECAM-1)

CD73, CD90 and CD105 are surface markers of *in vitro* MSC, and CD146 and CD271 are well established markers for MSC enrichment *ex vivo*. CD34 was included since $CD146^+$ or $CD271^+$ MSC progenitors were reported to be either $CD34^-$ or $CD34^+$, respectively, but MSC *in vitro* are $CD34^-$ **(Crisan, 2008; Quirici, 2002)**. MSC *in vitro* are defined to be negative for CD14 and CD45. Furthermore, we utilized CD45 and CD31 to identify and exclude hematopoietic cells and endothelial cells. By intracellular staining of α-smooth muscle actin (αSMA), we also assessed the distribution of smooth muscle cell populations within SVF cells.

In bulk cultures and sorted subset cultures, we monitored morphology, proliferation and surface marker expression in tight kinetics during the MSC derivation phase. The effect of two different culture conditions, namely MScult and ECcult (Table 1) on MSC derivation was investigated. Finally, gene expression of *ex vivo* sorted MSC progenitors and cultured MSC was compared using microarray, analyzed by Gene Set Enrichment Analysis (GSEA) and confirmed by quantitative Real Time-PCR (qPCR).

By this approach, we received a detailed overview about morphological and phenotypical transitions during MSC derivation and about underlying signaling cascades and transcriptional programs.

3. Materials & Methods

3.1. Cell isolation

Table 2: Materials needed for cell isolation.

Reagent / Buffer / Material	Manufacturer
PBS (Phosphate Buffered Saline)	
diluted from 10X PBS	Invitrogen, Darmstadt, Germany
PBS/BSA	
PBS	
+ 0.2% BSA (Bovine Serum Albumin)	PAA, Pasching, Germany
HBSS (Hank's Buffered Saline Solution)	Invitrogen
Collagenase NB4G	Serva, Heidelberg, Germany
Digestion Stopping Buffer	
DMEM, 1.5 g/L D-Glucose	Invitrogen
+ 20% FBS	Invitrogen
1L Storage Bottle	Corning
Buffer EL (Erythrocyte Lysis)	Qiagen, Hilden, Germany
70µm cell strainer	BD, Heidelberg, Germany
40µm cell strainer	BD

Adipose tissue samples of gynaecomastic breast, abdomen, hip or thigh from elective liposuctions from female and male donors were provided by the Aesthetical Surgery department of Dr. Bodo, Berlin. Donors were informed and consented to anonymized sample utilization. The procedure was approved by the local ethics committee.

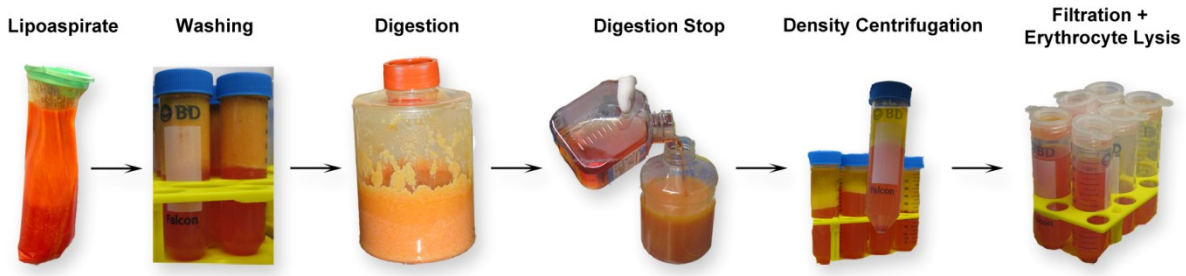

Figure 5: Schematic overview over SVF isolation procedure.

Stromal vascular fraction (SVF) cells were isolated by Collagenase digestion and density centrifugation (Fig. 5). In detail, 200-400 ml lipoaspirate were distributed to several 50ml Falcon tubes and washed with PBS at a ratio of 1:1 and centrifuged at 430xg for 10 min at 4°C. This washing step was repeated twice to remove peripheral lymphocytes and red blood cells. The washed lipoaspirate was transferred to a 1L Storage Bottle. Collagenase NB4G,

previously dissolved in HBSS at 37°C for about 10 min and sterile filtered using a 0.2µm sterile filter, was added at a final concentration of 0.3 U per ml of lipoaspirate. Digestion was performed for 45-60 min at 37°C. Reaction was stopped by adding Digestion Stopping Buffer (30% of digest volume). The cell suspension was transferred to 50ml Falcon tubes and centrifuged at 600xg for 10 min at 4°C. Thereby, dense mononuclear cells were pelleted, while less dense adipocytes and lipids remained in the supernatant that was then removed by pipetting and discarded. The pelleted mononuclear cells, the "Stromal Vascular Fraction" (SVF), was resuspended in 30 ml PBS/BSA per pellet and filtered through a 70µm cell strainer. After centrifugation at 430xg for 10 min at 4°C, pellets were resuspended in 5-10 ml of Buffer EL to remove remaining erythrocytes by erythrocyte lysis. After 10-15 min, cell suspension was filled up with PBS/BSA and centrifuged at 430xg for 10 min. Pellets were resuspended in PBS/BSA and filtered over a 40µm cell strainer. Cell concentration in the suspension was determined using CASY cell counter.

3.2. Cell Counting

Table 3: Materials needed for cell counting.

Reagent / Buffer / Material	Manufacturer
CASY Cell Counter and Analyzer	Roche Applied Science, Basel, Switzerland
Casy Tube	Roche
CasyTon (Running Buffer)	Roche

Casy cell counter determines cell concentration in a cell suspension and measures cell sizes and the ratio of viable cells by measuring electric impedance which is proportional to cell size. The membranes of dead cells are permeable, hence, only the nucleus influences the electric current and dead cells can be excluded due to size, generally smaller than 5 µm.

For measurement, 10 µl of a cell suspension were diluted 1:1000 in 10ml CasyTon in a special Casy tube. Three times 400 µl of the cell suspension are acquired and the mean of viable cells per ml is calculated.

3.3. Cell Culture

Table 4: Materials needed for cell culture.

Reagent / Buffer / Material		Manufacturer
NH Expansion Medium		Miltenyi, Bergisch-Gladbach, Germany
EGM-2 culture medium (Endothelial Growth Medium)		
EBM-2 (Endothelial Basal Medium)		Lonza
EGM-2 SingleQuot Kit	hEGF, Hydrocortisone, GA-1000 (Gentamicin, Amphotericin-B), 5% FBS, VEGF, h-FGF-B, R3-IGF-1, Ascorbic Acid, Heparin	Lonza
Porcine Gelatine		Sigma, St. Louis, MO, USA
2% Stock in PBS; diluted 1:10 in PBS, coating of 6-well plates over-night at 4°C		
Growth Medium (GM)		
DMEM, 1.5 g/L D-Glucose, 0.11g/L Sodium Pyruvate, Glutamate		Invitrogen
+ 10% FBS		Invitrogen
+ 100 U/ml Penicillin, 100µg/ml Streptomycin		PAA
Accutase		PAA
6 well plates		BD
T25 Tissue culture flask, polystyrene, 25cm^2		BD
T75 Tissue culture flask, polystyrene, 75cm^2		BD
T175 Tissue culture flask, polystyrene, 175cm^2		BD

Ex vivo bulk SVF cells were plated at a density of 1x10^5 cells/cm^2. Sorted cells were seeded at different ratios (1-5x10^4/cm^2), since different cell numbers were yielded after sorting. Cells were cultured either under MScult, i.e. on uncoated tissue culture polystyrene (TCPS) plates with NH expansion medium, or under ECcult, i.e. on gelatin-coated TCPS with EGM-2 medium. We used commercially available media to standardize and avoid medium differences, e.g. related to FCS batches. After 24 hours, medium was replaced to remove non-attached cells. AT-MSC were passaged when 80% confluence was reached. For passaging, cells were detached using Accutase, and re-seeded on uncoated TCPS in growth medium (GM) at a density of 4x10^3 cells/cm^2.

Cell counts at passaging were used to calculate expansion curves based on cumulative cell numbers. Cell numbers increase during expansion, but at each passaging, not all cells are reseeded in expansion cultures. To correct for this, following formula was used:

$$C_{+1} = \frac{N}{n} \times C_{-1}$$

N: Cell count of harvested cells

n: Cell count of initially plated cells

C-1: Cell number at previous passaging

C+1: Cell number at current passaging (hypothetical)

This calculation results in a hypothetical value of the total cell number at passaging. Continuing this for all passages, leads to cumulative cell numbers. $\frac{N}{n}$ represents the proliferation factor or proliferation rate.

3.4. Differentiation

Table 5: Materials needed for differentiation.

Reagent / Buffer / Material	Manufacturer
Growth Medium (GM)	
DMEM, 1.5 g/L D-Glucose, 0.11g/L Sodium Pyruvate, Glutamate	Invitrogen
+ 10% FBS	Invitrogen
+ 100 U/ml Penicillin, 100µg/ml Streptomycin	PAA
Adipogenic Medium	
GM	
+ 100µM Indomethacine	Sigma
+ 10 µg/ml Insulin	Sigma
+ 500µM 3-Isobutylmethylxanthine	Sigma
+ 1µM Dexamethasone	Sigma
Osteogenic Medium	
GM	
+ 250µM Ascorbic acid	Sigma
+ 10 mM β-Glycerophosphate	Sigma
+ 100 nM Dexamethasone	Sigma
Chondrogenic Medium	
GM	
+ 3 g/l D-Glucose	Sigma
+ 350 µM L-Proline	Sigma
+ 100 nM Dexamethasone	Sigma
+ 10ng/ml recombinant human Transforming Growth Factor β3	Sigma

AT-MSC in passage 2 were differentiated towards the adipogenic, osteogenic and chondrogenic lineage according to standard protocols **(Braun, 2010; Pittenger, 1999)**. For adipogenesis and osteogenesis, $5x10^3$ AT-MSC/cm^2 were plated, and stimulated with osteogenic differentiation medium directly or with adipogenic differentiation medium upon confluence. Chondrogenic differentiation was induced in micromass cultures of $4x10^5$ cells in chondrogenic medium in 96-well plates. Cultures were maintained for 21 days and medium was exchanged every 2^{nd} to 3^{rd} day.

3.5. Cytochemical stainings

Table 6: Materials needed for differentiation.

Reagent / Buffer / Material	Manufacturer
Oil Red Stock solution:	
Oil Red stock: 0.25 g Oil Red O	Sigma
in 50ml Isopropyl alcohol	Carl Roth, Karlsruhe, Germany
Oil Red Staining solution:	
30 ml Oil Red stock ad 50 ml dH_2O, filtration after overnight incubation	
Nile Red	
100µg/ml; 1 mg Nile Red S	Sigma
in 10 ml Acetone	Sigma
Alizarin Red	
0.7 g Alizarin Red in 50 ml dH_2O; pH 4.0	Sigma
TissueTek	Sakura Finetek Europe, Alphen adR, Netherlands
Alcian Blue	
0.5 g Alcian Blue	Sigma
+ 1.5 ml Acetic Acid	Merck, Darmstadt, Germany
ad 50 ml H_2O	
Formaldehyde (37%)	Merck
Methanol	J. T. Baker, Griesheim, Germany
Ethanol	Carl Roth
Glass slides	Thermo Scientific, Wilmington, DE, USA
Cover slip	Carl Roth
Dako Fluorescence Mounting Medium	Dako, Glostrup, Denmark

Differentiation was controlled by cytochemical stainings. Lipid vesicles, mineral deposits, and proteoglycans were detected using Oil Red or Nile Red staining, Alizarin Red, and Alcian Blue staining, respectively.

Oil Red, also known as Sudan Red, has strongly lipophilic aromatic groups that bind to triglycerides and lipids with high affinity. For Oil Red staining, cells were washed once with PBS and fixed with 4% formaldehyde for 15 min to permeabilize cell membranes. Cells were again washed twice with dH_2O (demineralized water) and then Oil Red O staining solution was incubated for 30 min. After a final three-times washing with PBS, cells were photographed using a Motic AE31 microscope with Moticam 2300.

Nile Red is a lipophilic fluorescent dye, the excitation (ex) and emission (em) wavelengths of which are altered dependent on the surrounding hydrophobicity. Therefore, less hydrophobic structures like membranes are stained with orange fluorescence, whereas highly hydrophobic lipid vesicles appear green. For Nile Red staining, cells were washed with PBS and fixed with 4% formaldehyde for 15 min. After washing twice with PBS, a pre-mixed staining mixture containing Nile Red (1:200) and DAPI (1:300) was applied and incubated for 10 min. After additional washing steps, cells were photographed with a Zeiss Axio Observer

fluorescence microscope using filter sets 49 (DAPI, ex 365-395nm, em 420-470nm), 43HE (membrane fluorescence, ex 535-560nm, em 570-640nm) and 38HE (lipid vesicle fluorescence, ex 450-490nm, em 500-550nm).

Alizarin Red, isolated from the plant Rubia tinctorum, complexes with calcium depositions and renders them stained in red. For Alizarin Red staining, cells were washed shortly with PBS and fixed and permeabilized using ice-cold methanol for 2 min. After washing with dH_2O, cells were incubated with Alizarin Red staining solution for 15 min, and then washed with PBS for 15 min. After dehydration using ice-cold ethanol for 5 min and additional washing steps, cells were photographed using a Motic AE31 microscope with Moticam 2300.

Alcian Blue is a copper-containing dye that binds to anionic residues of glycosaminoglycans via electrostatic interactions and stains them blue. To stain chondrogenic micropellets, the pellets were first prepared for cryosectioning. Pellets were harvested from 96 well plates and washed once in PBS for 5 min. Pellets were embedded in TissueTek in an alu-foil tube, and then shock frozen in liquid nitrogen. Until sectioning, the embedded and frozen pellets were stored at -80°C. Sectioning into 7µm slices was performed on a Leica Cryotom CM3050S. Slices were transferred onto glass slides, fixed in acetone and stored at -80°C. For Alcian Blue staining, slices were thawed, washed twice with dH_2O and incubated for 30 min in Alcian Blue staining solution. After washing with PBS twice, slides were shortly dried and covered with a coverslip using Dako Mounting Medium. Slides were photographed on a Zeiss AxioScope.

3.6. Antibody staining and flow cytometry

Flow cytometry enables multi-parametric analysis of individual cells within heterogeneous cell populations. Flow cytometry can provide information about single cells concerning cell size and granularity and in combination with the use of fluorescently labeled antibodies or fluorescent compounds also protein expression, protein phosphorylation, cytokine secretion and proliferation.

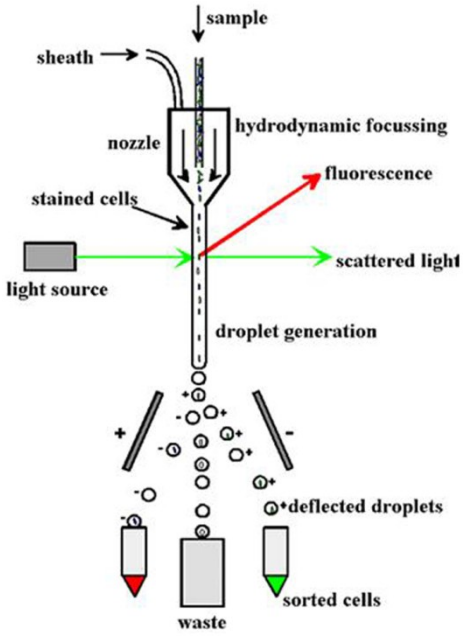

Figure 6: Schematic overview about the working principle of flow cytometers and cell sorters. (http://missinglink.ucsf.edu/lm/molecularmethods/flow.htm).

The working principle of a flow cytometer is the following (Fig. 6): cells in a cell suspension are collected by the fluidic system and singularized in small droplets by hydrodynamic focusing using a small nozzle and an ultrasound source. The cells then pass the so called interrogation point. Here, laser light at different wavelengths either is refracted or excites fluorochromes and refracted light or emitted fluorescence are recorded by photomultipliers (PMTs). The refracted light gives information about cellular size (forward scatter, FSC) and structural complexity, such as granularity (side scatter, SSC). The information conveyed by emitted fluorescence depends on the utilized antibodies or compounds and their specific fluorescence.

When many fluorochromes are employed for multi-parametric analysis the emission spectra of specific dyes may partly overlap, which may lead to false positive results. This is conventionally prevented by "compensation", i.e. the subtraction of detected signals of one PMT from another PMT. Prior to FACS-analysis, cells were surface-stained and/or intracellularly.

Ex vivo or cultured, detached SVF cells ($1x10^6$ cells) were transferred to FACS tubes, pelleted by centrifugation at 490xg for 10 min at 4°C and resuspended in 100µl PBS/BSA. Nonspecific antibody binding was prevented by adding Beriglobin (1:50) before surface staining with monoclonal antibodies. After incubation for 20 minutes, cells were washed with PBS/BSA, centrifuged at 490xg, 10 min, 4°C and resuspended in 300µl PBS/BSA. Dead cells were excluded by DAPI staining (1:250) prior to measurement.

Intracellular staining was performed for detection of alpha-Smooth Muscle Actin (aSMA). Surface-stained cells were washed and centrifuged (490xg, 10min, 4°C). Before fixation, dead cells were stained using Live/Dead Fixable Aqua Dead Cell Stain. Cells were fixed using 1ml BD FACS Lysing solution for 10 min at RT. After centrifugation, cells were permeabilized using 500µl BD Permeabilizing solution 2.

For proliferation assays, cells were labeled with a Cell Tracker Violet BMQC dye (CTV) according to manufacturer's protocol. In detail, *ex vivo* cells were incubated with DMSO-reconstituted CTV (dissolved in DMEM at a concentration of 5µM) at 37°C for 30 minutes. Cells were then transferred into fresh medium and incubated at 37°C for 30 minutes. Afterwards, CTV-labeled cells were washed with PBS, and cultured under MScult. At indicated time points, cells were harvested and antibody-stained.

Labeled cells were measured with a BD Canto II flow cytometer (provided by the BCRT Flow Cytometry Lab) and data were analyzed using FlowJo software.

Table 7: Materials needed for flow cytometry.

Reagent / Buffer / Material	**Clone**	**Manufacturer**
APC-H7 anti-CD14	MΦP9	BD
PE-Cy7 anti-CD31	WM59	Biolegend, San Diego, CA, USA
PerCP anti-CD34	8G12	BD
FITC anti-CD34	AC136	Miltenyi
Horizon V500 anti-CD45	HL30	BD
PE anti-CD73	AD2	BD
APC anti-CD90	5E10	Biolegend
AlexaFluor488 anti-CD105	43A3	Biolegend
PE anti-CD146	541-10B2	Miltenyi
APC anti-CD271	Me20.4	Miltenyi
PE anti-αSMA (α-smooth muscle actin)	1A4	R&D Systems, Minneapolis, MN, USA
BD FACS Lysing Solution		BD
BD Permeabilizing Solution 2		BD
Beriglobin		Sanofi-Aventis, Frankfurt/Main, Germany
DAPI (4'-6'-diamidino-2-phenylindole; 1µg/ml)		Invitrogen
Live/Dead Fixable Aqua Dead Cell Stain kit		Invitrogen
FACS tubes (5ml)		BD
FlowJo software v9		Tree Star Inc., OR, USA

3.7. Statistical analysis and integrated mean fluorescence intensity

All statistical analyses were performed using Prism5 (GraphPad Software, La Jolla, CA, USA). Mean values ± standard deviation (SD) are displayed. Significance was tested using Student T-test and results with p-value below 0.05 (*) and 0.001 (**) were regarded as statistically significant.

For comparison of surface marker expression between several experiments, we utilized the iMFI (integrated Mean Fluorescence Intensity) to correlate the increase in MFI with the percentage of positive cells according to **(Darrah, 2007)**. Positive cells were gated according to the respective marker and percentage and MFI were derived from FlowJo software. iMFI was calculated by multiplication of percentage and MFI. An increase in cell number together with an actual upregulation (increase in MFI) would result in a high iMFI value, whereas a few positive MFI^{high} cells would result in a low iMFI.

3.8. Fluorescence-activated cell sorting

Flow cytometers can also be equipped with an electrostatic deflection system, and serve as cell sorters (Fig. 6). For the so called fluorescence-activated cell sorting (FACS), the separate cell-containing droplets after the interrogation point receive an electrical charge dependent on parameters selected by the operator and later pass deflection plates where the cells are separated into different tubes. This system allows for the highly specific purification of up to 4 different cell populations in parallel. In this study, FACS-sorting was performed by the BCRT Flow Cytometry Lab (Dr. Desiree Kunkel).

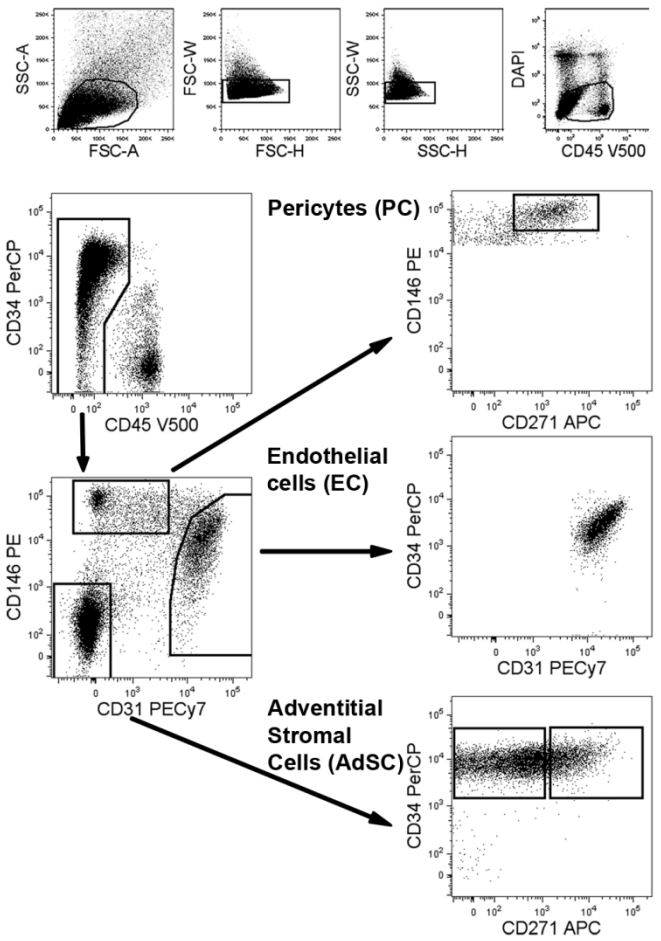

Figure 7: FACS-sorting scheme of SVF cell subsets *ex vivo*. SVF were antibody-stained, and then sorted as described.

For FACS, typically $2x10^8$ SVF cells were labeled with antibodies against CD31, CD34, CD45, CD146 and CD271 as described earlier. After staining, cells were filtered through a 30µm cell strainer. Subsets were sorted into medium-containing FACS tubes using a BD Aria II cell sorter according to the following sorting scheme (Fig. 7). First, cells were gated according to forward and sideward scatter (FSC vs. SSC), and dead cells and $CD45^+$ lymphocytes were excluded. In the remaining $CD45^-$ stromal vascular cells, $CD146^{high}$ $CD31^{low}$ $CD271^+$ pericytes (PC), $CD146^+$ $CD31^+$ endothelial cells (EC) and $CD146^-$ $CD31^-$ $CD34^+$ $CD271^-$ or $CD271^+$ adventitial stromal cells (AdSC) were gated and sorted. Purities were around 99%.

Sorted cells were cultured under MScult or ECcult. Cell numbers in the kinetic analysis were normalized to $1x10^3$ seeded cells/cm^2 because seeding densities varied from $1x10^4$ to $4x10^4$ cells/cm^2. In addition, RNA of sorted $CD271^+$ and $CD271^-$ AdSC was isolated for microarray analysis.

3.9. Magnetic Cell Separation

For magnetic cell separation (MACS), cells are labeled with monoclonal antibodies conjugated to paramagnetic microbeads and loaded onto special MACS columns positioned in a magnetic field. Thereby, bead-labeled cells are retained in the column whereas unlabeled cells are washed out. Labeled cells are later retrieved by removing the column from the magnetic field and flushing.

Table 8: Materials needed for magnetic cell separation.

Reagent / Buffer / Material	Manufacturer
PBS/BSA/EDTA	
PBS/BSA + 2mM EDTA	Carl Roth
Anti-human CD45 microbeads	Miltenyi
Anti-human CD146 microbeads	Miltenyi
MACS separation column LS	Miltenyi
30µm cell strainer	Partec, Münster, Germany
MidiMACS Magnet	Miltenyi

Up to $2x10^8$ SVF cells were resuspended in 20ml PBS/BSA/EDTA. EDTA (Ethylenediaminetetraacetic acid) prevents cell aggregations and clogging of the MACS columns. Unlabeled SVF cells were first ran over four LS columns to remove adhesive dead cells and debris. SVF cells were then labeled with anti-CD45 and anti-CD146 magnetic microbeads (1:5) and incubated for 15 minutes at 4°C in the dark. After incubation, cells

were washed with PBS/BSA/EDTA and centrifuged at 490xg for 10 minutes at 4°C, and the pellet was re-suspended in 20mL PBS/BSA/EDTA. Labeled SVF cells were filtered through a cell strainer and applied onto four LS columns placed in a MidiMACS magnet. By extensive washing with PBS/BSA/EDTA, unlabeled cells were collected since AdSC are contained in the $CD45^-$ $CD146^-$ flow through. After three washing steps, LS columns were removed from the magnet and flushed with 5ml PBS/BSA/EDTA using a plunger.

The cell number of both fractions was determined and aliquots of $1x10^5$ cells were then stained to assess purity by flow cytometry. The collected $CD45^-$ $CD146^-$ cells, mainly containing AdSC (Fig. 8), were cultured under MScult and ECcult, or RNA was isolated for expression analysis.

The MACS-enrichment method was chosen when AdSC only were cultured for further analyses.

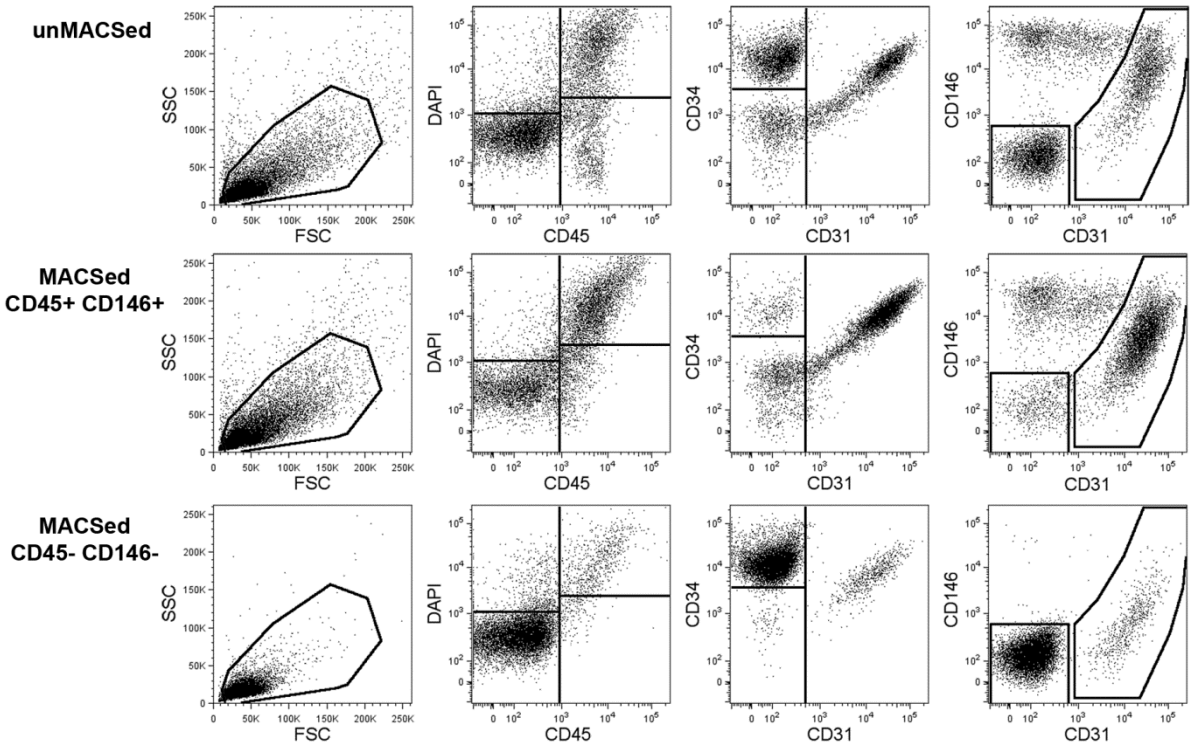

Figure 8: MACS-enrichment of AdSC *ex vivo*.
Freshly isolated SVF cells were labeled with anti-CD45 and anti-CD146 magnetic microbeads, and subjected to MACS. $CD45^-$ $CD146^-$ cells contained mainly AdSC (90% purity).

3.10. Kinetic analyses

For kinetic analysis, *ex vivo* bulk SVF cells were seeded under the indicated culture condition at a cell density of $1x10^5$ cells/cm^2; sorted subsets at densities ranging from $1\text{-}4x10^3$ cells/cm^2; MACSed cells at densities up to $1x10^5$ cells/cm^2. Medium was replaced after 24 hours and three times a week. At indicated time points, cells were photographed, detached, counted, and prepared for flow cytometrical analyses (see Materials & Methods 3.6.). Cellular diameters were recorded using a Casy cell counter as described above.

3.11. RNA isolation

Total RNA was isolated using a NucleoSpin II kit according to manufacturer's protocol (Macherey&Nagel, Düren, Germany). Briefly, $1–5x10^6$ cells were centrifuged at 490xg for 10 minutes at 4°C, the supernatant was removed and the pellet was resuspended and mixed in 350µL RA1 lysis buffer supplemented with 2% reducing agent β-mercaptoethanol. Cell lysates were stored at -80°C or directly processed. The cell lysates were homogenized using special filter columns. The homogenized lysate was mixed and 350µl of 70% ethanol were added to precipitate nucleic acids which were then applied on an isolation column with a membrane affine to nucleic acids under high salt conditions. After treatment with DNase to digest genomic DNA and repeated washing, the RNA was eluted from the filter with 100µl dH_2O.

RNA concentration was determined using a Nanodrop photometer (Thermo Scientific). Nucleic acids absorb ultraviolet light with maximum absorption at 260nm (OD260) due to the heterocyclic rings of the organic bases. The absorption wavelength of proteins is at 280nm (OD280) due to aromatic amino acids. The concentration of nucleic acids and proteins is proportional to the optical density at 260nm and 280nm (OD260 and OD280), respectively. Hence, the purity of RNA is expressed as the ratio of OD260/OD280 and should be below 1.8.

For measurement, the Nanodrop was first calibrated with dH_2O, and then RNA-concentrations of 1.5µL sample were measured.

3.12. Reverse Transcription

To quantify RNA expression using real-time PCR, the RNA was first reverse transcribed into complementary DNA (cDNA) using reverse transcriptase. RNA is easily degraded by

ubiquitous RNases, therefore the more stable cDNA is used for later PCRs. Reverse Transcriptase is an RNA-dependent DNA polymerase isolated from different retroviruses that use this enzyme to integrate the RNA genomes into the host's DNA genome.

For reverse transcription using TaqMan Reverse Transcription Reagents (Applied Biosystems, Life Technologies, CA, USA), 1µg of RNA was reverse transcribed into cDNA according to manufacturer's instruction. The reaction was performed in a thermo cycler using the following one-cycle program: (1) 95°C for 5', (2) 25°C for 10', (3) 48°C for 40", (4) 95°C for 5', (6) 4°C for indefinite time.

3.13. Quantitative PCR

Real-time PCR allows for continuous monitoring of DNA amplification by fluorescent dyes like TaqMan probes or SYBR green. SYBR green intercalates with double stranded DNA (dsDNA) and emits light upon excitation. Hence, the intensity of emitted light positively correlates with amount of dsDNA. Background detection is avoided by setting a threshold as three-fold standard deviation of measured fluorescence values within early cycles. The cycle, when the fluorescence exceeds this threshold, is called the cycle threshold (C_T). Quantification data can be calculated as absolute copy numbers or as relative expression normalized to a housekeeping gene.

Primers were designed using Primer Blast (www.ncbi.nlm.nih.gov/tools/primer-blast/; see Table 9). β-Actin or hypoxanthine phosphoribosyltransferase (HPRT) served as housekeeping genes. Real time-PCR was performed using RealMasterMix SYBR ROX kit according to manufacturer's instructions (5Prime, Hamburg, Germany). Forward and reverse primers were used at 500nM concentration. The measurements were done in triplicates, and were performed using Eppendorf epRealplex 2 Mastercycler with the following program: (1) 95°C for 5', (2) 95°C for 15", (3) annealing temperature (T_M, Table 17) for 30" and (4) 72°C for 30-45". The steps (2) to (4) were repeated for 40 cycles.

Relative quantification was calculated as ΔC_T to correlate expression of the gene of interest to the house-keeping gene:

$$Relative\ Expression = 2^{(C_{T\ Housekeeping\ Gene} - C_{T\ Target\ Gene})}$$

Table 9: Primer sequences.

Gene	Forward	Reverse	T_M
β-Actin	GACAGGATGCAGAAGGAGATCACT	TGATCCACATCTGCTGGAAGGT	64
HPRT	ATCAGACTGAAGAGCTATTGTAATGACCA	TGGCTTATATCCAACACTTCGTG	61
CD34	TGAAGCCTAGCCTGTCACCT	CGCACAGCTGGAGGTCTTAT	60
CD105	CAGCAGTGTCTTCCTGCATC	AGTTCCACCTTCACCGTCAC	60
CD146	CAACAGCACCTCCACAGAGA	GTGATCTCCTGCTTCCCTGA	60
CD271	GTATTCCGACGAGGCCAAC	CGTGCTGGCTATGAGGTCTT	60
ACTA2	ACGGCCCTAGCACCCAGCACCA	CAGAGAGGCCAGGATGGAGCCACCG	64
CDH2	GACAATGCCCCTCAAGTGTT	CCATTAAGCCGAGTGATGGT	60
CXCL12	CTACAGATGCCCATGCCGAT	GTGGGTCTAGCGGAAAGTCC	60
CXCR4	CAGCAGGTAGCAAAGTGACG	GCCCATTTCCTCGGTGTAGT	60
DKK1	TTGACAACTACCAGCCGTACC	TGGAATACCCATCCAAGGTGC	60
FGF1	CAGCCCTGACCGAGAAGTTT	ATAAAAGCCCGTCGGTGTCC	60
FGF2	GCTGTACTGCAAAAACGGGG	AGCCAGGTAACGGTTAGCAC	60
FGF5	AAGGAAGTGGCTTGGAGCAG	GCAGTCATCTGTGAACTTGGC	60
FOXD1	GACTCTGCACCAAGGGACTG	CCGAACCACCAAGACGAGAA	60
FOXM1	TGCCAACCGCTACTTGACAT	TCACCGGGAACTGGATAGGT	60
FOXO1A	CAAGAGCGTGCCCTACTTCA	CTGGAAAGGCTCTGGAGTCG	60
FSP1	GCTGCCCAGCTTCTTGGGGAAAAGG	TGGCGATGCAGGACAGGAAGACACA	62
GATA6	GAGCGCTGTTTGTTTAGGGC	CTGGAAAGGCTCTGGAGTCG	60
GDF10	AGGTGGACTTCGCAGACATC	AGGACCCCAAGGGAGTTCAT	60
GREM1	CACGCGTCGAAAGCGCAG	AGGGCTCCCACCGTGTAG	60
GREM2	GACCAAACTTAGACCCCGCT	CCTTGTAAGGCGAGGGGATG	60
PODXL	CCCCACAGCAGCATCAACTA	CACTTATCTTGGGCCGGGTT	60
REX1	TTACGTTTGGGAGGAGGTGG	CAGCTCAGCGATGGTTAGGT	60
SNAI1	CTGCTGCTGAGCTGAATGAC	GGACAGAGTCCCAGATGAGC	60
SNAI2	CCTTCCTGGTCAAGAAGCAT	ATCCGGAAAGAGGAGAGAGG	60
SOX17	TGTAGACCAGACCGCGACAG	CTGGTCGTCACTGGCGTATC	60

3.14. Microarray

Microarray is a fast and reliable tool for whole transcriptome analysis (Fig. 9). RNA of samples to be compared is fluorescently labeled and hybridized to small, specific nucleotide probes spotted on a glass slide. Laser excitation and fluorescence detection are used to identify genes expressed in the samples and to compare up- and downregulation between samples.

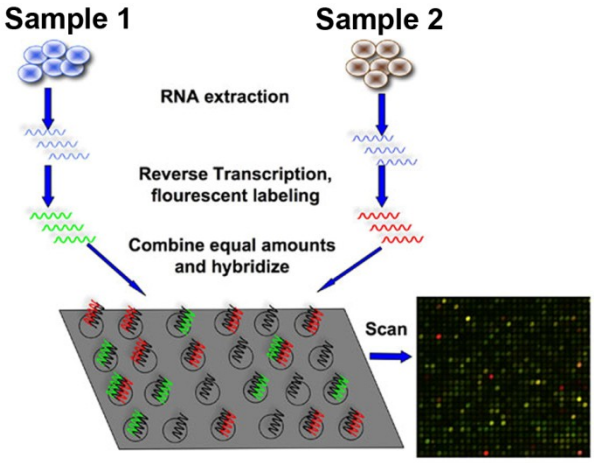

Figure 9: Principle of microarray experiment preparation. (www.bitesizebio.com)

Table 10: Materials needed for microarray experiments.

Reagent / Buffer / Material	Manufacturer
Whole Human Genome Microarray 44K	Agilent, Santa Clara, CA, USA
Quick Amp Labeling Kit, two color Plus	Agilent
Hybridization Gasket Slide Kit	Agilent
RNA Spike In Kit 2-color	Agilent
Gene Expression Hybridization Kit	Agilent
Gene Expression Wash Buffer Kit	Agilent
Stabilization & Drying Solution	Agilent

Ex vivo sorted $CD271^+$ and $CD271^-$ AdSC were cultured under MScult and RNA was isolated at d0 (after sorting) and at day 14 (at confluence) to perform microarray analysis. RNA labeling, hybridization and primary data analysis was performed in collaboration with AG Lauster (Technical University, Berlin) and kind support by AG Mollenkopf (Max-Planck-Institute for Infections Biology, Berlin).

For two-color ratio hybridization, RNA was labeled using the Quick Amp Labeling Kit according to manufacturer's instructions. 500ng of total RNA (extracted as described above) was first transcribed with oligo(dT)-T7 promoter primers using Moloney murine leukemia virus-Reverse Transcriptase (MMLV-RT) to synthesize cDNA. The fluorescent antisense strand of cRNA was then synthesized with T7 RNA polymerase, to incorporate either Cyanin 3 (Cy3)-cytidine-5´-triphosphate (3-CTP) or Cyanine 5 (Cy5)-5'-CTP (5-CTP). *Ex vivo* AdSC were Cy5-labeled, day 14 AdSC were Cy3 labeled and these pairs ($CD271^+$ and $CD271^-$) were co-hybridized on two chambers. The purified products were quantified by absorbance at 552nm for Cy3 and 650nm for Cy5. Labeling efficiency was determined using a Nanodrop

photometer. Prior to hybridization, labeled cRNA products were fragmented and mixed with control RNA using the RNA Spike In kit in hybridization buffer. Samples were hybridized to Whole Human Genome Microarray 44K for about 19hrs at 60°C overnight. The slides were washed according to the manufacturer´s protocol. Microarrays were scanned with 5-µm resolution using a DNA microarray laser scanner (Agilent Technologies). After measurement, the ratio of expected versus observed spiked-in RNAs serve as internal control for data quality. Fluorescent signals were evaluated with an image analysis tool version A 6.1.1 (Agilent Technologies) using default settings. Data analysis was conducted on the Rosetta informatics Platform Resolver Built 4.0. Results were exported as excel file for further analysis.

3.15. Gene Set Enrichment Analysis

To compare gene expression patterns yielded by microarray analysis with annotated gene sets describing regulation of gene expression during different cellular physiological processes, we conducted Gene Set Enrichment Analysis (GSEA). To this end, the expression data was prepared as a list of genes, annotated with gene symbol as identifier. Genes with a detection p-value above 0.005), a fold change less than two-fold (>2 or <-2) and fluorescence intensity values below 500 were excluded from analysis. Since we were interested in gene regulations that are common to both AdSC subsets, we further excluded genes that were differentially regulated between the two subsets. Thereby, gene list was reduced to 5971 genes (Fig. 10).

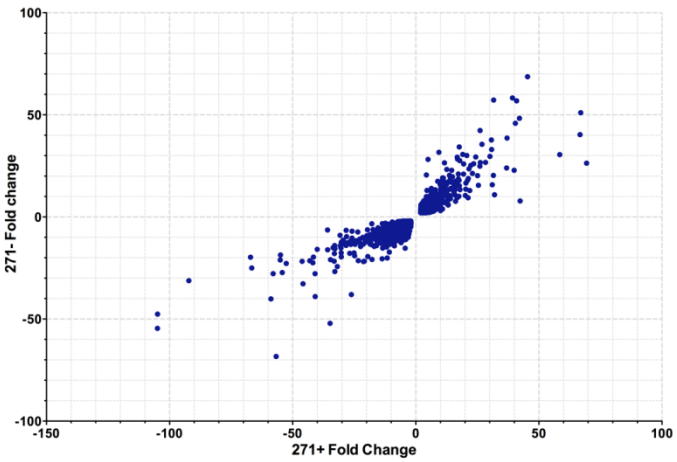

Figure 10: Expression matrix for GSEA analysis.
For GSEA, a gene list was prepared containing genes with a sufficient detection quality and fold change and similar regulation in $CD271^-$ and $CD271^+$ AdSC.

The GSEA software v.2.0 (www.broadinsitute.org/gsea; provided by the Broad Institute, Boston, MA, USA) ranks the genes in this gene list according to differences in expression intensities, i.e. ranging from highest expression at day 0 to highest expression at day 14. This is depicted at the bottom of the GSEA enrichment plot: the y-axis denotes the

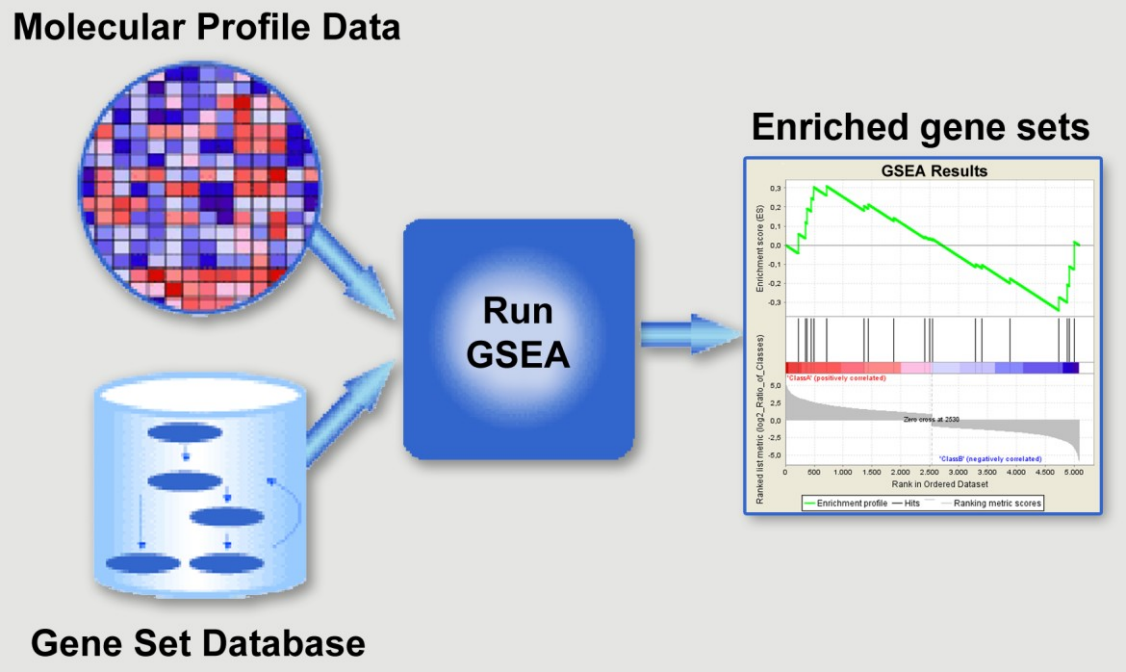

Figure 11: Workflow of Gene Set Enrichment Analysis with exemplary result.
(modified from www. broadinstitute.org/gsea)

expression differences between compared samples; the x-axis depicts the ranked order in our gene list (Fig. 11).

Next, selected gene sets from the database MSigDB (www.broadinstitute.org/gsea/msigdb) are matched and "aligned" to the ranked gene list, as shown in the middle scheme of the enrichment plot. The red-to-blue shaded bar illustrates expression intensities; the black bars indicate the position of genes from the gene set in the ranked gene list.

Based on this distribution, the enrichment score (ES) is calculated as depicted as the green line in the upper diagram of the enrichment plot. Whenever a gene from the gene set is found, the enrichment score is increasing; when no gene is found, the ES is decreasing. Finally, gene sets enriched at day 0 will have an ES above 0, and gene sets enriched at day 14 will have an ES below 0.

GSEA analysis was performed according to the following parameters: Permutation type: "gene_set"; enrichment statistic: "weighted_p2"; Metric for ranking genes: "log2_Ratio_of_Classes"; Gene list sorting mode: "real"; Max size of gene sets: "500"; Min size of gene sets: "15"; Collapsing mode for probe sets: "Median_of_probes"; Normalization mode: "mean_div"; Randomization mode: "equalize_and_balance"; Seed for permutation: "timestamp".

4. Results

The results comprise

1) Characterization of SVF cell-derived AT-MSC,

2) Isolation and characterization of AT-MSC progenitors,

3) Kinetic analysis of the MSC derivation phase of bulk SVF cells and sorted AT-MSC progenitors under two different culture conditions, and

4) Transcription analysis of *ex vivo* AT-MSC progenitors compared to cultured AT-MSC.

4.1. Characterization of Adipose Tissue-derived Mesenchymal Stromal Cells

To verify isolated and expanded SVF cells as MSC, cells were characterized according to the minimal criteria defined by the ISCT (International Society for Cellular Therapy) **(Dominici, 2006)**.

4.1.1. Long-term culture of AT-MSCs

To determine the long-term proliferative capacity, SVF cells from 7 donors were cultured for long term (up to 160 days, i.e. 16 passages; Fig. 12). In all preparations, we observed approx. 1.5 population doublings per passage that remained constant throughout culture. Also, the time required for a population doubling remained constant at about 8.5 days/population doubling. Differences in initial cell numbers (passage 1) correlated to differences in cell yields at later time points.

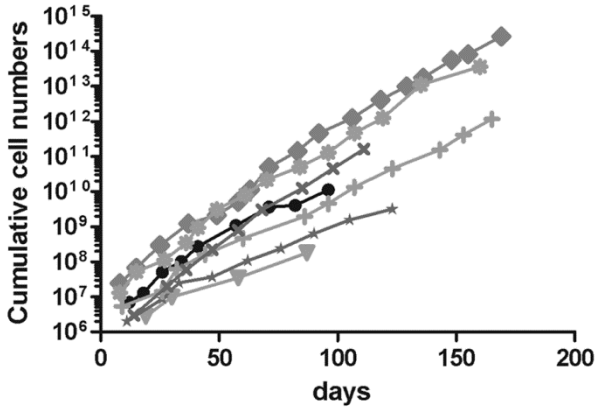

Figure 12: Long-term culture of AT-MSC.
Cumulative cell numbers during long term culture starting with passage 1 (n=7). Cells were counted at each passage.

Isolated SVF cells were capable of plastic-adherent proliferation and long-term expansion, and hence fulfilled the first essential characteristic of AT-MSC.

4.1.2. Differentiation of AT-MSCs

To assess the differentiation potential of our cell preparations, expanded SVF cells in passage 2 were differentiated towards the adipogenic, osteogenic and chondrogenic lineage (Fig. 13). In all preparations, lipid-containing vesicles or calcium depositions were detected after 21 days of adipogenic or osteogenic induction, by Oil Red or Alizarin Red staining, respectively. In comparison to BM-MSC (not shown), chondrogenic differentiation was less efficient, with only weakly Alcian Blue-stained micropellets.

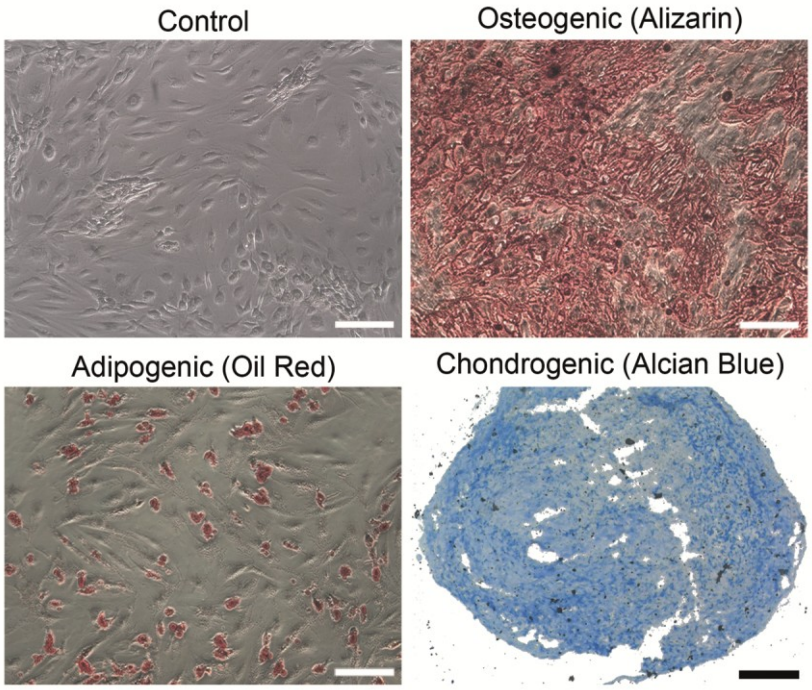

Figure 13: Differentiation of AT-MSC in passage 2.
AT-MSC in passage 2 were differentiated towards the osteogenic, adipogenic and chondrogenic lineage, and stained with Alizarin Red, Oil Red, and Alcian Blue, respectively. Undifferentiated cells cultured for 3 weeks served as control (control cells shown without staining). Magnification 100x; scale bar: 200µm. Representative images out of 7 individual experiments are shown.

According to these results, expanded SVF cells exhibited multipotent differentiation capacity, as required by the MSC minimal criteria.

4.1.3. Immunophenotyping of AT-MSC

To control for expression of MSC-typical surface markers, expanded SVF cells in passage 2 were analyzed. Flow cytometry results revealed the absence of CD14, CD34 and CD45 and presence of CD73, CD90 and CD105 (Fig. 14). Furthermore, AT-MSC in passage 2 were $CD146^-$ and partially $CD271^+$ (approx. 30%).

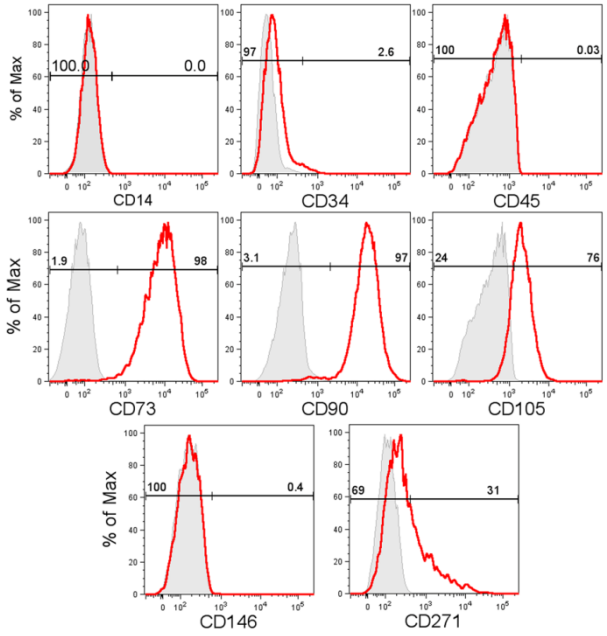

Figure 14: Immunophenotype of AT-MSC in passage 2.
AT-MSC in passage 2 were stained for indicated markers (red line), and compared to unstained control cells (grey area).

These initial results demonstrate that the isolated SVF cells give rise to *bona fide* AT-MSC defined as plastic-adherent growing cells with multipotent differentiation capacity and the specific immunophenotype, as defined by the ISCT **(Dominici, 2006)**.

4.2. Characterization and isolation of different SVF cell subsets

To identify potential AT-MSC progenitors, SVF subsets were characterized by flow cytometry. The SVF subsets that resulted from this initial phenotyping were FACS-sorted or MACS-enriched for analysis of separate culture.

4.2.1. Immunophenotypical characterization of SVF cells *ex vivo*

To dissect different subsets within the SVF, expression of surface markers CD45, CD31, CD34, CD105, CD146 and CD271 was determined on *ex vivo* SVF cells using flow cytometry.

Around 18% of $CD45^+$ hematopoietic cells were detected (Fig. 15A, D). Within the $CD45^-$ stromal vascular cells, around 50% were $CD34^+CD31^-$cells, 22% were $CD34^+CD31^+$ cells and 17% were $CD34^-CD31^-$ cells (Fig. 15B, D). Based on a recent report by Zimmerlin et al., we termed these subsets as Adventitial Stromal Cells (AdSC), Endothelial Cells (EC) and Pericytes (PC), respectively. These populations were characterized further for CD105, CD146 and CD271 expression. EC were $CD146^+$ and $CD105^{low}$. PC were $CD105^-$, $CD146^{high}$ and by around 50% $CD271^+$. AdSC were $CD105^-$, $CD146^-$ but by 30% $CD271^+$ (Fig. 15C).

SVF subset frequencies of different donors varied only marginally, especially in the frequencies of $CD45^+$, $CD45^-$ and AdSC (Fig. 15D, Table 11). For separate culture and subsequent analysis, we FACS-sorted or MACS-enriched these SVF subsets (see section 3.9. and 3.10.).

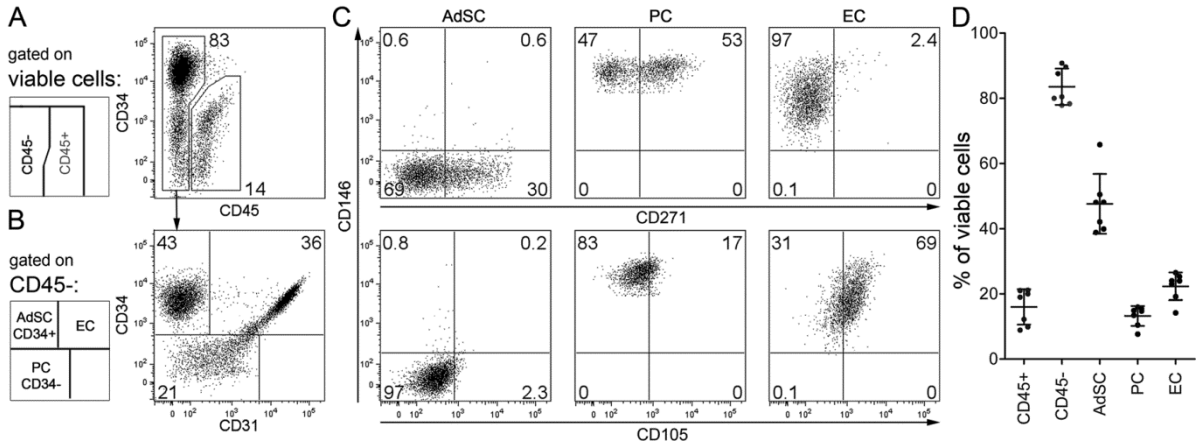

Figure 15: Immunophenotypic characterization of *ex vivo* SVF cells.
Ex vivo SVF cells were analyzed by flow cytometry for CD45, CD31, CD34, CD105, CD146, and CD271 expression. Gating strategy (see schemes): A) viable *ex vivo* SVF cells were separated into $CD45^+$ and $CD45^-$. B) Three subsets were identified within $CD45^-$ cells: adventitial stromal cells (AdSC, $CD34^+CD31^-$), pericytes (PC, $CD34^-CD31^-$), and endothelial cells (EC, $CD34^+CD31^+$). C) AdSC, PC, and EC were further analyzed for CD146, CD271 (upper row), and CD105 expression (lower row). (D) Summary of SVF subset frequencies in different donors [n=7; plots shown are Mean ± standard deviation (SD)].

Table 11: Adipose tissue-derived SVF subset frequencies in different donors.

Patient No	Gender	Age	Donor Site	Subset frequencies (%)				
				CD45+	CD45-	AdSC	PC	EC
A22	m	30	mas	12,20	87,60	75,10	8,73	26,40
A20	m	30	abd	8,91	90,80	55,60	16,20	28,36
A26	f	49	abd	9,86	89,60	53,70	17,80	33,10
A27	f	38	abd, hip	21,10	77,90	61,70	13,40	16,20
A29	f	29	abd, hip, thg	19,00	80,50	52,30	18,50	28,30
A30	f	40	thg	8,20	90,70	45,40	15,20	24,60
A31	f	27	thg	21,00	78,30	49,60	19,70	28,60
Mean				14,32	85,06	56,20	15,65	26,51
StDEV				5,83	5,91	9,74	3,71	5,23

Abbreviations: gender: m, male; f, female. Anatomical donor sites: mas, gynaecomastia; abd, abdomen; thg, thigh

According to these results consisted the $CD45^-$ stromal vascular cells of three distinct subsets, namely AdSC, PC and EC.

4.2.2. Long-term culture of sorted SVF subsets

To functionally compare the long-term proliferative capacity of putative MSC progenitors, FACS-sorted subsets were cultured separately (see Materials & Methods 3.8.). Direct *ex vivo* culture was performed either under MScult or ECcult. Following the first passage, cells were further cultured under MScult. Notably, during early culture under MScult, PC and EC rarely developed into proliferating fibroblastoid cells. Therefore, only ECcult-cultured PC and EC will be shown in the following analyses.

Cell numbers determined during long-term expansion revealed that AdSC proliferated steadily to passage 8 (day 111; Fig. 16) and proliferation rates were independent of CD271 expression. Cell counts of unsorted SVF cells as well as PC and EC cultures dropped at day 14, suggesting reduced proliferation during early culture compared to AdSC. After passaging, proliferation rates of unsorted SVF cells and PC were similar to AdSC. Cell numbers of EC decreased constantly and culture was ceased after the 2^{nd} passage.

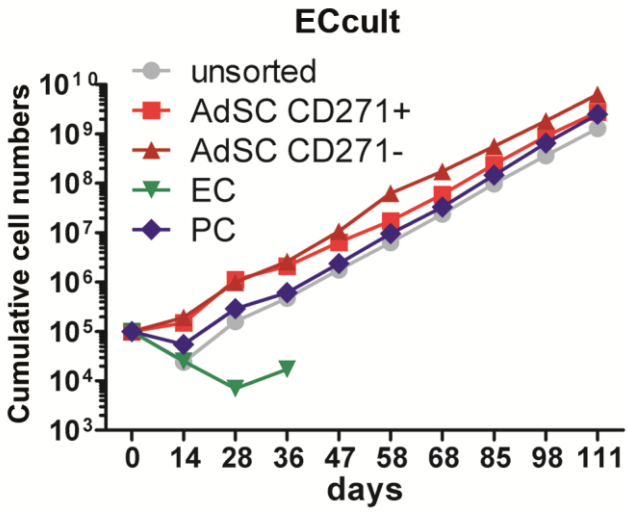

Figure 16: Long term expansion of sorted SVF cell subsets.
Ex vivo FACS-sorted SVF cell subsets and unsorted SVF cells were ECcult-cultured during early culture and after passaging, MScult-cultured until final passage 8 (n=1).

We conclude that both, AdSC and PC are AT-MSC progenitors with similar proliferation rates during long-term culture. Differences in the proliferation of AdSC and PC during early culture further attracted our interest (see section 4.3.1.).

4.2.3. Differentiation of AT-MSC derived from sorted AdSC and PC

To further verify AdSC and PC as AT-MSC progenitors, the differentiation potential of sorted SVF subsets was assessed. Sorted MScult- or ECcult-cultured AdSC and ECcult-cultured PC were expanded under MScult until passage 2 and differentiated towards the adipogenic and osteogenic lineage. EC were not included due to insufficient cell numbers in passage 2. Differentiation was evaluated by Alizarin Red staining for extracellular calcium depositions and by Oil Red and Nile Red staining for lipid vesicles. Differentiation results were compared to AT-MSC derived from unsorted SVF cells of the same donor (Fig. 17).

AdSC and PC successfully differentiated towards the osteogenic and adipogenic lineage. We observed only marginal differences in the osteogenic potential, with differentiated PC exhibiting the strongest Alizarin Red staining. Adipogenic differentiation appeared to be minimally enhanced in ECcult-cultured AdSC, whereas MScult-cultured AdSC exhibited less intracellular lipid vesicles as determined by Nile Red staining (Fig. 17b).

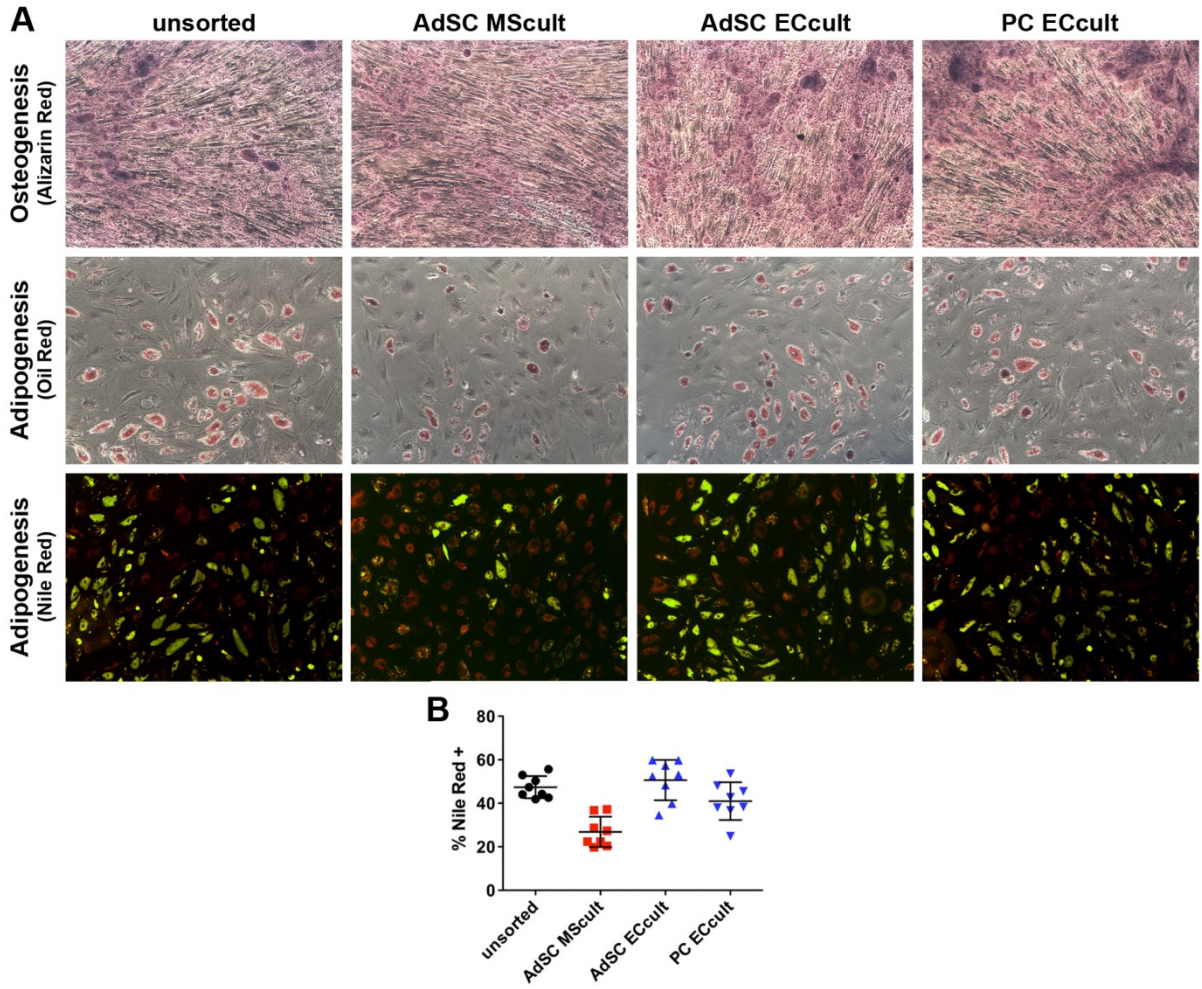

Figure 17: Differentiation of sorted SVF subsets.
A) Unsorted SVF cells and MScult- or ECcult-cultured AdSC or PC were differentiated in passage 2 and stained with Alizarin Red, Oil Red and Nile Red. B) Adipogenesis was quantified by counting Nile Red^{+} cells. Magnification: 100x. One representative result out of three experiments is shown.

In summary, these results demonstrate that both, AdSC and PC give rise to multipotent AT-MSC with long-term proliferative capacity and similar differentiation potential. Interestingly, MSC derivation from PC was restricted to ECcult and less efficient when compared to AdSC.

4.3. Analysis of the derivation phase of AT-MSC

To understand how MSC progenitors adapt to *in vitro* conditions, we next analyzed how bulk SVF cells and sorted AT-MSC progenitors behave during the MSC derivation phase concerning proliferation, morphology and cell size as well as immunophenotype.

4.3.1. Proliferation of bulk and sorted SVF cells

To monitor proliferation of bulk SVF cells during MSC derivation, *ex vivo* cells were seeded at a density of $1x10^5$ cells/cm^2 under the two different culture conditions, MScult and ECcult, and cultured until confluence. At indicated time points, adherent cells were detached for determination of cell counts using Casy Cell counter. Cell numbers are presented as cell densities, i.e. normalized to the harvested culture area.

In MScult-cultures, cell densities decreased to approx. 7-10% of seeded cells ($0.7\text{-}1x10^4$ cells/cm^2) at day 2 and then further to 5-7% at day 4 (Fig. 18A). This decrease was followed by a steady increase to confluence (10-20% of initial cell numbers) at day 8-11 (end of initial culture). In ECcult, cell densities similarly decreased to 10% at d2, then remained constant and after day 6 increased to 100% of seeded cells at day 8. Notably, ECcult-cultured cells proliferated more rapidly than under MScult.

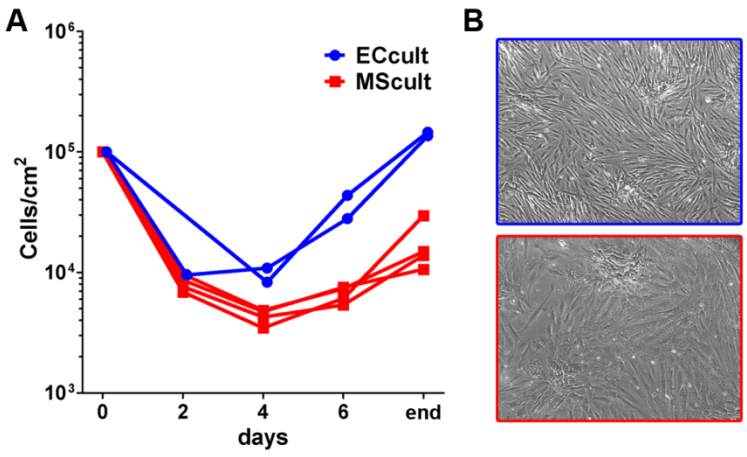

Figure 18: Cell count kinetic during MSC derivation of unsorted SVF cells.
A) *Ex vivo* SVF cells were MScult- (n=4) or ECcult-cultured (n=2) and cell counts were recorded at indicated time points of early culture ("end" denotes end of early culture at day 8 to day 11). B) At confluence, cultures were photographed to compare morphologies (magnification 100x).

Similar to unsorted bulk cultures, cell densities of *ex vivo* sorted AdSC, PC and EC were monitored in MScult- and ECcult-cultures. Due to differences in cell numbers yielded from

FACS-sorting, the subsets were seeded at varying cell densities. Therefore, cell numbers were normalized to 1,000 seeded cells/cm^2.

Under MScult, cell numbers initially reduced to about 30% of seeded cells (Fig. 19A); in detail, we retrieved 27±18% of AdSC, 29±29% of PC and 19±19% of EC. After day 8, AdSC proliferated up to 130% of seeded cells at confluence, whereas PC and EC cell numbers remained constant throughout culture at 33% and 14%, respectively. This confirms the observation of impeded PC proliferation under MScult (Fig. 16).

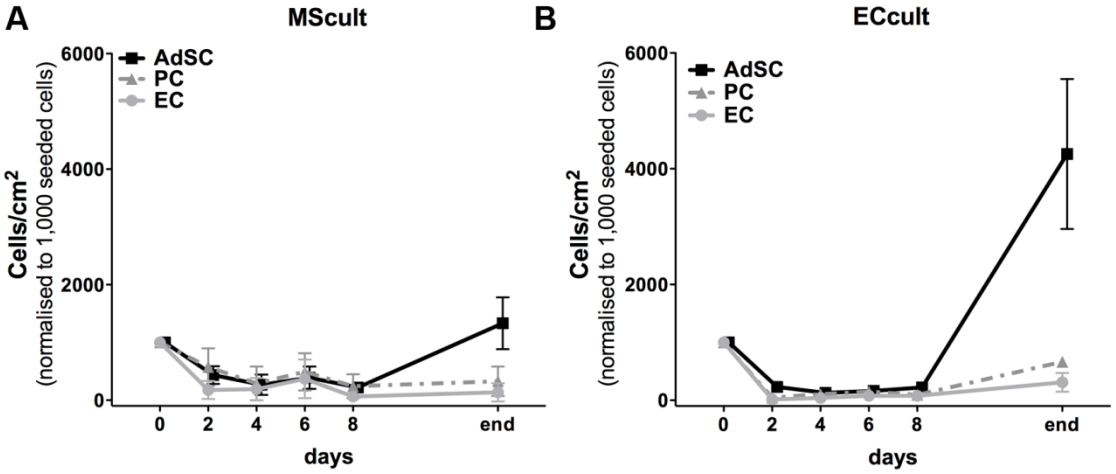

Figure 19: Cell count kinetic during MSC derivation of sorted SVF cell subsets.
Cell counts of sorted AdSC, PC and EC were recorded at indicated time points of early culture under MScult (A, n=5) or ECcult (B, n=3). “End” denotes end of early culture at day 11 or day 14.

Under ECcult, cell numbers initially decreased to 23% for AdSC, 4.6% for PC and 13.7% for EC at day 2. Thereafter, cell numbers remained constant until day 8, and AdSC increased to 426±183% at day 14 (Fig. 19B). Further, we observed proliferation of PC to 66±10% and of EC to 31±22%.

We defined *ex vivo* cultures as confluent, when cell densities of about 80% were reached. At confluence, ECcult cultures reached much higher cell numbers compared to MScult for bulk (100% versus 20% of seeded cells, respectively) and sorted subsets cultures (420% versus 130%, respectively). This was not only related to accelerated proliferation under ECcult, but also an altered morphology. ECcult-cultures exhibited a quite homogeneous monolayer of slim, spindle-shaped cells (Fig. 18B), whereas larger and more flattened-out cells were observed in MScult-cultures.

In summary, AdSC proliferated faster than PC, particularly under MScult. Therefore, we propose that predominantly AdSC contribute to MSC derivation from bulk cultures and that AdSC are the more clonogenic SVF cell subset. Finally, the overall behavior of cell numbers during the MSC derivation phase of SVF cells implies that (1) cells able to attach to TCPS are selected until day 4, and (2) these selected cells proliferate until confluence.

4.3.2. Changes in morphology and cell size

We have observed differences in cell morphology between culture conditions (Fig. 18B). To now follow how morphologies change during early culture, we monitored cell morphologies and cell diameters using microphotographs, Casy cell size data and FACS.

Photomicrographs revealed that, in bulk MScult-cultures, small round-shaped cells observed at day 2 and day 4 developed into larger spindle-shaped cells by day 6 and then proliferated to confluence (day 11, Fig. 20A). Under ECcult, cultures at day 2 and day 4 similarly consisted of small round-shaped cells, but in addition, some small cells with cobblestone morphology in tight colony formation were detectable as early as day 2 (Fig. 20B). Similar to MScult-cultures, small round-shaped cells were replaced by larger fibroblastoid cells beginning at day 4. Cells in cobblestone colonies also proliferated but disappeared until confluence.

According to Casy cell size data, cell diameters at day 0 were <15µm (Fig. 20C). At day 4, cells with diameters >15µm were observed under both conditions, which dominated the cultures until day 8. This development was identical in different preparations and also in ECcult-cultures (Fig. 20D). Using the MFI of FSC to measure cell size in flow cytometry, an increase in MFI of FSC was similarly observed, but in MScult-cultures to higher final values (Fig. 20F). Thus, differences in cell morphology and size were observed when the cultures reached confluence, as determined on photomicrographs (Fig. 20A+B), in the cell counting data (Fig. 20D+E) and flow cytometry data (Fig. 20F).

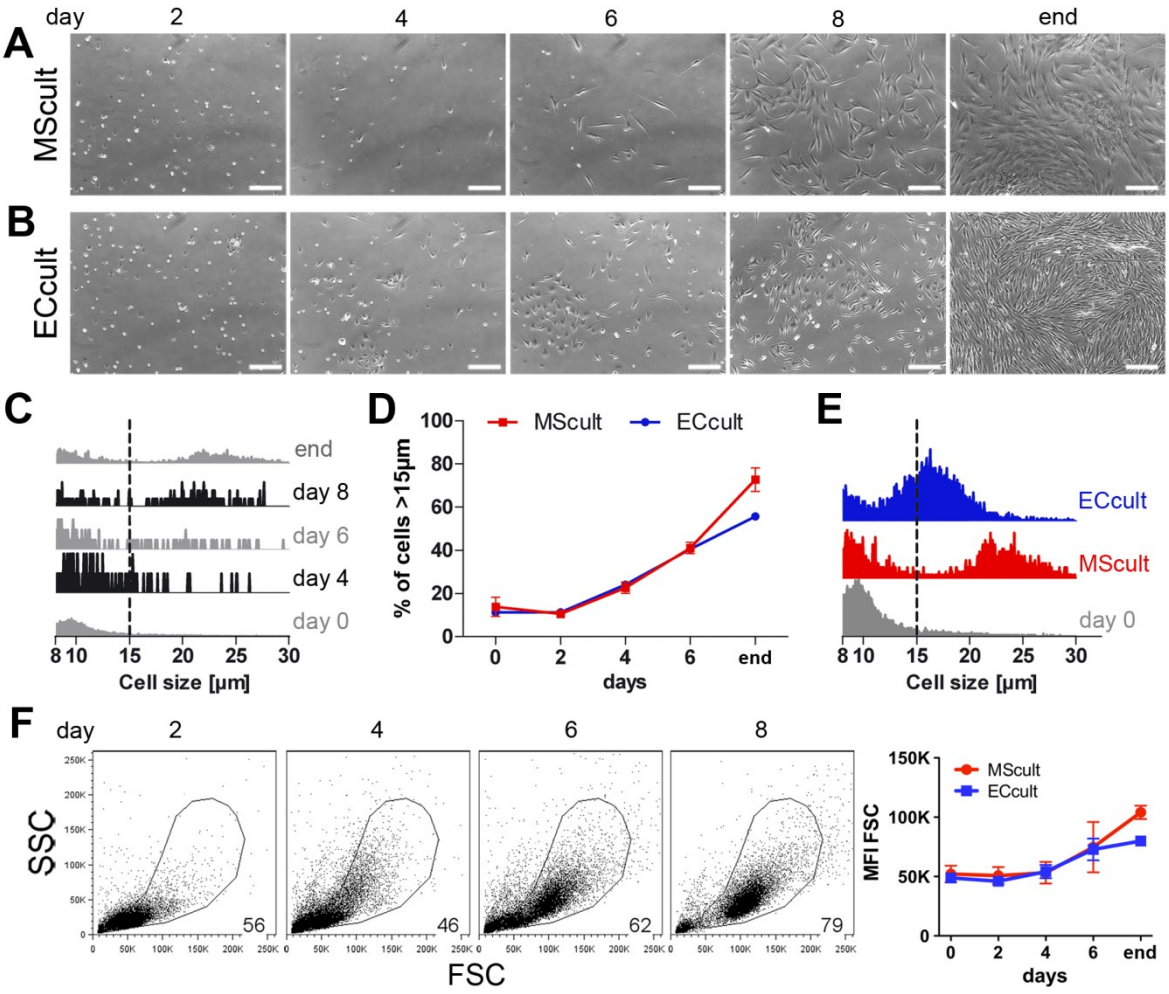

Figure 20: Morphological changes during MSC derivation of bulk cultures.
Photomicrographs of bulk cultures under MScult (A) and ECcult (B) at indicated time points reveal morphological changes (magnification: 100x; scale bar: 200µm). C) Cell diameters of detached cells in bulk cultures at indicated time points (as assessed by Casy cell counter). Dashed line at 15µm marks border between "small" and "big" diameter cells. D) Changes in percentage of "big" diameter cells under MScult (n=4) and ECcult (n=3). E) Differences in cell diameters at confluence of MScult and ECcult cultures compared to day 0. F) Scatter plots (FSC vs. SSC) at indicated time points and summarized as MFI of FSC for MScult (n=3) and ECcult (n=3).

Differences in morphologies of MScult- and ECcult-cultured sorted AdSC were also analyzed. An increase in cell size, as determined by flow cytometry, occurred already at day 6 (Fig. 21A). At confluence, cell sizes of MScult-cultured AdSC were bigger, not only of detached cells but also of attached cells in culture (Fig. 21B).

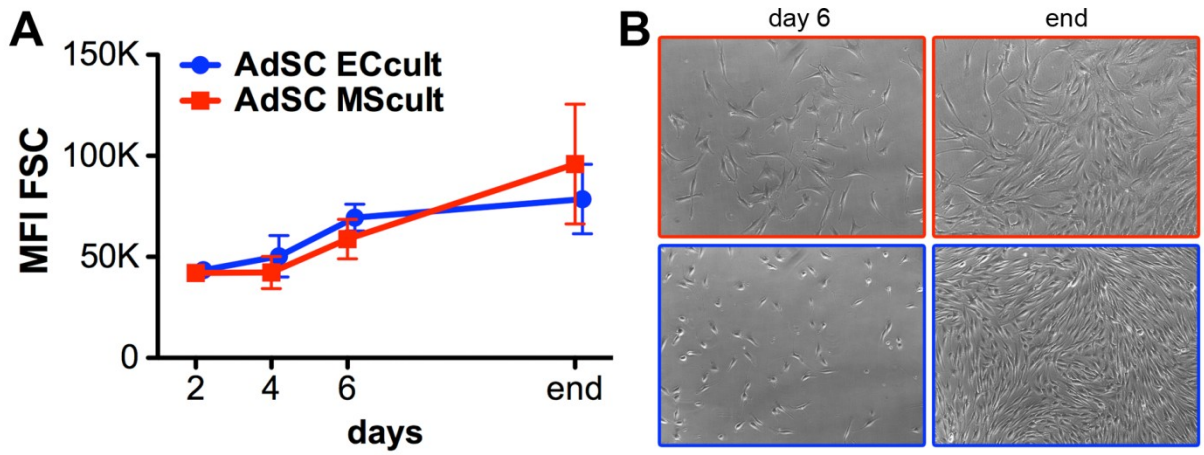

Figure 21: Changes in cell size of sorted AdSC during MSC derivation.
A) Diagram shows changes in MFI of FSC at indicated time points in AdSC cultured under MScult (n=3) and ECcult (n=2). B) Photomicrographs of AdSC under MScult and ECCult at day 6 and at confluence (magnification: 100x)

Confirming our cell count kinetic data, photomicrographs revealed a pronounced increase in cell numbers at day 8 under both culture conditions (Fig. 18+19). Cells with fibroblastoid morphologies and increased cell diameters appeared as early as day 4. The fibroblastoid cells in MScult-cultures were derived from AdSC; under ECcult, also PC may contribute to fibroblastoid colonies, yet to a lesser extent than AdSC. In ECcult-cultures, colonies with cobblestone morphology were observed and were most likely derived from EC.

4.3.3. Kinetic of bulk SVF cell phenotypes

To determine whether changes in surface marker expression occur during the early culture phase, bulk SVF cells were analyzed at indicated time points using the described multi-color flow cytometry analysis. Analysis focused (1) on $CD45^+$ cells, (2) on percentage of CD34 and CD31 expressing cells, and (3) comparison of CD146, CD271 and CD105 expression within these subsets over time.

Between day 0 and day 2, the decrease in $CD45^+$ cell frequencies indicated that the majority of blood cells were not able to adhere and removed by medium exchange (Fig. 22A). The amount of adhered lymphocytes further decreased during primary culture. Conversely, the $CD45^-$ stromal vascular cells increased in percentage and were analyzed further.

Within $CD45^-$ cells, percentages of $CD34^+CD31^-$ (AdSC), $CD34^-CD31^-$ (PC) and $CD34^+CD31^+$ (EC) were compared. At day 2, AdSC and PC frequencies were slightly increased compared to day 0 (Fig. 22B). In contrast, EC frequency decreased and this subset vanished over time. However, it has to be highlighted that $CD34^+CD31^+$ cells upregulated CD105 as early as day 2 (Fig. 22E), indicating activation of EC **(Nassiri, 2011)**.

Between day 4 and day 6, the percentage of $CD34^-CD31^-$ cells increased abruptly, together with a reduction of $CD34^+CD31^-$ cells. In line with previous reports showing CD34 downregulation of AT-MSC progenitors **(Suga, 2009)**, this process was rather due to CD34 downregulation by $CD34^+CD31^-$ AdSC, than proliferation of $CD34^-CD31^-$ PC.

The regulation of CD105, CD146 and CD271 may further support that CD34 downregulation by AdSC is the reason for the increase of the $CD34^-CD31^-$ subsets. To compare several experiments, we utilized the integrated MFI (iMFI) to weight the increase in MFI with the percentage of positive cells **(Darrah, 2007)**. An increase in cell number together with an actual upregulation (increase in MFI) will definitely result in a high iMFI value, whereas a few positive MFI^{high} cells will lead to a lower iMFI.

In $CD34^+CD31^-$, the percentage of $CD146^+$ and $CD105^+$ cells increased steadily starting (Fig. 22C). At day 8, only a few $CD34^+$ cells were detected, which were $CD105^+$ and to a lower extent also $CD146^+$ and $CD271^+$ cells. In $CD34^-CD31^-$ cells, a similar population of $CD105^+$ $CD146^+$ $CD271^+$ cells was detected as early as day 4 and superseded the previously present $CD105^-CD146^+CD271^{+/-}$ cells on day 6 (Fig. 22D).

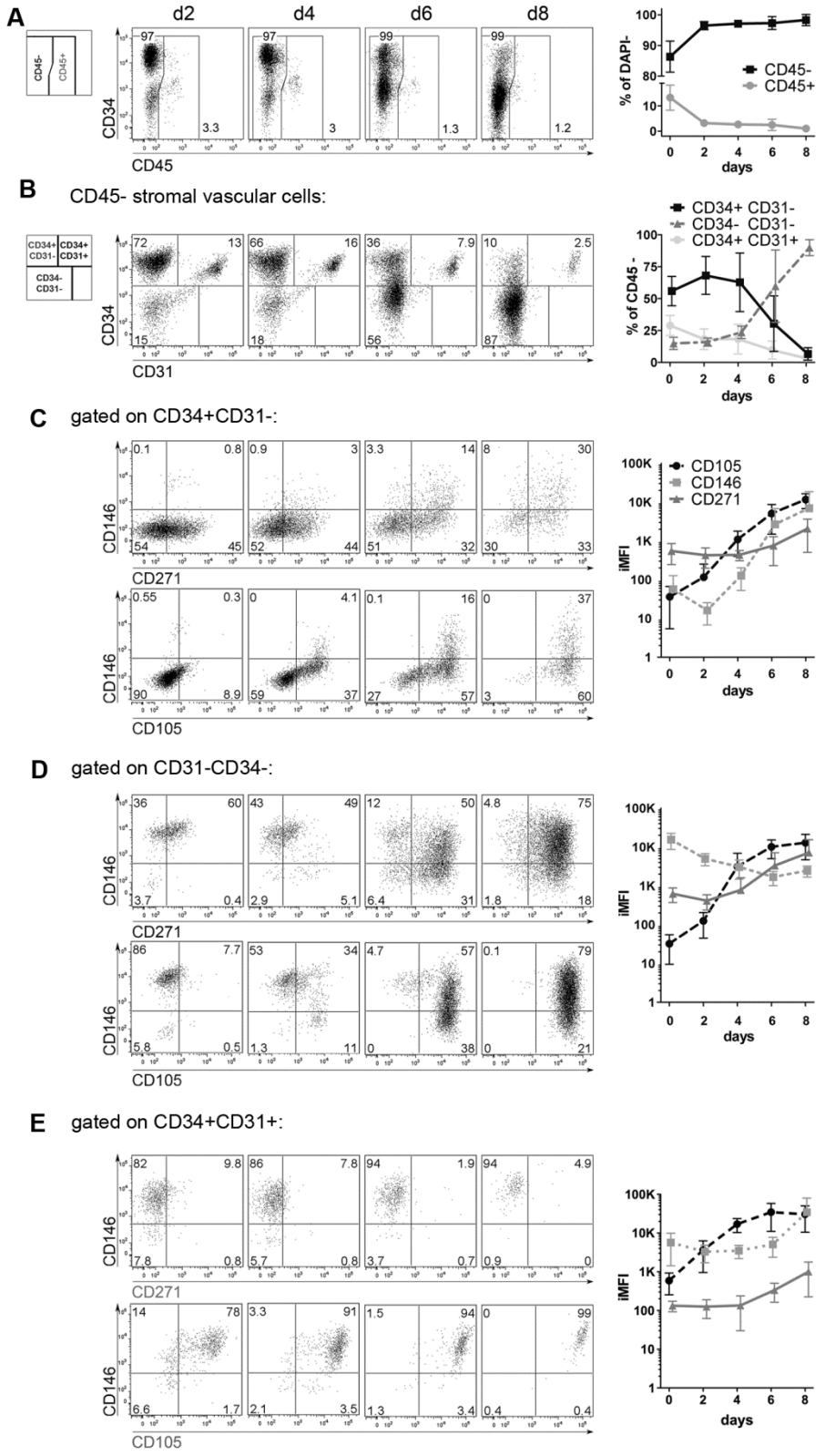

Figure 22: Immunophenotype kinetic of bulk cultures during MSC derivation.
SVF cells cultured under MScult were harvested at indicated time points and analyzed for surface marker expression by flow cytometry. One representative analysis and diagrams of kinetic experiments (d0–d8) are depicted (n = 4; mean ± SD). A) Changes in frequencies of $CD45^+$ and $CD45^-$ cells (see gating scheme). B) Changes in frequencies of $CD34^+CD31^-$, $CD34^-CD31^-$ and $CD34^+CD31^+$ cells within $CD45^-$ stromal vascular cells (see gating scheme). C, D, E) $CD34^+CD31^-$, $CD34^-CD31^-$ and $CD34^+CD31^+$ cells were further analyzed for CD146, CD271, and CD105 expression. Diagrams summarize the changes in integrated mean fluorescence intensity (iMFI).

These results provide no evidence for a contribution of PC to the final MSC population under MScult (Fig. 19A) implying that changes in marker expression during the early culture period of AdSC comprise (1) upregulation of CD105 and CD146 and (2) downregulation of CD34 by day 6 to day 8. Accordingly, AdSC eventually developed into $CD34^-$ $CD105^+$ $CD146^+$ $CD271^{+/-}$ cells.

4.3.4. Immunophenotype kinetic of sorted AdSC and PC

Changes in the immunophenotype of sorted AdSC and PC during MSC derivation were also analyzed. Sorted subsets were MScult- or ECcult-cultured and immunophenotypes were assessed at indicated time points. For a more comprehensive overview, results are depicted as histogram overlays.

CD34 expression gradually decreased after day 4 of culture which was highly reproducible in all analyzed donors (Fig. 23A). PC remained $CD34^-$ and $CD146^+$ throughout culture. Under both culture conditions, AdSC and PC upregulated CD105, as prominently detectable at day 6. CD146 upregulation by AdSC occurred by day 8 (Fig. 23B+C). Notably, although kinetics of CD146 upregulation by AdSC were similar in all conditions, the ratio of $CD146^+$ cells was lower at the end of initial culture under ECcult compared to MScult. PC and AdSC similarly downregulated CD271 under ECcult. In contrast, AdSC under MScult slightly upregulated CD271 resulting in a significant difference in percentage of $CD271^+$ cells at the end of initial culture (Fig. 23D).

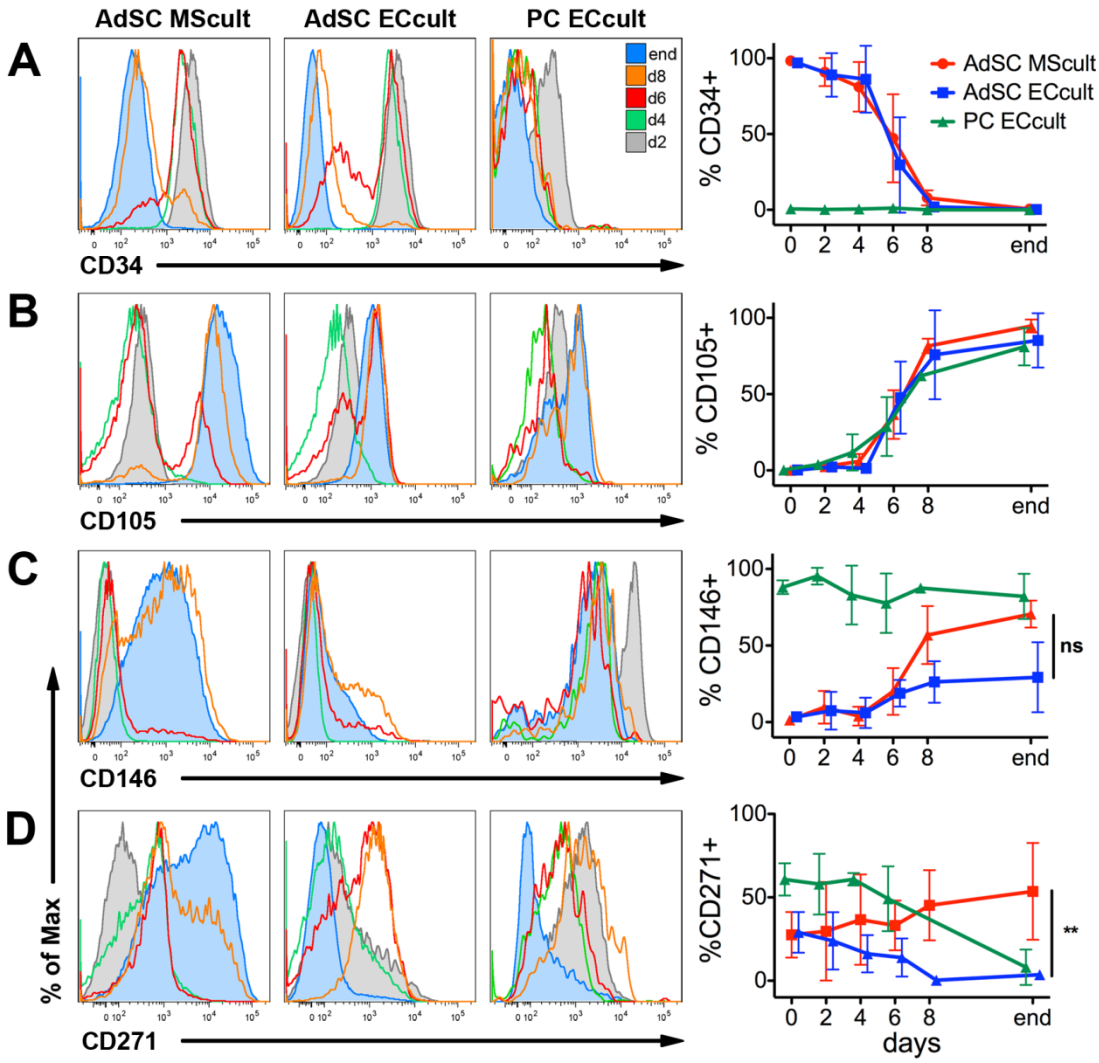

Figure 23: Immunophenotype kinetic of sorted AdSC and PC during MSC derivation.
MScult- and ECcult-cultured *ex vivo* sorted AdSC or PC were analyzed for expression of A) CD34, B) CD105, C) CD146 and D) CD271 at indicated time points. Overlay histograms show changes in marker expression from day 2 (grey area) to end of culture (blue area; see color code). Diagrams summarize percentage of marker-positive cells at indicated time points. Statistical test: unpaired t-test (**, $p<0.01$)

Interestingly, differences were observed in expression intensities of CD105, CD146 and CD271 under MScult and ECcult (Fig. 23B, C, D). These differences were depicted as the iMFI of surface marker-positive cells (Fig. 24). The iMFI of $CD105^{+}$ cells remained constant under ECcult, but increased under MScult (Fig. 24A). Also the iMFI of CD146 and CD271 were significantly lower under ECcult compared to MScult (Fig. 24B+C). In other words, ECcult-cultured AdSC upregulated CD105 less strongly compared to MScult; CD146 and CD271 were just weakly and transiently upregulated.

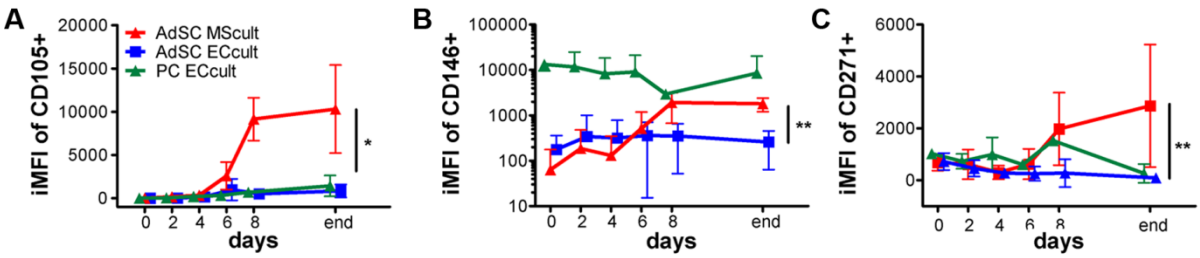

Figure 24: Culture-dependent differences in MFI of surface markers.
Kinetic of iMFI of CD105$^+$ (A), CD146$^+$ (B) and CD271$^+$ (C) in MScult- and ECcult-cultured AdSC and ECcult-cultured PC. Diagrams summarize iMFI of marker-positive cells at indicated time points. Statistical test: unpaired t-test (*, p<0.05; **, p<0.01)

Finally, we assessed surface marker expression on transcript level by qPCR in *ex vivo* PC, EC and AdSC as well as in MScult cultured AdSC at day 14 (Fig. 15). Confirming the *ex vivo* phenotyping results, low CD34 and high CD146 and CD271 transcript levels were detected in PC, while the highest CD105 transcript level was measured in EC (Fig. 25). Further, CD34 downregulation and CD105 upregulation was observed in CD271$^+$ AdSC at day 14. Transcript levels of CD146 and CD271 stayed rather constant in AdSC. The increased fluorescence in flow cytometry indicating increased protein levels may be associated with altered translation or protein processing (further discussed in section 5.4.3.).

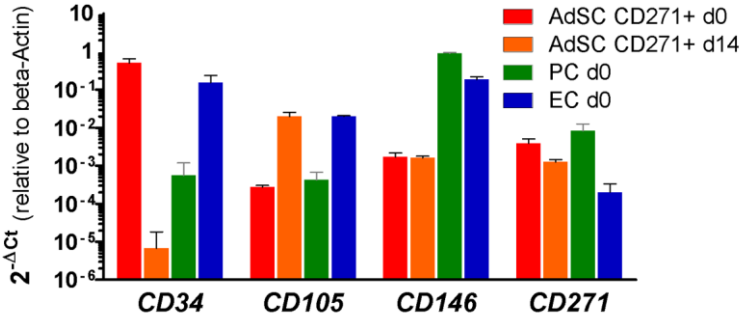

Figure 25: Validation of surface marker expression on transcript level.
Transcripts of CD34, CD105, CD146, and CD271 were quantified by qPCR in MScult-cultured CD271$^+$ AdSC at day 0 and day 14, and in PC and EC at day 0.

Hereby, we confirmed that AdSC downregulate CD34 and upregulate CD105 during the MSC derivation phase as assessed by flow cytometry and qPCR. In addition, we observed differential regulation of CD105, CD146 and CD271 expression depending on culture conditions.

4.3.5. Expression of CD73, CD90 and αSMA

MSC *in vitro* are characterized by expression of CD73 and CD90. Further, smooth muscle cells represent a substantial fraction within vascular walls and are marked by α-smooth muscle actin (αSMA) expression. To hence understand which subsets express MSC markers and αSMA *ex vivo*, we analyzed CD73, CD90 and αSMA expression by AdSC, PC and EC and on AdSC during early culture.

AdSC *ex vivo* were $CD90^{+}CD73^{+}$, PC were $CD90^{+/-}CD73^{-}$ and EC were $CD90^{+/low}CD73^{low}$ (Fig. 26A). During MSC derivation, CD73 and CD90 expression by AdSC changed only marginally (Fig. 26B).

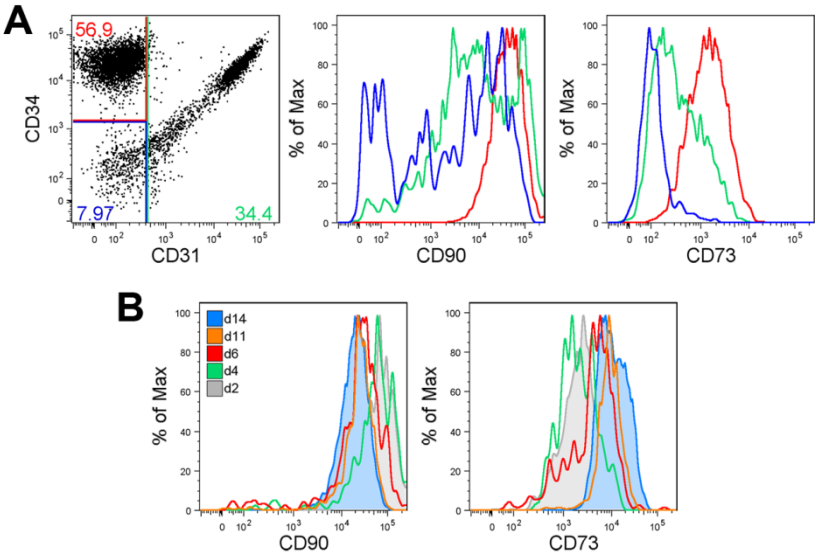

Figure 26: Expression of CD73 and CD90 in *ex vivo* SVF cell subsets and during MSC derivation.
A) *Ex vivo* SVF cells separated into $CD34+CD31^{-}$ AdSC (red), $CD34^{-}CD31^{-}$ PC (blue) and $CD34^{+}CD31^{+}$ EC (green) were analyzed for CD90 and CD73 expression. B) Overlay histograms show CD90 and CD73 expression of sorted AdSC monitored during MSC derivation from day 2 (grey area) to day 14 (blue area; see legend).

The majority of αSMA^{+} cells *ex vivo* was found in the PC population (60% αSMA^{+}), followed by EC with 21% αSMA^{+} cells (Fig. 27A). Only 2% αSMA^{+} cells were detected among AdSC at day 0. During culture however, the frequency of αSMA^{+} AdSC first increased slowly to about 10% at day 4 and then suddenly to 94% αSMA^{+} cells at day 6 (Fig. 27B). These results demonstrate that AdSC upregulate αSMA during MSC derivation.

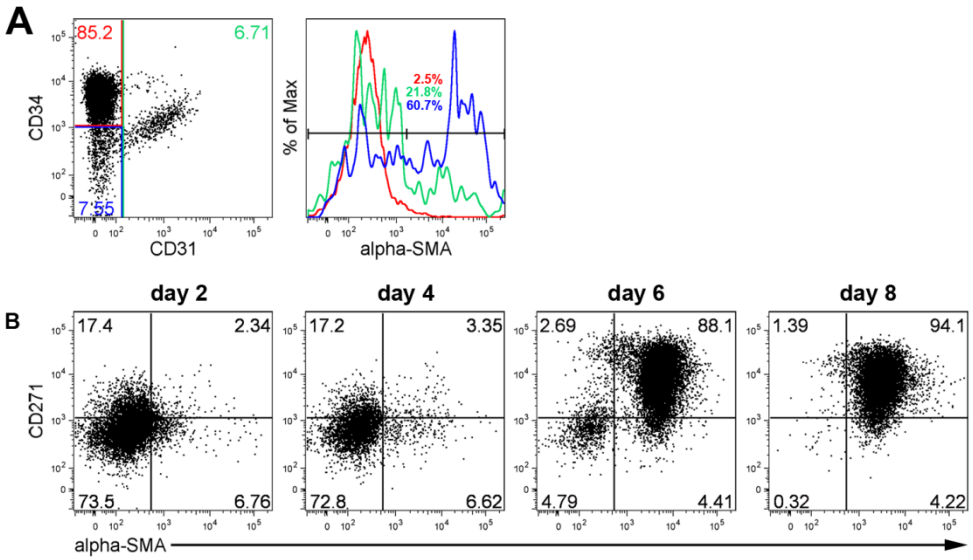

Figure 27: Expression of αSMA in *ex vivo* SVF cell subsets and during MSC derivation.
A) *Ex vivo* SVF cells separated into $CD34^{+}CD31^{-}$ AdSC (red), $CD34^{-}CD31^{-}$ PC (blue) and $CD34^{+}CD31^{+}$ EC (green) were analyzed for αSMA expression. Numbers indicate % of $αSMA^{+}$ cells in the respective fraction. B) αSMA vs. CD271 expression of sorted AdSC monitored during MSC derivation from day 2 to day 8.

4.3.6. Correlation of immunophenotype changes and onset of proliferation

Since surface marker regulations and onset of proliferation were observed at day 6, we questioned whether a possible correlation between these two events exists. To this end, *ex vivo* bulk SVF cells were labeled with a Cell Tracker Violet dye (CTV) that is diluted with cell divisions, resulting in weaker fluorescence by daughter cell generations.

Confirming our previous observations (Fig. 18), frequencies of proliferated, CTV^{-} cells increased prominently at day 6 (Fig. 28A+B). In the CTV^{+} population, i.e. non-proliferated cells, a slight increase in the percentage of $CD105^{+}$ and $CD146^{+}$ occurred. In contrast, CD34 downregulation was only observed in CTV^{-} cells. CD271 was apparently upregulated after cell division.

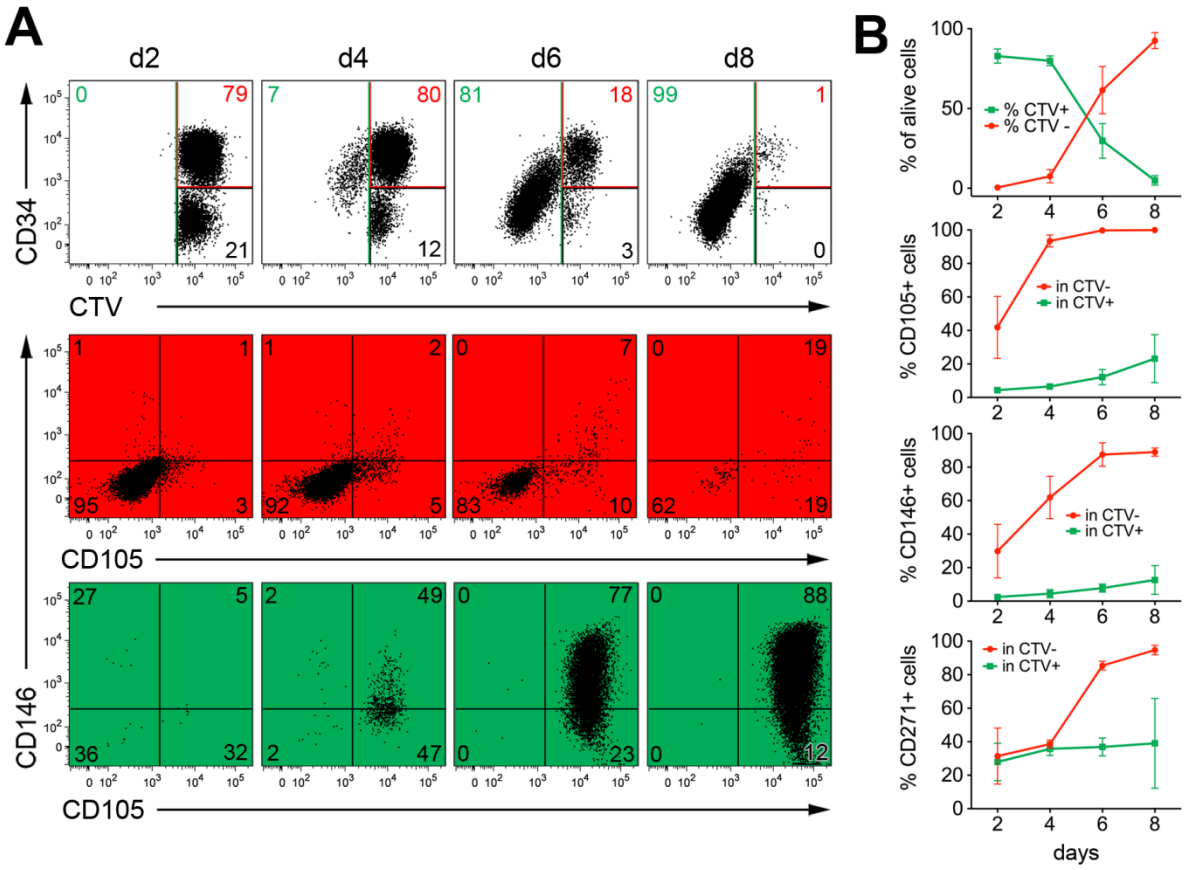

Figure 28: Surface marker regulation coincides with proliferation.
A) Non-proliferated, Cell Tracker Violet positive cells (CTV^+, red) and proliferated CTV^- cells (green) in bulk cultures were gated and analyzed for CD105 and CD146 expression at indicated time points. B) Diagrams summarize percentage of CTV^+ and CTV^- cells, and percentage of $CD105^+$, $CD146^+$ and $CD271^+$ cells within CTV^+ and CTV^- (n=3).

We conclude that there is a timely correlation of surface marker regulation and proliferation. In detail, CD105 and CD146 were already upregulated prior to cell division, whereas CD271 and CD34 were regulated after mitosis.

4.4. Transcriptome analysis of AdSC before and after early *in vitro* culture

Besides immunophenotypical changes and morphological adaptations to *in vitro* culture, we wanted to determine which other cellular processes are affected by early *in vitro* culture and understand which transcriptional programs govern these cellular alterations. To this end, microarray-based transcriptome analysis was performed to compare gene expression in *ex vivo* sorted MScult-cultured CD271$^+$ and CD271$^-$ AdSC at day 0 with the expression after MSC derivation at day 14. One microarray experiment was conducted for each subset.

We expected differences between CD271$^+$ and CD271$^-$ AdSC. However, with only about 8% of differentially regulated genes, CD271$^+$ and CD271$^-$ cells appeared highly similar, and thus, we concentrated the microarray analysis on similarly regulated genes to identify differences between *ex vivo* and cultured AdSC.

From 41,093 probes on the chip, about 9,800 had a sufficiently good detection p-value <0.005 and about 6,500 were regulated at least 2-fold. This high number of regulated genes already implies that vast transitional processes occurred during early culture.

For an initial quality control of the dataset, fluorescence intensities (i.e. expression strength) of all genes at d0 were compared to d14 (Fig. 29). Thereby, the results from flow cytometry and qPCR were confirmed (Fig. 23). For example, CD34 was downregulated by around 10-fold, and CD105 and CD146 appeared upregulated, CD271$^-$ AdSC at day 14 have upregulated CD271 by more than 2-fold. Interestingly, Dickkopf-1 (Dkk1), an inhibitor of WNT signaling, was extremely upregulated at day 14. Furthermore, VCAM1 were downregulated at day 14.

To gain deeper insights into changes in gene expression and associated cellular functions, we performed Gene Set Enrichment Analysis (GSEA).

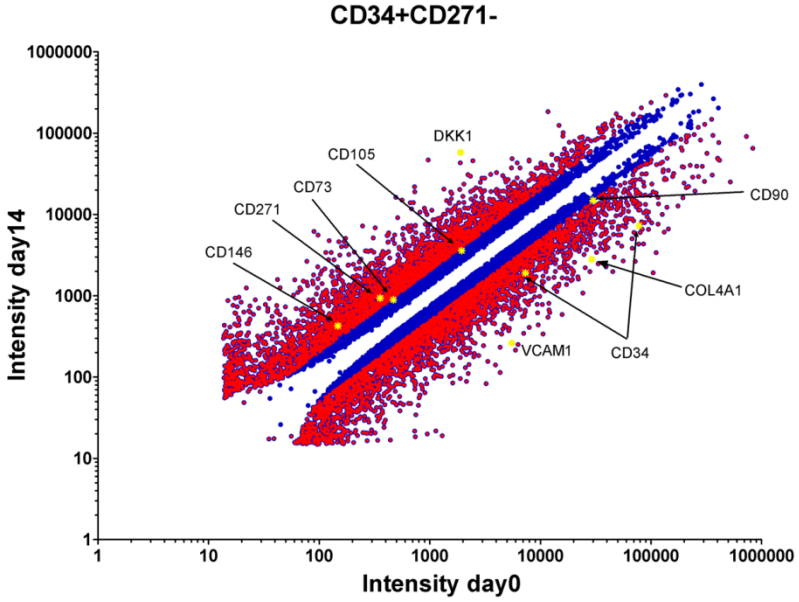

Figure 29: Overview about microarray results of CD271$^-$ AdSC. Intensity values of individual probes for day 0 and day 14 of CD271$^-$ AdSC are compared, and genes regulated less (blue) or more (red) than 2-fold are depicted.

The Broad Institute (Boston) provides a software tool for GSEA **(Subramanian, 2005)**. This software utilizes a huge database of gene sets with compiled gene annotations (e.g. Gene Ontology) or gene sets about different cellular processes published by institutions or researchers. The expression data of an experiment comparing two cellular states or classes are matched with these gene sets to calculate enrichment of a gene set within the one or the other cellular state (for details about GSEA, see Materials & Methods, 3.15.).

Screening our gene expression data by GSEA against all available gene sets pointed at the results of a previous study by Boquest et al. **(Boquest, 2005)** and at several different processes and pathways, such as proliferation, cell adhesion, extracellular matrix production and growth factor signaling. The major findings are explained in the following and a few genes of interest are highlighted. Furthermore, expression of several pivotal genes was validated by qPCR (section 4.4.9.).

4.4.1. Comparison with a previous study

Boquest et al. have performed a similar expression analysis **(Boquest, 2005)**. In that study, $CD31^-$ and $CD31^+$ SVF cells were isolated, and the $CD31^-$ subset was defined as "Stem Cells". Gene expression of *ex vivo* $CD31^-$ Stem Cells was compared to $CD31^+$ and to cultured $CD31^-$. Different to our study, AT-MSC from passage 4 were used, and not early culture MSC. Moreover, Boquest et al. have applied a less stringent sorting scheme and included also PC into the AdSC population.

The gene sets generated by Boquest et al. partially correlated with our expression data. On the one hand, we found gene set "Boquest Stem Cell UP" which compares *ex vivo* Stem Cells to *ex vivo* $CD31^+$ cells to be perfectly enriched at day 0 (Fig. 30A). Also gene set "Boquest Stem Cell Cultured vs Fresh DOWN" (not shown) was well enriched in AdSC d0. On the other hand, the gene set "Boquest Stem Cell Cultured vs Fresh UP" with genes upregulated in cultured $CD31^-$ stem cells was still enriched in AdSC at day 0 (Fig. 30B), although several genes contained in this gene set were upregulated at day 14. This incomplete matching might be due to the fact that we have utilized very early AT-MSC in contrast to Boquest et al. who used passage 4 AT-MSC which may be further matured. All in all, the overlap with the expression data set from Boquest et al. represents a confirmation of our microarray results.

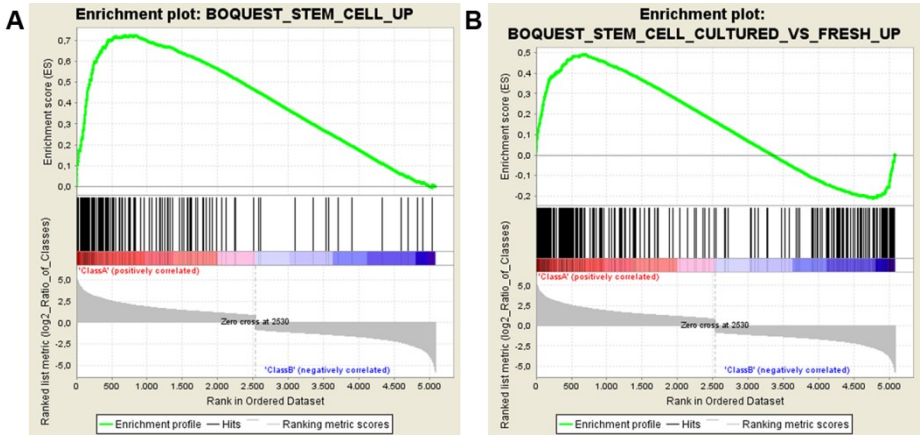

Figure 30: GSEA results – Boquest et al.
Gene sets "Boquest Stem Cell Up" (A) and "Boquest Stem Cell Cultured vs Fresh UP" (B) were enriched at day 0.

Several extracellular matrix components such as Laminins, Collagens and Fibulins as well as growth factors and cytokines including GDF-10, CXCL14, CXCL12 (SDF-1), and IGF-1 were downregulated at day 14. In contrast, different cytoskeletal components such as Cytokeratins (KRT18, KRT7), Myosin X, and cell adhesion molecules including N-Cadherin, CD105, AL-CAM and Podocalyxin were enriched at day 14. Furthermore, signaling inhibitors such as Dickkopf-1 and Gremlin were upregulated at day 14. These genes appeared to be involved in different cellular processes, as described in the following.

4.4.2. Proliferation

To assess whether induction of AdSC proliferation *in vitro* correlates to a changed gene expression profile, enrichment of proliferation-associated gene sets was determined.

Genes related to "Cell Cycle Arrest GO:0007050" were enriched in *ex vivo* AdSC (Fig. 31A). Cell cycle arrest-specific genes such as cyclin-dependent kinase inhibitors CDKN1C (p57/KIP2), CDKN1B (p27/KIP1), and tumor suppressors GAS1 (growth arrest-specific 1) and GAS7 were clearly upregulated at day 0 (Fig. 31C).

In contrast, the gene set "Reactome Cell Cycle Mitotic" was clearly enriched in AdSC at day 14 (Fig. 31B+C). Genes with strongest expression were several Cyclins (CCNA2, D1, E1, B2) and Cyclin-Dependent Kinases (CDK6, 7) and other Cell Division Cycle genes (CDC20). Also, factors involved in chromosome separation during M-phase, such as Aurora Kinase A (AURKA) and Polo-Like Kinase 1 (PLK1) were upregulated at day 14, suggesting the presence

of cells in all cell cycle phases. Note the almost exclusive expression of CDC20 and CCNA2 at day 14. CCNA2 is critical for S/G2 and also G2/M-phase transition; and CDC20 is a pivotal inducer of the Anaphase-Promoting Complex during M-phase **(Malumbres, 2009)**. This exclusive presence of these factors underlines cell cycle activity at day 14 compared to day 0. In summary, these results not only confirm that proliferation is initiated upon *in vitro* culture but also reveal that AdSC *in vivo* are quiescent.

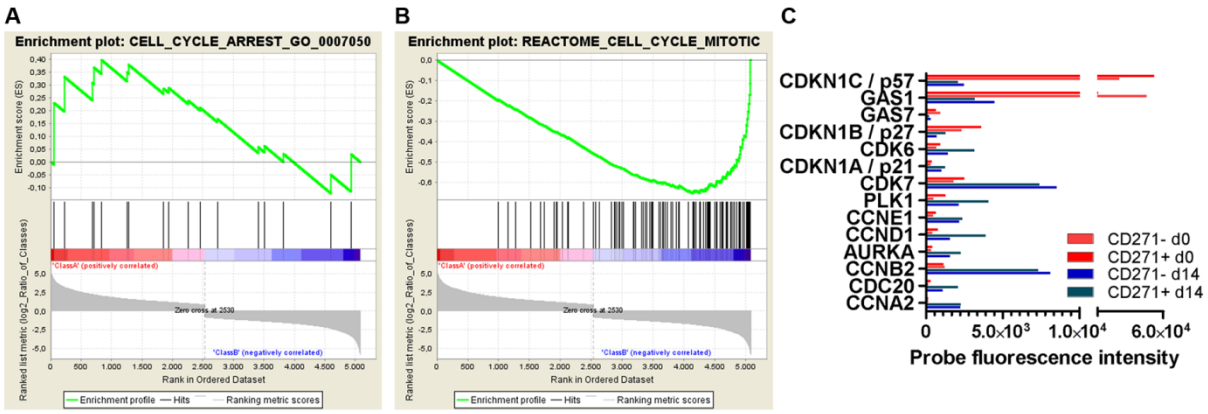

Figure 31: GSEA results – Proliferation
Gene sets "Cell Cycle Arrest GO0007050" (A) and "Reactome Cell Cycle Mitotic" (B) were enriched at day 0 and day 14, respectively. C) Probe intensity values of $CD271^-$ and $CD271^+$ AdSC at day 0 and day 14 for example genes involved in cell cycle arrest and mitosis.

4.4.3. Morphology

Gene set "Gobert Oligodendrocyte Differentiation UP" was enriched at day 14 (Fig. 32A). Gobert et al. induced oligodendrocyte differentiation in murine OPC Oli-Neu cells, a neuronal progenitor cell line, by different treatments that vary in induction efficiency **(Gobert, 2009)**. These differently treated cells were sampled at different time points, and gene expressions were compared.

The genes enriched in cultured AdSC comprised cell cycle regulating genes such as Maternal Embryonic Leucine Zipper Kinase (MELK) or Checkpoint Kinase 1 (CHEK1) (Fig.32B), but also genes like the Sialomucin Podocalyxin (PODXL), tropomyosin-1 (TPM1) and cytokeratin-18 (KRT18) which are involved in cytoskeleton organization and cellular morphology.

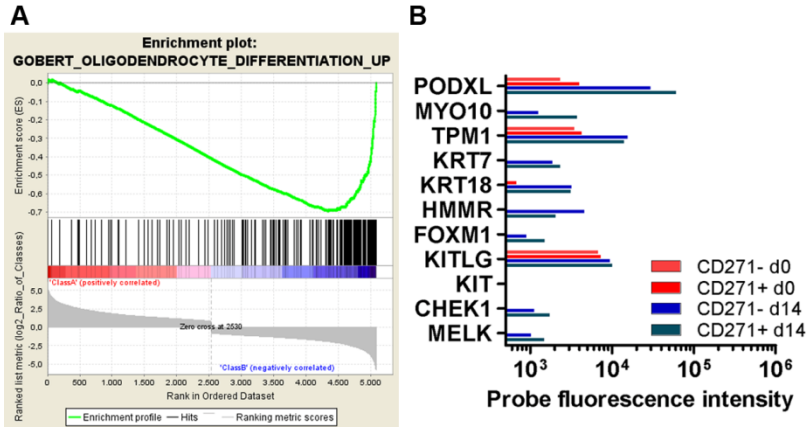

Figure 32: GSEA results – Oligodendrocyte Differentiation – Morphology
A) Gene set "Gobert Oligodendrocyte Differentiation UP" was enriched at day 0.Probe intensity values of $CD271^-$ and $CD271^+$ at day 0 and day 14 for example genes involved in immune response (B) and HLA molecules (C).

Based on these results, we reasoned that oligodendrocyte signatures were enriched at day 14 because MScult-cultured AdSC share morphological features with oligodendrocytes, e.g. multiple filopodial extensions. Hence, we compiled other cytoskeletal and morphology-regulating genes (also from gene sets by Boquest et al.) and observed quite exclusive expression of Myosin X (MYO10), hyaluronan-mediated motility receptor (HMMR) and cytokeratin-7 (KRT7) at day 14 (Fig. 32B). In addition, in this oligodendrocyte gene set, we found transcription factor FOXM1 expressed at day 14. Also of high interest is that *ex vivo* and cultured AdSC expressed KITLG, the so called Stem Cell Factor, but not the receptor c-KIT (CD117) which is associated with stemness and recruitment in HSC and early myeloid and lymphoid progenitors and cancer **(Okada, 1991)**.

These findings suggested that during MSC derivation cytoskeletal rearrangements occurred with a tendency towards more complex morphologies at day 14.

4.4.4. Cell adhesion molecules

The gene set "KEGG Cell Adhesion Molecules CAMs" was enriched in *ex vivo* cells (Fig. 33A) including Vascular Cell Adhesion Molecule 1 (VCAM1), CD34, Claudin 5 (CLDN5), neuronal growth regulator 1 (NEGR1) and neuroligin 2 (NGLN2) (Fig. 33B). In contrast, Claudin 11 (CLDN11), N-Cadherin and activated leukocyte-CAM (ALCAM) were expressed at day 14. These data suggest that AdSC undergo a switch in CAM expression during MSC derivation, probably associated with different attachment properties to different surfaces.

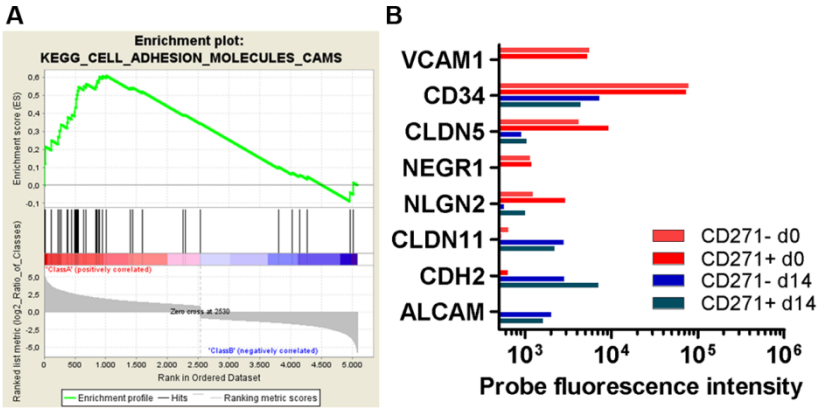

Figure 33: GSEA results – Cell Adhesion Molecules
A) Gene set "Cell Adhesion Molecules CAMs" was enriched at day 0. B) Probe intensity values of $CD271^-$ and $CD271^+$ at day 0 and day 14 for selected cell adhesion molecules.

4.4.5. Extracellular matrix

Clear enrichment of the gene set "Proteinaceous Extracellular Matrix" (GO: 0005578) at day 0 led to analysis of genes involved in extracellular matrix formation (Fig. 34A). The enriched genes comprised matrix constituents such as Laminins, Collagens and other matrix components (Fig. 34B+C). Some Collagens were downregulated more than five-fold (COL4A1, COL8A2), other Collagens remained constant (COL1A1, COL6A1, COL12A1), but COL13A1 was expressed exclusively at day 14. Laminins (LAMA2, LAMA4, LAMB2, LAMC1;) and other ECM components such as Fibulin-1, (FBLN1), Lumican (LUM), Nidogen 2 and Tenascin XB (TNXB) were expressed at higher rates at day 0 (some probe intensity values are shown in Figure 34B). Matrix metalloproteinase 9 (MMP9) was exclusively expressed in *ex vivo* AdSC. In contrast, at day 14, expression of Fibronectin-1 (FN1), MMP1 and MMP3 were upregulated.

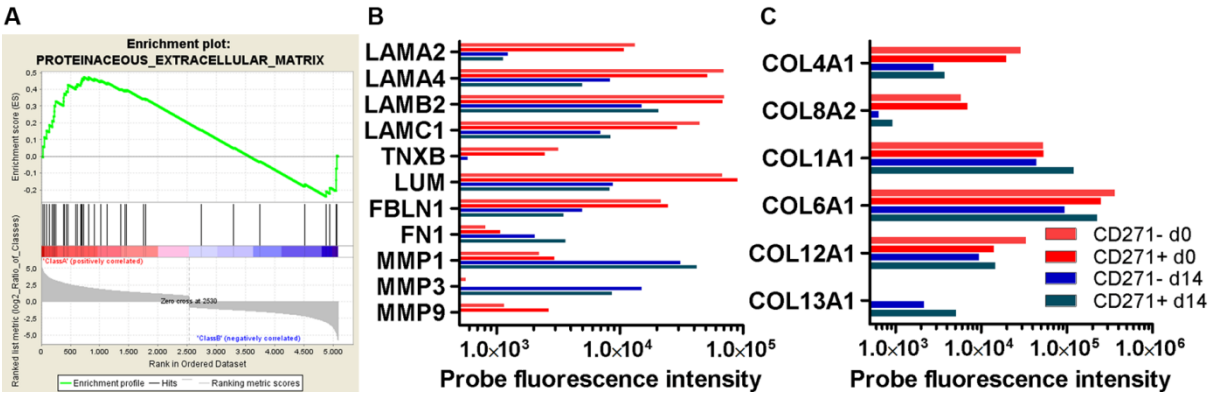

Figure 34: GSEA results – Extracellular Matrix
A) Gene set "Extracellular Matrix" was enriched at day 0. Probe intensity values of $CD271^-$ and $CD271^+$ at day 0 and day 14 for example genes from GSEA and for selected Laminins (B) and Collagens (C).

These results suggest that ECM production was clearly changed *in vitro*. Especially Laminins and proteins required for matrix organization and maturation (e.g. LUM, FBLN1, TNXB) were downregulated. Collagens were mainly maintained but COL8 was downregulated and COL13 was induced *in vitro*. MMPs required for matrix turnover were upregulated at day 14.

4.4.6. Immune response

The gene sets "Response To Wounding" (GO: 0009611) and "Immune Response" (GO: 0006955) were similarly enriched at day 0 (Fig. 35A). Several genes were redundantly found in both gene sets. Examples of regulated genes are displayed in Figure 35B+C.

Several chemokines were exclusively expressed at day 0 (Fig. 35B), such as tumor necrosis factor ligand superfamily member 13B (TNFSF13B, B-cell activating factor, BAFF, CD257), CXCL9 (Monokine induced by gamma interferon, MIG) and CX3CL1 (Fractalkine). Other chemokines were strongly downregulated during culture, like CCL2 (monocyte chemotactic protein-1, MCP-1), CCL19 (macrophage inflammatory protein-3-beta; MIP-3-beta), CXCL14 (BRAK, breast and kidney-expressed chemokine) and CXCL12 (Stromal cell-derived Factor-1, SDF1). Furthermore, the chemokine receptor CXCR4 was only expressed at day 0, and CXCR7 was constantly transcribed. Egr1 (Early Growth Response 1) was upregulated at day 0, and maintained until day 14, albeit at lower levels (Fig. 35B). Similarly, the IL13 receptor α1 (IL13RA1) was expressed constantly

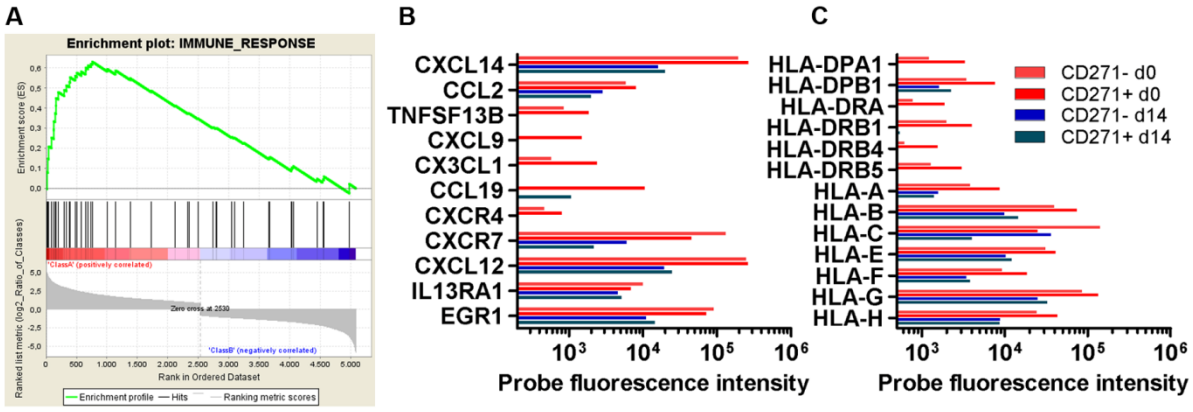

Figure 35: GSEA results – Immune response and wound healing
A) Gene set "Immune Response" was enriched at day 0.Probe intensity values of $CD271^-$ and $CD271^+$ AdSC at day 0 and day 14 for (B) example genes involved in immune response and wound healing and (C) HLA molecules.

MHC class I (Human Leukocyte Antigen HLA-A, -B, -C) and minor MHC (HLA-E, -F, -G, -H) were expressed constantly, but were slightly downregulated at day 14 (Fig. 35C). In contrast, MHC class II molecules (HLA-DP, HLA-DR) were exclusively expressed at day 0.

These results implied that inflammatory responses are ongoing in *ex vivo* AdSC and that MSC downregulate MHC class II expression during early culture.

4.4.7. Growth factor signaling pathways

Concerning growth factor signaling pathways, enrichment of WNT, PDGF, TGFβ, and FGF signaling was observed.

WNT signaling

Gene set "WNT signaling" was enriched at day 0 (Fig. 36) due to upregulated WNT ligands and receptors: Frizzled-4 and -5 (FZD4, FZD5), WNT11, and Low-density lipoprotein receptor-related protein 5 (Lrp5), further, Kremen-1 and Sox17. FZD2, FZD6, WNT5A and Dkk1 were upregulated at day 14. WNT6 was transcribed at similar rates at both time points. All in all, WNT signaling was reduced upon *in vitro* culture, probably related to expression of Dkk1 as a major repressor of WNT signaling **(Bao, 2012)**.

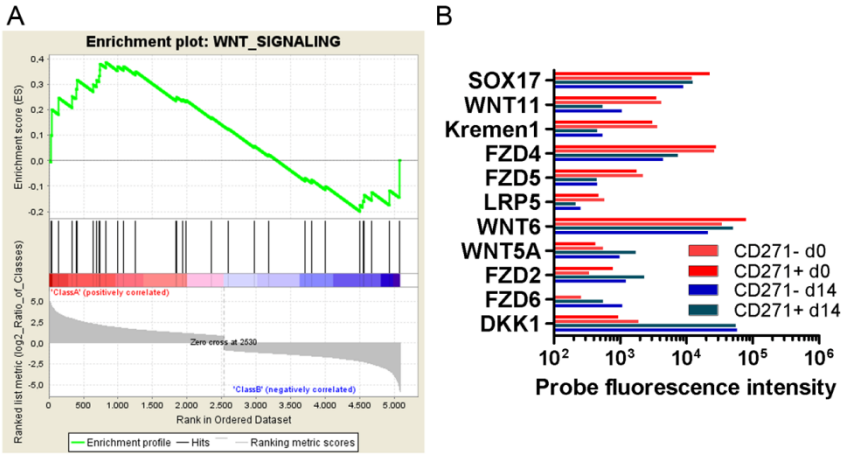

Figure 36: GSEA results – WNT Signaling
Enrichment of gene set "WNT Signaling" and probe intensity values for example genes.

PDGF signaling

Gene set “Reactome Signaling by PDGF” was enriched in *ex vivo* AdSC (Fig. 37). Platelet-derived Growth Factor Receptor A (PDGFRA) and PDGFRB as well as PDGF-D and the mediators STAT-5A, -6 and -3 were upregulated at day 0. Neither PDGF-A or PDGF-B was transcribed by AdSC, but at day 14, PDGF-C and STAT1 were upregulated. This implies a switch in major involved signaling molecules, especially from PDGF-D to PDGF-C.

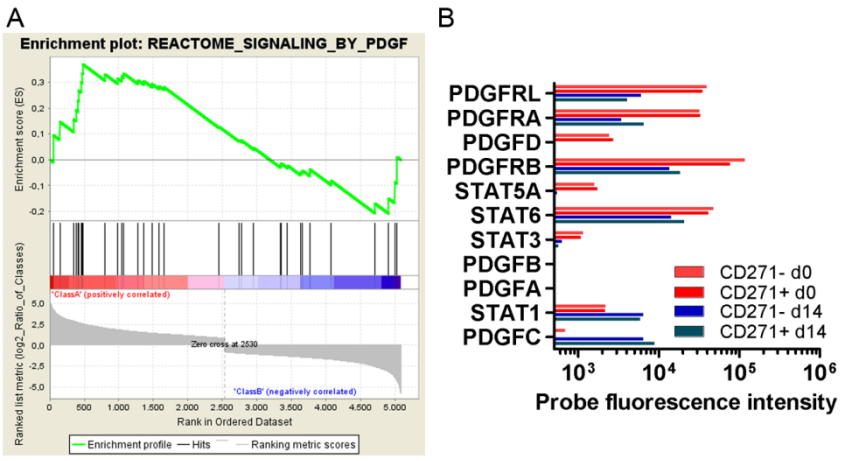

Figure 37: GSEA results – PDGF Signaling
Enrichment of gene set “Reactome Signaling By PDGF” and probe intensity values for example genes.

TGF-β signaling

Gene set “Reactome Signaling By TGF-β Receptor Complex” was slightly enriched at day 14, although it appears that involved genes are only marginally regulated (Fig.38). Looking at TGF-β ligands and receptors further supported this notion. TGF-β3, Activin-B (INHBB) and TGF-β Receptor Type 3 (TGFBR3) were slightly downregulated at day 14. Activin receptor-like Kinase 1 (ACVRL1, ALK-1) was only expressed at day 0, whereas TGF-β Induced (TGFBI) and Activin-A (INHBA) were upregulated at day 14. All present ligands (TGFB3, INHBA, INHBB) can signal via ALK-2 which is constantly expressed, but also via CD105 which is 2-fold upregulated at day 14, as already shown by flow cytometry and qPCR (Fig. 23+25). These results imply that TGF-β signaling is constantly active throughout MSC derivation, although upregulated CD105 may modulate TGF-β-mediated effects.

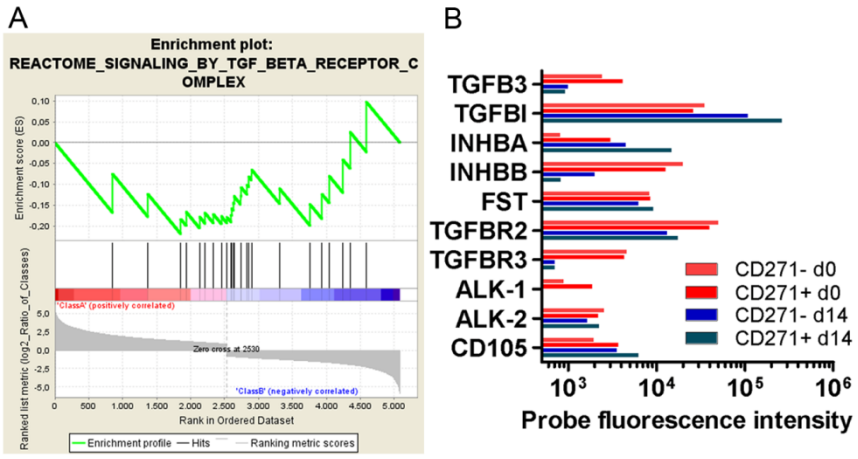

Figure 38: GSEA results – TGFβ Signaling
Enrichment of gene set "Reactome Signaling By TGF Beta Receptor Complex" and probe intensity values for TGFβ ligands and TGFβ receptors.

FGF signaling

Gene set "Reactome Signaling by FGFR" was enriched in cultured AdSC (Fig. 39). But the FGF receptor FGFR1 was downregulated at day 14 and FGFR2 was even completely absent. But FGF1 and FGF5 were upregulated at day 14, while FGF2 appears constantly expressed. Finally, most importantly, at day 0, growth factor signaling inhibitors Sprouty-1/2 (SPRY1/2) were expressed which may render AdSC unable to respond to extracellular, growth factor-mediated cues **(Hanafusa, 2002)**. Hence, FGF signaling may be more influential at day 14.

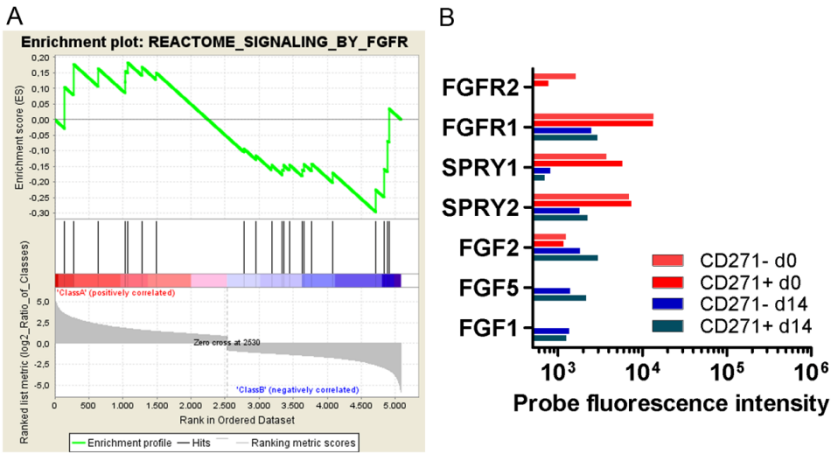

Figure 39: GSEA results – PDGF Signaling
Enrichment of gene set "Reactome Signaling By FGFR" and probe intensity values for example genes.

4.4.8. Epithelial-to-mesenchymal transition

Gene set "Sarrio Epithelial Mesenchymal Transition UP" was highly enriched at day 14 (Fig. 40B), and conversely, gene set "Sarrio Epithelial Mesenchymal Transition DN" was found enriched at day 0 (Fig. 40A). Sarrio et al. have compared genes expression of MCF10A breast cancer cells grown at low confluence (mesenchymal phenotype) compared to those grown at high confluence (epithelial, basal-like phenotype).

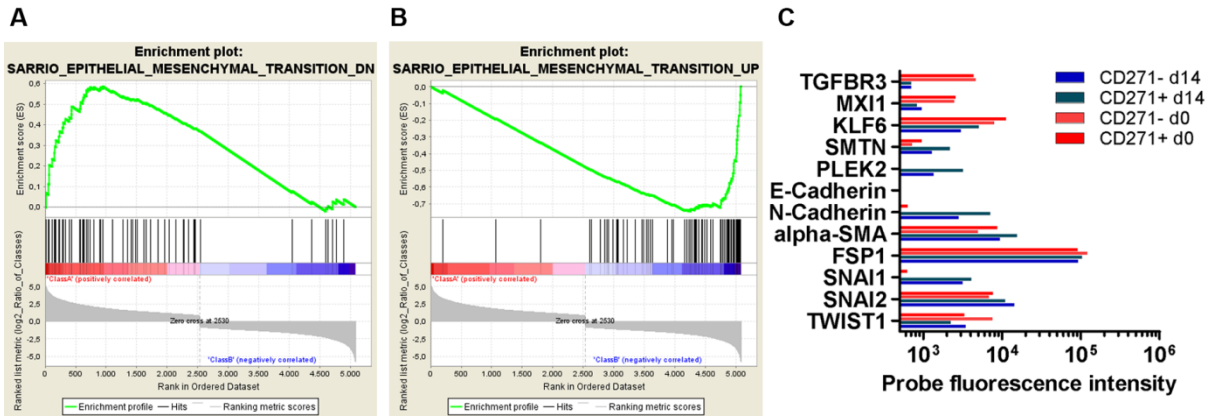

Figure 40: GSEA results – Epithelial-to-Mesenchymal Transition (EMT)
Gene sets "Sarrio Epithelial Mesenchymal Transition DN" (A) and "Sarrio Epithelial Mesenchymal Transition" (B) were enriched at day 0 and day 14, respectively. C) Probe intensity values of $CD271^-$ and $CD271^+$ at day 0 and day 14 for example genes involved EMT.

At day 0, the potent Myc-inhibitor MAX-inhibitor 1 (MXI1) and TGF-β receptor 3 (TGFBR3) were upregulated, which is consistent with cell cycle quiescence. At day 14, genes involved in formation of fibroblastoid cell morphology were upregulated (Fig. 40C), such as actin-binding proteins SMTN (smoothelin) and PLEK2 (pleckstrin-2). Concerning the major EMT-related genes, we found N-Cadherin (CDH2) and Snail (SNAI1) to be upregulated. In contrast, Fibroblast-specific Protein 1 (FSP1), α-Smooth Muscle Actin (ACTA2), Slug (SNAI2) and TWIST1 were constantly expressed at both time points.

4.4.9. Validation of microarray results by qPCR

To validate the microarray results, AdSC were MACS-enriched and cultured to confluence. Different to the FACS-sorted AdSC used for the microarrays, MACS-enriched AdSC reached confluence already as early as day 8 (not at day 14). RNA was isolated at day 0, day 5 and day 8. These samples were used to verify expression of different genes by qPCR. Expression

of several different growth factors, cytokines and receptors, transcription factors and EMT-related genes were assessed (Fig. 41).

Changes in gene expression as determined by qPCR were in most cases consistent with the microarray results. For example, a drastic, 60-fold upregulation of Dkk1, the potent WNT signaling inhibitor, was confirmed, with the peak of transcription already reached at day 5.

Moreover, Gremlin-1 and -2 (GREM1, GREM2) were strongly upregulated (100-fold and 100-fold, respectively). Gremlins are potent antagonists of BMP signaling and were reported to be involved in cancer cell proliferation and metastasis, as well as fibrosis **(Farkas, 2010; Mulvihill, 2012)**.

In addition, GDF10 (BMP3B) expression was almost exclusively expressed at day 0 (50-fold downregulation at day 8). GDF10 is predominantly expressed by pre-adipocytes **(Hino, 2012; Upadhyay, 2011)**. Interestingly, GDF10 was recently linked to expression of Sca-1, the murine Stem Cell Antigen-1, Ly-6A **(Upadhyay, 2011)**. In detail, Sca-1 marks murine adult stem cells, such as HSC, but is also elevated in malignancies. Especially in cancer, Sca-1 inhibits TGF-β signaling by GDF-10 via TGF-β receptor I and II. Upadhyay et al. suggested that Sca-1/Ly6-A disturbs TGF-β receptor heterodimerization following GDF10 ligation and thereby inhibits SMAD3signaling. In humans, Ly6D and Ly6K, homologs of murine Ly-6A, have analogously been associated with breast cancer **(Choi, 2009)**. Intriguingly, Ly6K is upregulated by AdSC during MSC derivation (data not shown). Future studies will further analyze the role of Ly6K and GDF10 in MSC.

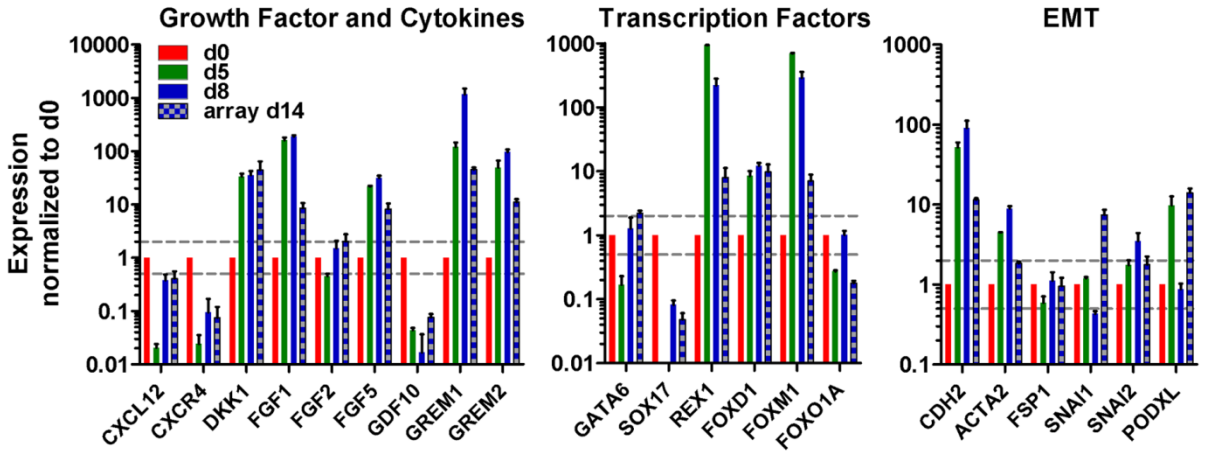

Figure 41: Confirmation of gene expressions by qPCR.
Expression results from microarray (blue/white patterned bars; fold change d14/d0 of $CD271^-$ and $CD271^+$ AdSC) were confirmed by qPCR (fold change: dCt relative to HPRT, normalized to d0). Values from day 0 (red bars), day 5 (green bars) and day 8 (blue bars) are shown. One biological replicate, three technical replicates.

Expression of several selected transcription factors was determined. The only GATA family member expressed, GATA6 was slightly upregulated at day 8 (2-fold). But at day 5, GATA6 was about 5-fold downregulated. Moreover, Sox17, a transcription factor recently discovered as marker for vascular stem cells was downregulated during MSC derivation **(Tang, 2012)**. Furthermore, during MSC derivation, REX1 was upregulated already at day 5 and then maintained.

Finally, regulation of major EMT-related genes was assessed **(Zeisberg, 2009)**. Upregulation of N-Cadherin (CDH2, 100-fold) and αSMA (ACTA2, 10-fold) during MSC derivation was confirmed. In contrast, central EMT transcription factors SNAI1 and SNAI2 showed ambiguous expression patterns. According to microarray, SNAI1 was strongly upregulated (10-fold) and SNAI2 expression was maintained. qPCR yielded inverse results, namely a slight downregulation of SNAI1 but upregulation of SNAI2 (4-fold). Upregulation of Podocalyxin (PODXL) could not be confirmed. Instead of being about 10-fold upregulated at confluence (microarray d14), PODXL was expressed at basal levels at day 8, but peaked at day 5 (10-fold).

In summary, microarray analysis revealed enrichment of cell cycle-promoting and morphology-associated genes at day 14, corroborating the observed coincidence of proliferation onset and morphological transition. Inflammatory responses were enriched *ex vivo*. Growth factor signaling was altered by expression of Gremlin at day 14 (BMP inhibition), Sprouty at day 0 (FGF inhibition) and Dickkopf at day 14 (WNT inhibition). qPCR results confirmed expression and regulation of several genes of interest, further corroborating the validity of the microarray dataset.

5. Discussion

In this study, immunophenotypical and morphological transitions of MSC progenitors during the early culture phase, the MSC derivation phase, were investigated and linked to changes in gene expression. We identified two different AT-MSC progenitors, namely AdSC (Adventitial Stromal Cell) and PC (Pericytes) and discovered changes in morphology and immunophenotype that tightly correlated to the proliferation status. MSC derivation turned out to be culture-dependent, i.e. the two MSC progenitor types reacted differently to the two employed culture conditions. MScult (conventional MSC culture condition) and ECcult (Endothelial cell culture condition) not only altered proliferation rates of MSC progenitors, but also morphological appearance and immunophenotype of derived AT-MSC.

Transcriptome analysis corroborated these findings, and in addition, shed light on major transcriptional programs that regulate MSC derivation. Accordingly, early inflammatory response upon tissue damage and stimulation by different growth factors may represent the initial pivotal regulators for MSC progenitor proliferation during MSC derivation.

5.1. Characterization of AT-MSC

Cultured SVF cells from adipose tissue developed into fibroblastoid cells with long-term proliferative capacity (Fig.12) that expressed CD73, CD90 and CD105, were negative for CD14, CD34 and CD45 (Fig. 14), and differentiated towards the adipogenic and osteogenic lineage (Fig. 13). Proliferation rates of AT-MSC during long-term expansion varied slightly between donors (Fig. 12), but these differences did not correlate with donors' age (data not shown). The proliferation rates were consistent with previous reports about human AT-MSC **(Kern, 2006)**. Differentiation was efficient towards the adipogenic and osteogenic lineage, but we rarely observed well differentiated chondrogenic micropellets. This is in accordance with the reportedly weak chondrogenic potential of AT-MSC **(Im, 2005)**, which according to previous studies, can be enhanced by addition of either higher growth factor concentrations or BMP-2 or BMP-7 **(Kim, 2009a**, **b; Mehlhorn, 2007)**.

Hereby, we confirmed that the cells derived from SVF cells fulfill the minimal criteria for AT-MSC, defined by the ISCT **(Dominici, 2006; Zuk, 2002)**.

5.2. Identification of SVF cell subsets and AT-MSC progenitors

In order to identify AT-MSC progenitors, the different cellular subsets in the SVF were dissected by analyzing expression of CD45, CD31, CD34, CD105, CD146, CD271, CD73, CD90 and αSMA by flow cytometry (Fig. 15, 26, 27). Four major cell fractions in the SVF were identified:

1) $CD45^+$ **hematopoietic cells**,

and within $CD45^-$ stromal vascular cells:

2) **Endothelial Cells (EC):** $CD34^+$ $CD31^+$ $CD105^{low}$ $CD146^+$ $CD90^+$ $\alpha SMA^{+/-}$ $CD73^{-/low}$,

and MSC progenitors:

3) **Pericytes (PC):** $CD34^-$ $CD31^-$ $CD105^-$ $CD146^{high}$ $CD271^{+/-}$ $CD90^{+/-}$ CD73- $\alpha SMA^{+/-}$

3) **Adventitial Stromal Cells (AdSC):** $CD34^+$ $CD31^-$ $CD105^-$ $CD146^-$ $CD271^{+/-}$ $CD73^+$ $CD90^+$ and αSMA^-

We observed only minor differences in the percentage of these cell subsets between individual donors, and no correlation with donors' age, gender or anatomical site of liposuction was found (Table 11). Thus, the cellular composition of the SVF appeared quite constant, independent of age and gender. However, to draw a definitive conclusion, our sample size was too small and donors' age ranged merely from 27 to 49 years. A recent study showed a reduced antigenic potential of AdSC in elderly patients (55 to 81 years), although frequencies of AdSC were independent of age, confirming our observation **(Madonna, 2011)**.

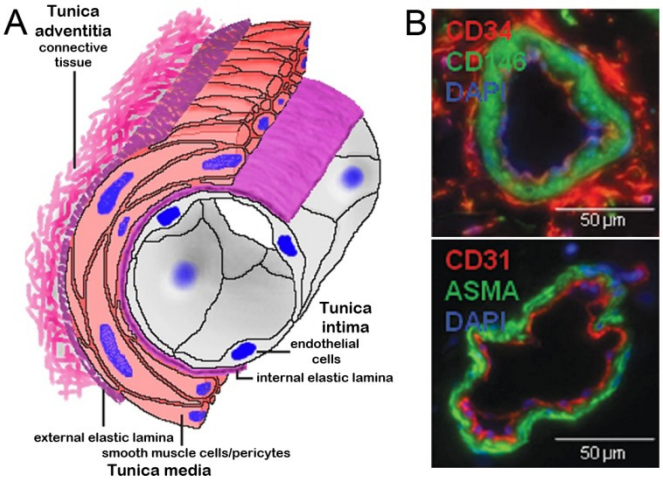

Figure 42: SVF subset localization.
A) Scheme of blood vessel wall architecture (http://www.lab.anhb.uwa.edu.au). B) Staining of blood vessels for CD31, CD34, CD146 and αSMA **(Zimmerlin, 2010)**.

Several recent studies have utilized similar markers for MSC progenitor phenotyping, but have also clarified the *in situ* localization of identified subsets by histology **(Corselli, 2011; Lin, 2008; Maumus, 2011; Zimmerlin, 2010)**. These publications provided clues about the histological localization of our characterized subsets (Fig.42). The majority of $CD45^+$ leukocytes reside in the blood vessel lumen, yet mast cells

for example are also located in the tissue stroma **(Galli, 2010)**. In the Tunica intima, $CD34^+$ $CD31^+$ endothelial cells line the blood vessel lumen and are attached to the internal elastic lamina. In the tunica media, $CD34^-$, $CD31^-$, αSMA^+ and $CD146^+$ pericytes and smooth muscle cells can be found **(Corselli, 2011; Lin, 2008; Zimmerlin, 2010)**. Finally, distal to the blood vessel lumen, in the Tunica adventitia or Tunica externa reside $CD34^+$ $CD31^-$ AdSC, fibroblasts and different progenitor cells **(Corselli, 2010)**. Based on this, we termed our cell subsets, EC, PC and AdSC (see above). We basically adopted this nomenclature from Zimmerlin et al., but termed "Supra-Adventitial ASC" as Adventitial Stromal Cells, AdSC.

Our marker selection has proven to be appropriate for characterization of different SVF cell types. However, we suggest improvements for future phenotyping studies. Firstly, EC and PC separation can definitely be enhanced by including CD90 as an additional criterion. EC and PC were incompletely separated by gating only according to CD34 and CD31, as especially manifested in the inhomogeneous distribution of αSMA and CD90 expressing cells (Fig. 26, 27). Zimmerlin et al. have additionally identified $CD31^+$ $CD34^-$ mature endothelial cells that were $CD90^-$ **(Zimmerlin, 2010)**. We find a similar population at the border between EC and PC. Hence, by including CD90, these mature EC may be better separated. Secondly, other markers have been described as MSC enrichment markers, such as PDGF-receptor A and B (CD140a and CD140b), and Stro-1 **(Jones, 2002; Uezumi, 2010)**. The finding that PDGFR-A and -B were expressed in AdSC underscores that inclusion of such markers in our staining panel will further improve identification of MSC progenitors *ex vivo*.

CD34, CD146 and CD271 - markers for MSC progenitor characterization

Ex vivo MSC progenitors were partially positive for CD271, but differed in expression of CD146 and CD34 (Fig. 15). We have sorted AdSC and PC, and both subsets – when initially cultured under ECcult – developed into AT-MSC that exhibited long-term expansion capacity and differentiated towards the adipogenic and osteogenic lineage (Fig. 16, 17).

CD34 has been already reported as a marker for non-hematopoietic stem/progenitor cells, and a perivascular localization was also described **(Campagnolo, 2010; Suga, 2009; Traktuev, 2008)**. In a study about CD271 expressing cells in AT, $CD271^+$ SVF cells were $CD34^+$ or $CD34^-$ **(Quirici, 2010)**, which is matching to our observations on AdSC an PC. Recently, Tormin et al. have identified similar $CD271^+$ $CD146^-$ and $CD271^+$ $CD146^+$ MSC progenitors in the BM **(Tormin, 2011)**. Perivascular cells in spatial proximity to blood vessels were $CD146^+$, whereas

bone-lining cells and cells more distal to blood vessels appeared $CD146^-$. This *in situ* localization suggests a correlation of CD146 expression to the distance to the blood vessel, which is also consistent with the observations in adipose tissue **(Corselli, 2011)**.

Based on the facts about MSC progenitor phenotypes in BM and AT, it would be interesting to know whether the $CD146^-$ cells in the BM express CD34. In this case, the immunophenotype of MSC progenitors from AT and BM would be identical. However, an older report by Quirici et al. about $CD271^+$ BM cells definitely provided no evidence for a $CD34^-$ population within CD271 expressing cells **(Quirici, 2002)**. Accordingly, also $CD146^+$ $CD271^+$ "pericytes" in BM must be $CD34^+$. Nonetheless, these data demonstrate that MSC progenitors from BM and AT show phenotypic similarity and can be identified by CD271, and partly by CD146 or CD34 expression.

In summary, we have demonstrated that both, AdSC and PC are AT-MSC progenitor subsets. Both successfully developed into bona fide AT-MSC that could be long term expanded and differentiated into osteoblasts and adipocytes in passage 2.

5.3. Expression analysis of AdSC during MSC derivation

Transcriptomes of MScult-cultured $CD271^+$ and $CD271^-$ AdSC at day 0 and day 14 of early culture were compared by microarray. Around 6,500 genes were differentially regulated more than 2-fold either at day 0 or day 14 (approx. 50%-50%) in both, $CD271^+$ and $CD271^-$ AdSC.

Since the microarray analysis was performed with cells of only one donor, donor-specific effects cannot be excluded. But the microarray results were thoroughly validated in different ways: 1) genes regulated during MSC derivation were highly similar in $CD271^+$ and $CD271^-$ AdSC; 2) microarray results confirm the observations concerning surface marker expression (Fig. 23, 25, 29); 3) results from a previous study by Boquest et al. **(Boquest, 2005)** confirm similar regulation of several genes (Fig. 30); 4) expression of selected genes was confirmed by qPCR on MACS-enriched AdSC from another donor (Fig. 41). Hence, the microarray experiments yielded reliable results.

For the validation by qPCR, an intermediate time point (day 5) was additionally included to investigate whether there are transient gene regulations occurring that could not have been detected in the microarray experiment.

To identify important functions and processes out of approx. 6,500 regulated genes, we eventually decided to perform Gene Set Enrichment Analysis (GSEA). GSEA offers a convenient analysis and returns gene sets, i.e. genes associated with distinct cellular processes (details on GSEA, see Mateials & Methods 3.15.).

GSEA pointed to different processes and genes regulated during MSC derivation, such as proliferation, immune response, extracellular matrix production and turnover as well as WNT, PDGF, TGF-β and FGF signaling.

5.4. The MSC derivation process

We have analyzed sorted AdSC and PC as well as bulk SVF cells for proliferation, morphology and immunophenotype during the MSC derivation phase and compared the effect of two different culture conditions. Furthermore, transcriptomes of sorted AdSC were assessed by microarray and analyzed by GSEA. In the following, our major findings are summarized with an attempt to combine the results from kinetic experiments and transcriptome analysis.

5.4.1. Culture-dependent differences in proliferation during MSC derivation

AdSC- and PC-derived AT-MSC exhibited similar proliferation rates during long-term culture (Fig. 16), whereas differences in the proliferation of AdSC and PC during initial culture under two culture conditions were observed (Fig. 19). AdSC proliferated sufficiently under both conditions, yet faster under ECcult, while PC did not proliferate under MScult. Confirming this observation, Corselli et al. have recently shown that AdSC proliferate faster than PC; yet, this was evaluated only under ECcult as culture condition for early culture **(Corselli, 2011)**. In a different study, Maumus et al. have not identified PC as MSC progenitors since only MScult was applied **(Maumus, 2011)**. Our results combine these findings and clearly demonstrate that different progenitor types obviously need specific culture conditions to adhere and proliferate.

There are similarities between AT and BM concerning the reduced proliferative potential of PC. Tormin et al. have also shown that PC-like $CD271^+$ $CD146^+$ cells from the BM were less clonogenic than AdSC-like $CD271^+$ $CD146^-$ **(Tormin, 2011)**. In other studies, medium supplementation with mitogens like dexamethasone, EGF and FGF-2, enhanced proliferation of PC **(Paul, 2012; Zimmerlin, 2010)**. Also, coating of culture dishes with e.g. gelatin

promoted MSC derivation from PC **(Crisan, 2008)**. Hence, we conclude that MSC derivation from different progenitor cells is culture-dependent.

According to the histological analysis by Corselli et al., AdSC were mainly found around larger blood vessels, such as arteria and venae, due to their localization in the Tunica adventitia **(Corselli, 2011)**. Hence, the amount of AdSC may correlate to the vascular architecture of a given tissue. Combining this finding with our observation of culture-dependent MSC derivation, the type and size of blood vessels present in a tissue may predetermine the amount of adventitia-derived MSC progenitors and, consequently, also which culture condition is favorable for MSC derivation from a specific tissue.

In summary, AdSC are the more clonogenic MSC progenitors that can sufficiently proliferate under both culture conditions. ECcult did not only enable PC culture but also accelerated AdSC expansion.

5.4.2. Proliferation kinetic during MSC derivation

Kinetic monitoring of cell numbers revealed that onset of proliferation of bulk SVF cells was observed around day 6 independent of the utilized culture condition (Fig. 18), whereas proliferation of sorted AdSC occurred about two days later (Fig. 19). This delay may, on the one hand, be due to increased cell stress after sorting. On the other hand, PC, EC and – not to forget – $CD45^+$ lymphocytes may have pro-proliferative effects on AdSC, which they can only exert in bulk cultures. These pro-proliferative effects may be mediated by cytokines and growth factors. This assumed pro-proliferative effect of lymphocytes on MSC derivation was already demonstrated by Friedenstein et al. who ascribed this effect to platelets and megakaryocytes **(Friedenstein, 1992)**.

During MSC derivation, cell numbers of bulk SVF cells under any culture condition dropped drastically to 5-10% relative to seeded cells until day 4 of culture (Fig. 18). This reduction probably represents the selection of living cells and cells capable to adhere. Sorting of AdSC and PC increased the number of adhering cells at day 4 to around 30% (Fig. 19). The low frequency of adherent cells at this time point could be due to lower viability, however, only apoptosis assays can clarify this aspect. Another explanation could be that cells with adhesion potential may only make up a minor subset within AdSC and PC and they can still be further enriched by inclusion of additional surface markers, as already suggested above (Discussion 5.2.).

Concerning expression of proliferation-associated genes during MSC derivation, GSEA revealed that several quiescence-related genes (GAS1, GAS7, p27, p57, MXI1) were upregulated at day 0 (Fig. 31, 40), whereas at day 14, genes involved in cell cycle progression and active mitosis (CCNA2, CCNE1, CCNB2, CDK6, CDK7, CDC20, AURKA, PLK1, CHEK, MELK) were upregulated (Fig. 31, 32) **(Malumbres, 2009)**. But also cell cycle inhibitors were expressed at day 14, such as p21 or CDKN3. Both are involved in G1-phase arrest triggered by contact inhibition **(Ritt, 2000)** implying that some cells are still actively cycling, while others are already arrested due to confluence. This outcome is an example of heterogeneities that have to be considered throughout the whole analysis of these microarray results.

In summary, kinetic of cell densities and microarray results demonstrate that *ex vivo* AdSC are quiescent, that adherent cells are selected until day 4 and that proliferation commences around day 6 to day 8 of culture.

5.4.3. Immunophenotype changes during MSC derivation

Summarizing our findings, the major hallmarks in surface marker expression changes during MSC derivation are downregulation of CD34 and upregulation of CD105, CD146, and CD271 (Fig. 22, 23, 25). In addition, CD73 and αSMA were upregulated (Fig. 26+27).

CD105 and αSMA upregulation and CD34 downregulation was confirmed in MScult-cultured AdSC by qPCR (Fig. 25, 41). In contrast, CD271 and CD146 transcription rates remained constant despite increased staining intensities during MSC derivation (Fig. 23, 24, 25). AT-MSC in passage 2, however, were $CD146^-$ and the ratio of CD271 expressing cells was reduced to initial values of about 20% (Fig. 14). Thus, the upregulation of CD146 and CD271 on protein level during MSC derivation seems to be a transient effect, possibly regulated by post-translational modifications or altered protein transport to the membrane. This intermittent upregulation may be of functional relevance for MSC derivation. The changes in surface marker expression were closely associated with onset of proliferation, as measured by proliferation staining using CTV (Fig. 28). In particular, CD105 and CD146 were already upregulated in non-proliferated cells, whereas CD34 was downregulated just after cell division.

CD105 and CD146 are involved in cell attachment, migration and morphology and may be important for AdSC to attach and develop the typical MSC morphology. CD146 (Melanocyte-

cell adhesion molecule, MCAM, Muc18) is associated with tumor progression and metastasis, i.e. contributes to increasing cellular motility **(Zeng, 2011)**. In addition, CD146 is upregulated on BM-MSC as a response to higher oxygen tensions in culture **(Tormin, 2011)**. Thus, CD146 upregulation occurs as a response to higher oxygen concentrations *in vitro*.

CD105 (Endoglin, ENG) promotes cellular attachment and morphological spreading of rat myoblasts **(Guo, 2004)**, while it is a co-receptor of the TGF-β receptor type 2 and is induced upon TGF-β exposure **(Bellon, 1993)**. Interestingly, CD105 signaling was reported to counteract the TGF-β-mediated suppression of proliferation in endothelial cells **(Li, 2000)**. For this aspect, AdSC may upregulate CD105 during MSC derivation upon stimulation by TGF-β which leads to activation and proliferation of AdSC, therefore we can suggest CD105 as activation marker for AT-MSC progenitors.

CD34 downregulation by AT-MSC progenitors is an established fact as shown by several previous reports **(Quirici, 2010; Quirici, 2002; Suga, 2009)**. We demonstrated that CD34 downregulation in *ex vivo* AdSC occurs between d4 to d6 in daughter cells after cell division. The timing and correlation with proliferation is supported by Maumus et al. who have convincingly shown a coinciding delay of proliferation onset and CD34 downregulation under serum-starvation conditions (2% FCS) **(Maumus, 2011)**.

CD34, a Sialomucin surface glycoprotein, is expressed on HSC, EC, cancer stem cells, and tumor stroma amongst others **(Furness, 2006; Malanchi, 2008; Nickoloff, 1991; Watt, 1987)**. CD34 is involved in maintenance of an undifferentiated hematopoietic progenitor pool **(Krause, 1996)** and in lymphocyte adhesion to endothelium **(Baumhueter, 1993)**. Furthermore, myoblasts express CD34 in the quiescent state **(Beauchamp, 2000)**. Interestingly, CD34 is downregulated by activated endothelial cells upon proliferation and simultaneous upregulation of other adhesion molecules such as CD105 **(Delia, 1993)**. Similarly, quiescent AdSC may require CD34 for cell-cell interactions *in vivo* (maybe in their putative niche), but no longer upon activation *in vitro*, when CD34 may even have inhibitory effects on MSC derivation. Consequently, CD34 might be a quiescence marker, being only expressed until cell division.

The transient upregulation of CD271 may be associated with morphological changes during MSC derivation (also discussed in section 5.4.3.). CD271 (low-affinity nerve growth factor receptor, NGFR, p75NTR) is involved in the development of peripheral neurons by

supporting axon outgrowth **(Lee, 1994; Lee, 1992)**. Similarly, CD271 may be involved in filopodia formation by AdSC.

Transcriptome analysis further extended the immunophenotyping insights: at day 0, VCAM1 and CLDN5 were expressed, whereas cultured AdSC were positive for CLDN11, N-Cadherin and ALCAM (Fig. 33).

Claudins are a family of transmembrane proteins that establish tight junctions **(Steed, 2010)**. Expression of CLDN5 and CLDN11 at day 0 and day 14, respectively, reflects that AdSC both *in vivo* and *in vitro* form tight junctions to neighboring cells, but with changing binding partners. The formation of tight junctions was not expected *in vitro*, since loose monolayers were formed. However, colony-like structures are present and occupy denser areas where cells may connect by tight junctions.

MSC are in general be negative for VCAM1 (Vascular cell adhesion molecule-1, CD106), with exception of lineage-committed MSC and MSC from elderly donors **(Lepperdinger, 2011)**. Yet, VCAM1 was recently shown to inhibit the migratory potential of MSC under high cell density conditions **(Nishihira, 2011)**. Thus, in our experiment AdSC may have not reached a sufficiently high cell density at day 14. In addition, the migratory potential of AdSC may have increased after VCAM1 downregulation.

ALCAM (activated leukocyte cell adhesion molecule, CD166) mediates homophilic and heterophilic (with CD6) cell adhesions and was reported to be expressed by MSC **(Gronthos, 2001; Weidle, 2010)**. ALCAM is also involved in neurite extension by neurons, and interacts with CD271 to modulate nerve growth factor (NGF) signaling **(Wade, 2012)**. The exact function of ALCAM on MSC remains to be elucidated; however, similar to CD271, ALCAM may be involved in filopodia formation of MSC.

In summary, immunophenotype kinetic and microarray analysis revealed downregulation of CD34 and Vcam1 as well as upregulation of CD105, CD146, CD271 and ALCAM during MSC derivation.

5.4.4. Morphological changes during MSC derivation

We investigated the morphological development during MSC derivation in detail and in general observed a pronounced change from a round-shaped to a spindle-shaped morphology around day 4 to day 6, irrespective of the culture condition (Fig. 20). This transition was accompanied by increase in cell size. Yet, differences in morphologies

between culture conditions were observed. Besides increased proliferation rates, higher cell numbers were yielded at confluence under ECcult (Fig. 18, 19). MSC form discrete monolayers without overgrowing spheroid clusters, implying that higher cell densities under ECcult are responsible for higher cell counts at confluence. Under MScult, AdSC developed a more flattened-out morphology, whereas a very lean spindle-shaped morphology was observed under ECcult (Fig. 20). Hence, the difference in cell numbers at confluence between MScult and ECcult can hence also be ascribed to a leaner cell morphology allowing for higher cell densities.

The factors involved in the formation of these different morphologies are of interest. Differences in surface marker expression correlated with morphological differences between culture conditions. Under MScult, CD271 was upregulated by AdSC, but downregulated under ECcult, and similarly, also PC downregulated CD271 under ECcult (Fig. 23). In addition, CD146 upregulation was less pronounced under ECcult, but PC maintained their CD146 expression. Finally, the expression intensity of CD105 and CD146 was lower at the end of early culture under ECcult.

CD271 was shown to be involved in axon outgrowth, and hence, may be also involved in filopodia formation by MSC **(Lee, 1994)**. In line with this assumption, we observed less prominent cell body extensions under ECcult, together with a lower expression of CD271.

All in all, it seems obvious that factors in the ECcult medium, EGM-2 – together with gelatin-coating – modulate morphology to a leaner spindle-shaped cell body.

By transcriptome analysis, genes involved in cytoskeletal rearrangement and morphology were found enriched at day 14 (Fig. 32, 40), such as Cytokeratins (KRT7, KRT18), Tropomyosin (TPM1), Myosin X (MYO10), Smoothelin (SMTN) and Pleckstrin-2 (PLEK2). In addition, αSMA was upregulated during MSC derivation (Fig. 41) which is associated with increased motility and stress fiber formation. Cytokeratins are intermediate filaments that locate to the cell membrane and provide stability against mechanical strains **(Kirfel, 2003; Magin, 2007)**. Myosin X is associated with intrafilopodial transport and filopodia formation **(Berg, 2002)**. Tropomyosin is involved in smooth muscle cell contraction and increases cellular motility **(Webb, 2003; Zheng, 2008)**. Smoothelin is specific for smooth muscle cells and involved in formation of filamentous structures such as stress fibers **(van Eys, 1997)**.

Pleckstrin-2 is associated with morphological spreading and induced downstream of PI3K **(Bach, 2007)**.

Kinetic experiments and monitoring of morphology revealed that the MSC-typical fibroblastoid morphology develops during early culture, and is associated with changes in surface marker expression. Differences between culture conditions were observed with ECcult culture resulting in leaner spindle-shaped cell bodies. Expression analysis revealed KRT7, KRT18, TPM1, MYO10, SMTN, PLEK2, αSMA and PODXL to be putative candidates being involved in the morphological changes during MSC derivation.

5.5. Regulation of MSC derivation

The expression data gave insights into signaling pathways and transcription factors regulated during MSC derivation. Active signaling mainly occurs by rapid chemical modifications of different pathway components, e.g. by phosphorylation, and not necessarily by transcription regulation. Thus, from the microarray results only the expression of signaling pathway mediators can be determined.

5.5.1. Early inflammatory response as a trigger of Egr1 expression

Gene sets “Immune Response” and “Response To Wounding” were enriched at day 0 (Fig. 35), since different chemokines were exclusively expressed *ex vivo* in comparison to cultured AdSC (Fig. 35B). These chemokines are all involved in early inflammatory responses as well as recruitment and activation of lymphocytes. For example, TNFSF13B/BAFF regulates B cell proliferation and differentiation, and acts as a T cell co-stimulator **(Huard, 2001; Schneider, 1999)**. TNFRSF13B was shown to be expressed by MSC at low levels and increased after adipogenic differentiation **(Wang, 2011)**. Moreover, CXCL9 is a chemoattractant induced by Interferon-γ **(Rotondi, 2003)**, and in BM-MSC induced after TNF-α stimulation **(Shin, 2010)**. Finally, CCL2 is associated with early inflammation upon injury-induced tissue trauma and results in monocyte, T cell and dendritic cell (DC) recruitment **(Carr, 1994; Xu, 1996)**. Thus, these findings suggest that the harvested *ex vivo* cells already responded towards tissue damage evoked by cell isolation with upregulation of pro-inflammatory cytokines. Consequently, the observed downregulation of pro-inflammatory cytokines during MSC derivation implies that AdSC may acquire low immunogenicity during early culture.

Moreover, *ex vivo* MSC progenitors do not represent the *in vivo* state of MSC progenitors, but rather a pre-activated state.

MSC in vitro are characterized by absence of MHC class II **(Dominici, 2006)**. Yet surprisingly, MHC class II receptors were expressed at day 0 and downregulated at day 14 (Fig. 35C). It was reported that MHC class II expression by MSC *in vitro* is stimulated by IFN-γ or TGF-β signaling, mediators of acute inflammatory responses **(Romieu-Mourez, 2007)**. Hence, the low MHC class II expression may be the result of IFN-γ or TGF-β stimulation and reflect the early activated state after cell isolation.

Supporting this line of argumentation, we found Egr1 (Early Growth Response 1) upregulated already at day 0, and maintained until day 14, albeit at lower levels (Fig. 35). Egr1 is a major pro-proliferative factor and was shown to be rapidly induced upon inflammatory signals **(Cho, 2006)**. In passaged MSC, Egr1 induces production and secretion of other growth factors and receptors **(Tamama, 2013)**. Thus, induction of Egr1 after early immune response may lead to AdSC activation and proliferation as well as expression of growth factors later during MSC derivation.

These results indicate that MSC progenitors are already activated *ex vivo*, probably as a result of tissue damage. Isolation of cells from solid tissues may always trigger inflammatory cascades and it appears hence almost impossible to isolate an “untouched”, not activated MSC progenitor for expression analysis, neither from BM nor AT.

The hypothesis of inflammation-induced AdSC activation may however be challenged by the recent discovery that follicular DCs (fDC) arise from perivascular fDC progenitor cells that express PDGFR-B and VCAM1 **(Krautler, 2012)** and lack expression of CD45 **(Schriever, 1989)**. PDGFR-B and VCAM1 were expressed in AdSC *ex vivo* (Fig. 33, 37) making the presence of fDC progenitors possible. The low expression of MHC class II further supports the notion that antigen-presenting cells contaminate the AdSC population. Moreover, CXCL9 and CCL19 were expressed in $CD271^+$ AdSC, and not in $CD271^-$ AdSC (Fig. 35B). Both CXCL9 and CCL19 are produced by latent or activated DCs **(Muthuswamy, 2010; Ohtani, 2009; Padovan, 2002)**. Furthermore, fDC isolated from tonsils and cultured in fibroblast medium, were also reported to grow plastic adherently and besides showing typical fDC functions, also exhibited MSC-like traits **(Munoz-Fernandez, 2006)**. Together, these facts imply that fDC progenitors may be contained in the AdSC compartment and are responsible – at least in part – for the detection of immune response-like signatures *ex vivo*. fDC progenitors may

also represent MSC progenitors. Future work will identify fDC progenitors in SVF cells and determine their potential role as MSC progenitors. Greatest care must be taken to exclude unwanted cell fractions in future expression analyses.

5. 5.2. Extracellular matrix production and turnover

Expression of ECM compounds decreased during MSC derivation, especially of Laminins and components that are involved in matrix maturation such as Tenascin XB, Lumican and Fibulin. MMP expression was increased at day 14 (Fig. 34), promoting ECM turnover and modulation as well as migration **(Alberts, 2002)**. Collagen expression was mainly maintained, with COL8A2 and COL13A1 being the only collagens expressed only at day 0 and day 14, respectively. Furthermore, upregulation of Fibronectin-1 (FN1) occurred during culture.

Early attachment to the tissue culture surface is mediated by Integrin-binding to FN1 that stems from serum and binds to TCPS by negative charges (mainly hydroxyl groups) **(Curtis, 1983; Steele, 1992)**. The FN1 film then serves as attachment matrix and as scaffold for collagens **(McDonald, 1982)**. The upregulation of FN1 may reflect that serum does not provide sufficient FN1 for proliferating AdSC or additional FN1 is needed after matrix degradation by MMPs. FN1 is also essential for MSC migration *in vitro* **(Veevers-Lowe, 2011)**.

Probably great differences in ECM component transcription can be observed when AT-MSC progenitors at initial early culture, e.g. day 2, are compared with later time points around confluence. AdSC may first increase ECM synthesis, and after an intact and functional ECM has been formed, AdSC reduce ECM production.

De novo production of ECM by AdSC *in vitro* may reflect the generation of a desired niche, which is necessary for long-term culture. However, this niche may not be identical to the *in vivo* niche, since communication with neighboring cells and appropriate growth factor signaling are missing in the *in vitro* niche, which may support activation of MSC progenitors and an altered immunophenotype.

5.5.3. Dkk1 suppresses WNT signaling

According to the GSEA results, WNT signaling appeared more active at day 0. Ligand expression switched from WNT11 to WNT5A, and receptor expression shifted from FZD4 and FZD5 to FZD2 and FZD6 (Fig. 36). Most importantly however was the upregulation of the

WNT signaling inhibitor, Dkk1 (Dickkopf-1) occurring already early during MSC derivation (Fig. 41).

Previous studies have shown that Dkk1 is necessary for MSC expansion *in vitro* **(Gregory, 2003; Horwitz, 2004)**. Prockop and colleagues have intensively investigated the role of Dkk1 during MSC expansion in later passages. They have identified Dkk1 as pivotal for undifferentiated expansion of MSCs by inhibiting the canonical Wnt/b-catenin signaling pathway that would otherwise induce differentiation **(Larson, 2008)**. Dkk1 interacts with Lrp5/6 and Kremen1/2 to antagonize WNT signaling **(Bao, 2012)**. These Dkk1 binding partners were indeed downregulated by AdSC. Supporting this observation, Prockop et al. have also demonstrated downregulation of Lrp5/6 and Dkk1 during expansion of MSC **(Gregory, 2003)**. Accordingly, Dkk1 is expressed during the early and intermediate phase together with its receptor Lrp6. Near confluence, Dkk1 and Lrp5/6 were not expressed but WNT-5a was upregulated to suppress proliferation. Our results confirm this kinetic of Dkk1 expression, but for the first time, directly during initial culture of *ex vivo* AT-MSC progenitors.

5.5.4. Autocrine PDGF signaling

PDGF signaling signatures were more enriched at day 0 of MSC derivation (Fig. 37). However, both PDGF-receptors PDGFR-A and PDGFR-B were expressed constantly, yet slightly downregulated at day 14, and neither PDGF-A nor PDGF-B were expressed by AdSC. More obvious was a shift from PDGF-D to PDGF-C expression.

The family of platelet-derived growth factors consists of four different types, namely PDGF-A, PDGF-B, PDGF-C and PDGF-D that form homo- and heterodimers (AA, BB, CC, DD, AB). PDGF-A and PDGF-B are intracellularly processed and secreted. In contrast, PDGF-C and PDGF-D are secreted with a CUB domain that renders them inactively bound to the ECM **(Andrae, 2008)**. The CUB domain is cleaved off by e.g. tissue plasminogen activator (TPA) which was expressed constantly by AdSC (not shown) and reportedly by MSC **(Neuss, 2010)**. Thereby, AT-MSC are enabled for autocrine/juxtacrine PDGF signaling. PDGF-C induces proliferation in murine embryonic palatal mesenchymal cells **(Han, 2006)**. In addition, PDGF-C was shown to be induced via an Egr1-mediated pathway **(Midgley, 2004)**. We have already described that Egr1 may play a pivotal role in regulating growth factor secretion during MSC derivation. Thus, the induction of PDGF-C may be a result of Egr1 activity.

In contrast to our results, Caplan et al. suggested PDGF-BB as a major trigger for MSC activation **(Caplan, 2011b)**. PDGF-BB was expressed neither by MSC progenitors nor by MSC at confluence, which excludes autocrine signaling by PDGF-BB, but PDGF-BB might be present in the serum.

5.5.5. CD105 upregulation and TGF-β signaling

We have also investigated the role of TGF-β signaling during MSC derivation (Fig. 38). The major components of the TGF-β signaling cascade were only marginally regulated. Yet, we observed upregulation of CD105 which has a complex role in TGF-β signaling. As a co-receptor of the TGF-β type II receptor, CD105 can antagonize the TGF-β-mediated suppression of cell proliferation **(Li, 2000)**. Thereby, the upregulation of CD105 may change the effect that the constantly active TGF-β signaling has on AdSC proliferation.

5.5.5. Sprouty may inhibit FGF signaling *in vivo*

FGF signaling signatures were enriched at day 14 of culture (Fig. 39). FGF2 was constantly expressed which may be correlated with its pivotal function in maintaining multipotency in MSC **(Tsutsumi, 2001)**. Growth factor signaling *in vivo* was probably inhibited by SPRY1/2 (Sprouty-1 and Sprouty-2) expression. SPRY1/2 are intracellular regulators of Ras-dependent MAPK signaling and inhibit the recruitment of Grb2 or Shp2 to the receptor **(Hanafusa, 2002)**, resulting in suppression of proliferation **(Lee, 2010)**. Consequently, Sprouty-1 plays a major role in the regulation of reversible muscle satellite cell quiescence **(Shea, 2009)**. Similarly, by blocking FGF signaling *in vivo*, Sprouty-1 may keep AdSC quiescent.

FGF5 was upregulated at day 14. FGF5 is a potent monogenic and antigenic growth factor **(Clase, 2000)** and also induces connective tissue fibroblast expansion **(Clase, 2000)**. FGF1 signaling via FGFR1 was implicated in early adipogenesis and involved in maintaining the pre-adipocyte progenitor pool **(Widberg, 2009)**. Hence, FGF1 and FGF5 expression may be upregulated by AdSC as response to activation, and to preserve the pre-adipocyte characteristics and plasticity *in vitro*.

5.5.7. Gremlins may suppress BMP signaling during MSC derivation

Expression of different BMP signaling ligands, receptor and mediators was also detected by microarray, but not taken into account, since no BMP-related gene set was clearly enriched during MSC derivation. However, looking at BMP genes in detail revealed that BMP receptor 1 and 2 were expressed throughout MSC derivation. As ligands only BMP8 was expressed constantly whereas BMP4 was only weakly present at day 0 (data not shown). Gremlin-1 and Gremlin-2 (Grem1, Grem2), potent antagonists of BMP signaling, were upregulated early during MSC derivation (Fig. 41). Grem1 specifically inhibits BMP4 signaling **(Gazzerro, 2006)**. Furthermore, Grem1-dependent inhibition of BMP signaling was pivotal for FGF induction and fibrosis **(Farkas, 2010)**. Most interestingly, however, Grem1 is overexpressed in a variety of cancers and induces proliferation and increases invasiveness of cancer cell lines in a BMP-independent manner **(Kim, 2012; Namkoong, 2006)**. In other words, Grem1 induces epithelial-to-mesenchymal transition in cancer cells.

BMPs are in general involved in induction of differentiation **(Gazzerro, 2006)**. However, due to Grem1 and Grem2 expression during MSC derivation, BMP signaling was inhibited, enabling undifferentiated expansion of MSC progenitors.

In summary, our analysis revealed pivotal roles for WNT, PDGF, TGF-β, and FGF signaling during AT-MSC derivation. WNT signaling is repressed by Dkk1 to allow for induction of proliferation and migration by PDGF, TGF, and FGF signaling *in vitro*. Egr1 expression may link early activation to changes in growth factor signaling.

Kuznetsov et al. have determined which growth factors are necessary for efficient BM-MSC derivation **(Kuznetsov, 1997)**. A mix of five growth factors including TGF-β, PDGF-AB, EGF, FGF-2 and IGF-1 in serum-free medium stimulated MSC derivation of mouse marrow cells, but not of human marrow cells. This implicates that other factors, maybe PDGF-C as we suggest here, are involved in human MSC derivation. Determination of the different temporal roles of growth factors during MSC derivation will be the aim of future investigations.

5.5.8. Transcription factors regulated during MSC derivation

Several transcription factors were regulated during MSC derivation, as determined by microarray and confirmed by qPCR (Fig. 41). Gata6 was the only GATA family member

expressed. Gata6 is associated with proliferation arrest and hypertrophy in cardiomyocytes **(Liang, 2001; Morrisey, 2000)**. Notably, Gata6 also represses Dkk1 expression **(Zhong, 2011)**. Thus, Gata6 may play a role in proliferation arrest *ex vivo* and in MSC derivation. On the one hand, during MSC derivation, Gata6 was transiently downregulated at day 5, the time point where Dkk1 was induced and proliferation commenced. On the other hand, Gata6 was again upregulated when proliferation ceased and subsets of AdSC acquired huge and flattened out morphologies, resembling hypertrophic cells. Yet, the precise role of Gata6 in MSC derivation has to be analyzed further.

Sox17 was downregulated during MSC derivation already at day 5. Sox17 was discovered as a marker for vascular stem cells **(Tang, 2012)** and is a transcriptional repressor of Cyclin D1 and other cell cycle-promoting genes **(Chew, 2011)**.Hence, AdSC may be retained in a quiescent state *in vivo* by Sox17 expression. Conversely, FoxM1 was upregulated early during MSC derivation. FoxM1 acts as a transcriptional activator of proliferation by inducing several S/G2-phase transition-promoting genes **(Laoukili, 2005)**. In addition, FoxM1 was reported to be capable of inducing EMT in tumor cells **(Bao, 2011)**. FoxO1A was transiently downregulated but returned to initial values. FoxO1 is expressed in the major insulin-responsive tissues, such as liver, adipose tissue and pancreas, and was associated with prevention of adipogenesis in pre-adipocytes **(Nakae, 2003)**. Moreover, FoxO1 induces p21 **(Nakae, 2003)**, a cell cycle inhibitor also upregulated in confluent AdSC. This suggests that FoxO1 is also involved in cell cycle regulation during MSC derivation.

Finally, we found Rex1 to be upregulated already at day 5 and then maintained during MSC derivation. Rex1 (Reduced Expression Gene 1; ZFP42, Zinc Finger Protein 42) is expressed in ES cells and associated with, yet dispensable for pluripotency **(Masui, 2008; Scotland, 2009)**. Furthermore, Rex1 was shown to be expressed by MSC and was critical for MSC proliferation **(Bhandari, 2010)**. In addition, Rex1 may play a role in epigenetic setting during spermatogenesis and early embryogenesis **(Kim, 2011)**.

We speculate that Rex1 upregulation during MSC derivation is associated not only with positive regulation of proliferation, but also with epigenetic modifications. These would be necessary to endow AdSC with stem cell-like traits. In other words, Rex1 may be the mediator of de-differentiation of AdSC into MSC-like cells during MSC derivation.

5.5.9. Epithelial-to-Mesenchymal-Transition

Epithelial-to-mesenchymal-transition (EMT) is defined as the transition from an epithelial to a mesenchymal cell phenotype. EMT is an evolutionary conserved process centrally involved in embryogenesis of vertebrates and invertebrates, and in cancer metastasis **(Cano, 2000; Thiery, 2006)**. In principal, EMT endows a previously epithelial cell with the potential to migrate and invade into other regions and tissues. Epithelial cells are characterized by an apical-basolateral polarization with strong intercellular connections, e.g. tight junctions, and strong contact to the basal lamina. In contrast, mesenchymal cells are not rigidly embedded in the surrounding tissue, but contact neighboring cells and extracellular matrix by flexible formation of focal adhesions **(Potenta, 2008)**.

During EMT, E-cadherin and other epithelial-specific cell-adhesion molecules and structural proteins, such as Claudins, Occludins and Cytokeratin-8, -9 and -18 are downregulated **(Zeisberg, 2009)**. Simultaneously, mesenchymal transcripts are upregulated such as N-cadherin, Fibronectin, Vimentin, Smooth muscle actin and FGF-Receptors. Main transcription factors of EMT are Snail (SNAI1), Slug (SNAI2) and Twist. EMT can be induced by several extracellular signals, including WNT, BMP and TGF-β signaling.

MSC derivation was overall reminiscent of EMT including the transition from an epithelial to a mesenchymal morphology accompanied by the onset of proliferation. Furthermore, the EMT-related genes N-Cadherin and αSMA were upregulated (Fig. 40, 41). In contrast, the central EMT transcription factors Snail (SNAI1) and Slug (SNAI2) exhibited an unclear expression pattern, being either up or downregulated during MSC derivation. This aspect has to be further validated. Nonetheless, we wanted to discuss EMT and its role in stem cell biology in detail.

Involvement of EMT and its reversion, mesenchymal-epithelial transition (MET) in stem cell biology was already reported. On the one hand, MET occurs early in the generation of iPS cells by ectopic expression of Oct-4, Sox2, KLF4 and c-Myc, as proven by Snail downregulation and E-cadherin upregulation; accordingly, pluripotent cells are considered rather epithelial than mesenchymal **(Samavarchi-Tehrani)**. In other contexts, EMT endows epithelial cells with stem-like properties, as reported for murine mammary epithelial cells **(Mani, 2008)**.

With the perivascular origin of MSC progenitors in mind, a recent report by Medici et al. focusing on Fibrodysplasia ossificans progressiva (FOP) is of high interest. The FOP-typical ectopic bone formations were demonstrated to be derived from endothelial cells in a murine model. *In vitro*, endothelial cell lines differentiated into chondrogenic or osteogenic cell types after EMT **(Medici, 2010)**. Similarly, transfection of endothelial cell lines with SNAI1-expressing vectors induced EMT and a conversion towards an MSC-like cell type with full differentiation potential **(Battula, 2010)**. Concerning our results, it might be that fibroblast-like MSC progenitors undergo partial EMT, accompanied by e.g. REX1 upregulation, which endows them with greater plasticity.

Together, in line with previous studies, our data underscore a potential role of EMT during MSC derivation and the acquisition of stem cell-like traits by MSC progenitors.

5.6. Summary and Conclusion

This study was conducted to understand how MSC progenitors adapt to *in vitro* culture conditions and develop into MSC. We identified two subsets of AT-MSC progenitors, namely $CD34^+$ $CD31^-$ $CD271^{+/-}$ AdSC and $CD34^-$ $CD31^-$ $CD146^+$ $CD271^{+/-}$ PC. The MSC derivation phase was investigated for the first time in great detail focusing on immunophenotype, morphology, and gene expression regulations of especially AdSC. Transcriptome analysis was conducted using microarray to compare *ex vivo* AdSC and derived AT-MSC. Thereby, we confirmed observations from the kinetic analyses and identified different cellular processes and growth factor signaling pathways governing MSC derivation.

The key findings are summarized in the following:

- **Culture-dependence of MSC derivation**

  The two MSC progenitor cell types, AdSC and PC gave rise to equally potent MSC with similar proliferation and differentiation capacity. However, MSC derivation from PC was restricted to ECcult. In contrast, AdSC proliferated under MScult and even faster under ECcult, and can thus be regarded as the more clonogenic MSC progenitor cell type.

- **Immunophenotype changes and proliferation during MSC derivation**

  Our kinetic analysis of the early culture phase revealed that CD34 downregulation and CD105, CD146 and CD271 upregulation coincided with the first round of cell division. According to the microarray results, *ex vivo* cells exhibited features of quiescent cells and proliferation-related transcripts were induced during culture. Thus, CD34 may mark quiescent cells *in vivo*, while CD105 may serve as an activation marker for MSC progenitors *in vitro*.

- **Morphological changes during MSC derivation**

  MSC progenitors *ex vivo* are small and round-shaped, and develop into fibroblastoid cells around day 4 to day 6 of culture. Cytoskeletal components were identified as candidate genes involved in the development of this MSC-typical morphology.

  Moreover, ECcult culture resulted in cells with leaner spindle-shaped morphology, whereas MScult-cultured MSC exhibited more filopodia and a more spread-out

morphology. These differences may correlate with differences in expression of adhesion molecules CD105, CD146 and CD271.

- **Early response to injury**

  Microarray results indicated that MSC progenitors *ex vivo* expressed injury / cell isolation-induced chemoattractants for lymphocytes and progenitor cells. This initial trigger may lead to expression of Egr1, the putative major mediator of proliferation and growth factor expression during MSC derivation.

- **Modulation of ECM production**

  Production of extracellular matrix is altered during culture. Basal lamina-specific Laminins were downregulated, while fibronectin, required for adhesion *in vitro*, was upregulated. These changes probably represent the generation of an adequate matrix for *in vitro* culture, resembling the formation of a novel niche *in vitro*.

- **Modulation of growth factor signaling**

  Involvement of different signaling cascades was suggested by the expression analysis. In particular, FGF signaling *in vivo* may be suppressed by expression of Sprouty, but takes over an essential role *in vitro* as represented by Sprouty downregulation and Fgf-1 and Fgf-5 upregulation. BMP signaling may be active *in vivo*, but following quick induction of Gremlin, a potent BMP inhibitor, is suppressed *in vitro*. CD105 upregulation during MSC derivation may alter the responsiveness to TGF-β signaling. Finally, WNT signaling maintains AdSC in a dormant state *in vivo*, but is inhibited *in vitro* by increased expression of Dkk1.

- **Transcription factors involved in MSC derivation**

  Transcription factor FoxD1 and Sox17 characterized AdSC *ex vivo* and negatively regulate cell cycle progression. In contrast, FoxM1, Egr1 and Rex1 may be the essential drivers of proliferation during MSC derivation. Last but not least, the upregulation of Rex1 may implicate that epigenetic modifications occur that are associated with de-differentiation.

Based on these findings, we want to propose a model for the MSC derivation process, here described for bulk SVF cells cultured under MScult (Fig. 43):

Firstly, isolation of EC, PC and AdSC from adipose tissue mimics tissue injury and results in inflammatory responses followed by Egr1 induction. Egr1 is a potent trigger of cell proliferation, migration and growth factor production, and thus, may play a pivotal role in MSC derivation.

Secondly, as the next step, SVF cells are plated and a minor fraction of bulk-cultured SVF cells attach as round-shaped cells with small diameters. At day 2, more AdSC and PC can be detected compared to EC and $CD45^+$ lymphocytes. Attached cells further reduce in number until d4. This initial cell loss represents the functional selection of cells capable to attach to tissue culture plastic. This adhesion potential requires ECM production by individual cells, but in return attachment also regulates ECM production.

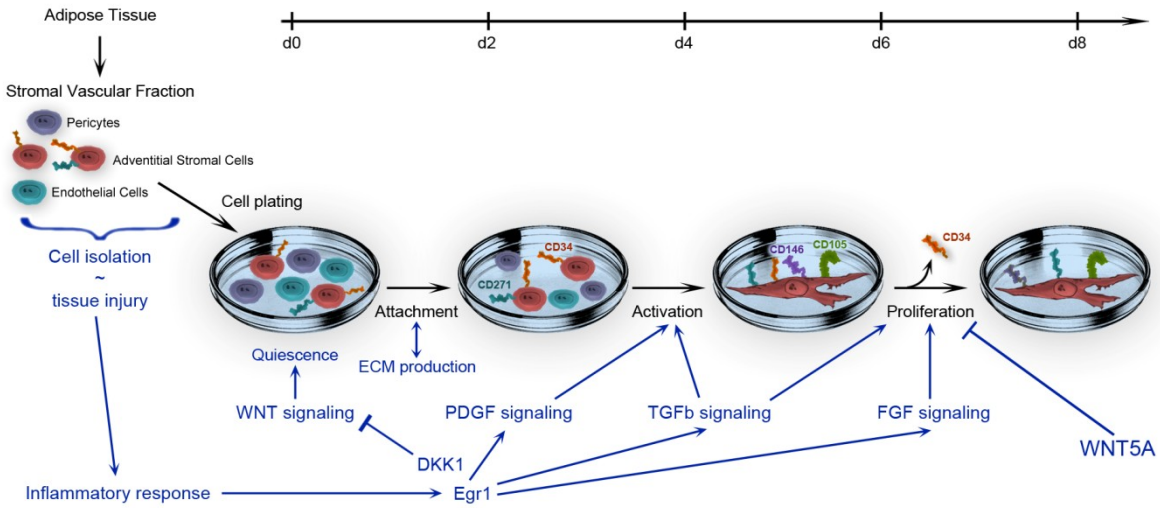

Figure 43: Proposed model for the MSC derivation process.
The scheme depicts the central events in the MSC derivation process under MScult between d0 to d8. Detailed explanation provided in the text. Hypothetical processes concluded from microarray are depicted in blue. Scheme modified from **(Braun, 2012)**.

Thirdly, at day 4 and later, AdSC acquire a spindle-shaped morphology with increased cell diameters, and upregulate CD105 and CD146. This coincidence of morphological changes and upregulation of especially CD105 can be interpreted as a sign of cellular activation. This activation may be a result of the initial inflammatory respose but may be further regulated by a multitude of signals. For example, TGF-β signaling via CD105 and PDGF signaling induced by Egr1 may further promote cell cycle entry, i.e. activation; WNT and BMP signaling suppression by Dkk1 and Gremlin, respectively, may enable undifferentiated proliferation.

Finally, from day 6 on, AdSC proliferate vigorously, daughter cells downregulate CD34, and thus eventually exhibit the typical MSC immunophenotype. At confluence, MSC undergo cell cycle arrest.

This model is based on our kinetic and microarray analysis, however, different aspects of this model will have to be verified by future experiments, e.g. by knock-down of different genes like Dkk1, Gremlin, etc.

This study provides the first detailed analysis of the early *in vitro* culture phase, the MSC derivation phase of MSC progenitors, in particular AT-MSC progenitors. We identified phenotypic conversions of MSC progenitors during early culture which are associated with activation and proliferation.

Activation of MSC progenitors was preceded by inflammatory response-like signatures *ex vivo* which may be triggered by cell isolation. In recent publications, Caplan et al. have postulated for the *in vivo* situation that activation upon injury or inflammation may be the essential, initial trigger for perivascular cells to become 'medicinal signaling cells', MSC **(Caplan, 2011a**, **b)**. Referring to Caplan et al., we speculate that the *in vitro* processes mimic *in vivo* activation of perivascular cells upon wounding or inflammation. Yet, appropriate controlling signals provided by the healing surrounding are lacking *in vitro*, which may lead to a partly artificial *in vitro* cell type.

In the course of the MSC derivation process, multipotency may also be acquired. The upregulation of the transcription factor Rex1 suggests that epigenetic modifications occur, which may be associated with de-differentiation of stromal vascular cells into their mesenchymal progenitors **(Roobrouck, 2011)**. Previous works have described higher adipogenic differentiation efficiencies for SVF cells cultured *ex vivo* in the absence of FBS **(Entenmann, 1996; Hauner, 1989)** suggesting that growth factors contained in FBS might further promote de-differentiation.

The MSC derivation process can be assumed to be similar for MSC from different tissues, since they are all derived from perivascular cells **(Crisan, 2008)**. Different tissue-specific stem/progenitor cells reside in perivascular niches, and for example, especially the adventitia in adipose tissue harbors several types of progenitor cells such as smooth muscle cell progenitors, adipocyte progenitors and fDC progenitors **(Tallone, 2011)**. Hence, MSC

may be derived from some of these progenitors, and therefore MSC in culture exhibit vast heterogeneity concerning differentiation potential and proliferative capacity **(Bianco, 2008)**.

All in all, different hypotheses exist about the origin of MSC in different tissues, based on evidences favoring either MSC progenitors as true stem/progenitor cells or MSC as *in vitro* artifacts. Our data indicate that both may be true: tissue-specific progenitor cells undergo culture-dependent de-differentiation, thereby acquire a broader differentiation spectrum and develop into MSC-like cells with tissue-specific minor differences.

This new perspective offers also new strategies for therapeutic applications. As before can in *vitro* cultured MSC be used in cell therapies, but the tissue-specific differences should now be considered as well. In the one clinical setting, it may be advantageous to utilize MSC from BM or AT, whereas MSC from placenta may have better effects in treatment of another disease. In addition, our findings suggest that also *ex vivo* cells may be useful in therapies. Application of less potent, tissue-specific progenitors may lead to improved clinical outcomes. It may even be possible to isolate one specific progenitor type needed in a respective condition. However, to this end, characterization of tissue-specific progenitors will have to be further improved, and a clear comparison of their potencies will be needed.

6. References

Alberts, B. (2002). Molecular biology of the cell, 4th edn (New York, Garland Science).

Andrae, J., Gallini, R., and Betsholtz, C. (2008). Role of platelet-derived growth factors in physiology and medicine. Genes Dev *22*, 1276-1312.

Anghileri, E., Marconi, S., Pignatelli, A., Cifelli, P., Galie, M., Sbarbati, A., Krampera, M., Belluzzi, O., and Bonetti, B. (2008). Neuronal differentiation potential of human adipose-derived mesenchymal stem cells. Stem Cells Dev *17*, 909-916.

Antonitsis, P., Ioannidou-Papagiannaki, E., Kaidoglou, A., Charokopos, N., Kalogeridis, A., Kouzi-Koliakou, K., Kyriakopoulou, I., Klonizakis, I., and Papakonstantinou, C. (2008). Cardiomyogenic potential of human adult bone marrow mesenchymal stem cells in vitro. Thorac Cardiovasc Surg *56*, 77-82.

Augello, A., Kurth, T.B., and De Bari, C. (2010). Mesenchymal stem cells: a perspective from in vitro cultures to in vivo migration and niches. Eur Cell Mater *20*, 121-133.

Bach, T.L., Kerr, W.T., Wang, Y., Bauman, E.M., Kine, P., Whiteman, E.L., Morgan, R.S., Williamson, E.K., Ostap, E.M., Burkhardt, J.K.*, et al.* (2007). PI3K regulates pleckstrin-2 in T-cell cytoskeletal reorganization. Blood *109*, 1147-1155.

Bai, L., Lennon, D.P., Eaton, V., Maier, K., Caplan, A.I., Miller, S.D., and Miller, R.H. (2009). Human bone marrow-derived mesenchymal stem cells induce Th2-polarized immune response and promote endogenous repair in animal models of multiple sclerosis. Glia *57*, 1192-1203.

Banas, A., Teratani, T., Yamamoto, Y., Tokuhara, M., Takeshita, F., Osaki, M., Kato, T., Okochi, H., and Ochiya, T. (2009). Rapid hepatic fate specification of adipose-derived stem cells and their therapeutic potential for liver failure. J Gastroenterol Hepatol *24*, 70-77.

Bao, B., Wang, Z., Ali, S., Kong, D., Banerjee, S., Ahmad, A., Li, Y., Azmi, A.S., Miele, L., and Sarkar, F.H. (2011). Over-expression of FoxM1 leads to epithelial-mesenchymal transition and cancer stem cell phenotype in pancreatic cancer cells. J Cell Biochem *112*, 2296-2306.

Bao, J., Zheng, J.J., and Wu, D. (2012). The structural basis of DKK-mediated inhibition of Wnt/LRP signaling. Sci Signal *5*, pe22.

Bartholomew, A., Sturgeon, C., Siatskas, M., Ferrer, K., McIntosh, K., Patil, S., Hardy, W., Devine, S., Ucker, D., Deans, R.*, et al.* (2002). Mesenchymal stem cells suppress lymphocyte proliferation in vitro and prolong skin graft survival in vivo. Exp Hematol *30*, 42-48.

Battula, V.L., Evans, K.W., Hollier, B.G., Shi, Y., Marini, F.C., Ayyanan, A., Wang, R.Y., Brisken, C., Guerra, R., Andreeff, M.*, et al.* (2010). Epithelial-mesenchymal transition-derived cells exhibit multilineage differentiation potential similar to mesenchymal stem cells. Stem Cells *28*, 1435-1445.

Baumhueter, S., Singer, M.S., Henzel, W., Hemmerich, S., Renz, M., Rosen, S.D., and Lasky, L.A. (1993). Binding of L-selectin to the vascular sialomucin CD34. Science *262*, 436-438.

Beauchamp, J.R., Heslop, L., Yu, D.S., Tajbakhsh, S., Kelly, R.G., Wernig, A., Buckingham, M.E., Partridge, T.A., and Zammit, P.S. (2000). Expression of CD34 and Myf5 defines the majority of quiescent adult skeletal muscle satellite cells. J Cell Biol *151*, 1221-1234.

Bellon, T., Corbi, A., Lastres, P., Cales, C., Cebrian, M., Vera, S., Cheifetz, S., Massague, J., Letarte, M., and Bernabeu, C. (1993). Identification and expression of two forms of the human transforming growth factor-beta-binding protein endoglin with distinct cytoplasmic regions. Eur J Immunol *23*, 2340-2345.

Berg, J.S., and Cheney, R.E. (2002). Myosin-X is an unconventional myosin that undergoes intrafilopodial motility. Nat Cell Biol *4*, 246-250.

Bhandari, D.R., Seo, K.W., Roh, K.H., Jung, J.W., Kang, S.K., and Kang, K.S. (2010). REX-1 expression and p38 MAPK activation status can determine proliferation/differentiation fates in human mesenchymal stem cells. PLoS One *5*, e10493.

Bianco, P., Robey, P.G., and Simmons, P.J. (2008). Mesenchymal stem cells: revisiting history, concepts, and assays. Cell Stem Cell *2*, 313-319.

Boquest, A.C., Shahdadfar, A., Fronsdal, K., Sigurjonsson, O., Tunheim, S.H., Collas, P., and Brinchmann, J.E. (2005). Isolation and transcription profiling of purified uncultured human stromal stem cells: alteration of gene expression after in vitro cell culture. Mol Biol Cell *16*, 1131-1141.

Braun, J., Hack, A., Weis-Klemm, M., Conrad, S., Treml, S., Kohler, K., Walliser, U., Skutella, T., and Aicher, W.K. (2010). Evaluation of the osteogenic and chondrogenic differentiation capacities of equine adipose tissue-derived mesenchymal stem cells. Am J Vet Res *71*, 1228-1236.

Braun, J., Kurtz, A., Barutcu, N., Bodo, J., Thiel, A., and Dong, J. (2012). Concerted Regulation of CD34 and CD105 Accompanies Mesenchymal Stromal Cell Derivation from Human Adventitial Stromal Cell. Stem Cells Dev.

Brizzi, M.F., Tarone, G., and Defilippi, P. (2012). Extracellular matrix, integrins, and growth factors as tailors of the stem cell niche. Curr Opin Cell Biol *24*, 645-651.

Campagnolo, P., Cesselli, D., Al Haj Zen, A., Beltrami, A.P., Krankel, N., Katare, R., Angelini, G., Emanueli, C., and Madeddu, P. (2010). Human adult vena saphena contains perivascular progenitor cells endowed with clonogenic and proangiogenic potential. Circulation *121*, 1735-1745.

Cano, A., Perez-Moreno, M.A., Rodrigo, I., Locascio, A., Blanco, M.J., del Barrio, M.G., Portillo, F., and Nieto, M.A. (2000). The transcription factor snail controls epithelial-mesenchymal transitions by repressing E-cadherin expression. Nat Cell Biol *2*, 76-83.

Caplan, A.I. (1991). Mesenchymal stem cells. J Orthop Res *9*, 641-650.

Caplan, A.I. (1994). The mesengenic process. Clin Plast Surg *21*, 429-435.

Caplan, A.I. (2009). Why are MSCs therapeutic? New data: new insight. J Pathol *217*, 318-324.

Caplan, A.I., and Correa, D. (2011a). The MSC: an injury drugstore. Cell Stem Cell *9*, 11-15.

Caplan, A.I., and Correa, D. (2011b). PDGF in bone formation and regeneration: new insights into a novel mechanism involving MSCs. J Orthop Res *29*, 1795-1803.

Carr, M.W., Roth, S.J., Luther, E., Rose, S.S., and Springer, T.A. (1994). Monocyte chemoattractant protein 1 acts as a T-lymphocyte chemoattractant. Proc Natl Acad Sci U S A *91*, 3652-3656.

Chakkalakal, J.V., Jones, K.M., Basson, M.A., and Brack, A.S. (2012). The aged niche disrupts muscle stem cell quiescence. Nature *490*, 355-360.

Chew, L.J., Shen, W., Ming, X., Senatorov, V.V., Jr., Chen, H.L., Cheng, Y., Hong, E., Knoblach, S., and Gallo, V. (2011). SRY-box containing gene 17 regulates the Wnt/beta-catenin signaling pathway in oligodendrocyte progenitor cells. J Neurosci *31*, 13921-13935.

Cho, S.J., Kang, M.J., Homer, R.J., Kang, H.R., Zhang, X., Lee, P.J., Elias, J.A., and Lee, C.G. (2006). Role of early growth response-1 (Egr-1) in interleukin-13-induced inflammation and remodeling. J Biol Chem *281*, 8161-8168.

Choi, S.H., Kong, H.K., Park, S.Y., and Park, J.H. (2009). Metastatic effect of LY-6K gene in breast cancer cells. Int J Oncol *35*, 601-607.

Clase, K.L., Mitchell, P.J., Ward, P.J., Dorman, C.M., Johnson, S.E., and Hannon, K. (2000). FGF5 stimulates expansion of connective tissue fibroblasts and inhibits skeletal muscle development in the limb. Dev Dyn *219*, 368-380.

Corselli, M., Chen, C.W., Crisan, M., Lazzari, L., and Peault, B. (2010). Perivascular ancestors of adult multipotent stem cells. Arterioscler Thromb Vasc Biol *30*, 1104-1109.

Corselli, M., Chen, C.W., Sun, B., Yap, S., Rubin, J.P., and B, P.A. (2011). The Tunica Adventitia of Human Arteries and Veins as a Source of Mesenchymal Stem Cells. Stem Cells Dev.

Costa, G., Kouskoff, V., and Lacaud, G. (2012). Origin of blood cells and HSC production in the embryo. Trends Immunol *33*, 215-223.

Covas, D.T., Panepucci, R.A., Fontes, A.M., Silva, W.A., Jr., Orellana, M.D., Freitas, M.C., Neder, L., Santos, A.R., Peres, L.C., Jamur, M.C.*, et al.* (2008). Multipotent mesenchymal stromal cells obtained from diverse human tissues share functional properties and gene-expression profile with CD146+ perivascular cells and fibroblasts. Exp Hematol *36*, 642-654.

Crisan, M., Yap, S., Casteilla, L., Chen, C.W., Corselli, M., Park, T.S., Andriolo, G., Sun, B., Zheng, B., Zhang, L.*, et al.* (2008). A perivascular origin for mesenchymal stem cells in multiple human organs. Cell Stem Cell *3*, 301-313.

Curtis, A.S., Forrester, J.V., McInnes, C., and Lawrie, F. (1983). Adhesion of cells to polystyrene surfaces. J Cell Biol *97*, 1500-1506.

da Silva Meirelles, L., Sand, T.T., Harman, R.J., Lennon, D.P., and Caplan, A.I. (2009). MSC frequency correlates with blood vessel density in equine adipose tissue. Tissue Eng Part A *15*, 221-229.

Darrah, P.A., Patel, D.T., De Luca, P.M., Lindsay, R.W., Davey, D.F., Flynn, B.J., Hoff, S.T., Andersen, P., Reed, S.G., Morris, S.L.*, et al.* (2007). Multifunctional TH1 cells define a correlate of vaccine-mediated protection against Leishmania major. Nat Med *13*, 843-850.

de Bruijn, M.F., Speck, N.A., Peeters, M.C., and Dzierzak, E. (2000). Definitive hematopoietic stem cells first develop within the major arterial regions of the mouse embryo. EMBO J *19*, 2465-2474.

Delia, D., Lampugnani, M.G., Resnati, M., Dejana, E., Aiello, A., Fontanella, E., Soligo, D., Pierotti, M.A., and Greaves, M.F. (1993). CD34 expression is regulated reciprocally with adhesion molecules in vascular endothelial cells in vitro. Blood *81*, 1001-1008.

Dezawa, M., Ishikawa, H., Itokazu, Y., Yoshihara, T., Hoshino, M., Takeda, S., Ide, C., and Nabeshima, Y. (2005). Bone marrow stromal cells generate muscle cells and repair muscle degeneration. Science *309*, 314-317.

Di Nicola, M., Carlo-Stella, C., Magni, M., Milanesi, M., Longoni, P.D., Matteucci, P., Grisanti, S., and Gianni, A.M. (2002). Human bone marrow stromal cells suppress T-lymphocyte proliferation induced by cellular or nonspecific mitogenic stimuli. Blood *99*, 3838-3843.

Doan, P.L., and Chute, J.P. (2012). The vascular niche: home for normal and malignant hematopoietic stem cells. Leukemia *26*, 54-62.

Dominici, M., Le Blanc, K., Mueller, I., Slaper-Cortenbach, I., Marini, F., Krause, D., Deans, R., Keating, A., Prockop, D., and Horwitz, E. (2006). Minimal criteria for defining multipotent mesenchymal stromal cells. The International Society for Cellular Therapy position statement. Cytotherapy *8*, 315-317.

Driskell, R.R., Clavel, C., Rendl, M., and Watt, F.M. (2011). Hair follicle dermal papilla cells at a glance. J Cell Sci *124*, 1179-1182.

Entenmann, G., and Hauner, H. (1996). Relationship between replication and differentiation in cultured human adipocyte precursor cells. Am J Physiol *270*, C1011-1016.

Farkas, L., Farkas, D., Gauldie, J., Warburton, D., Shi, W., and Kolb, M. (2010). Transient overexpression of Gremlin results in epithelial activation and reversible fibrosis in rat lungs. Am J Respir Cell Mol Biol *44*, 870-878.

Friedenstein, A.J., Deriglasova, U.F., Kulagina, N.N., Panasuk, A.F., Rudakowa, S.F., Luria, E.A., and Ruadkow, I.A. (1974). Precursors for fibroblasts in different populations of hematopoietic cells as detected by the in vitro colony assay method. Exp Hematol *2*, 83-92.

Friedenstein, A.J., Latzinik, N.V., Gorskaya Yu, F., Luria, E.A., and Moskvina, I.L. (1992). Bone marrow stromal colony formation requires stimulation by haemopoietic cells. Bone Miner *18*, 199-213.

Friedenstein, A.J., Piatetzky, S., II, and Petrakova, K.V. (1966). Osteogenesis in transplants of bone marrow cells. J Embryol Exp Morphol *16*, 381-390.

Frisbie, D.D., Kisiday, J.D., Kawcak, C.E., Werpy, N.M., and McIlwraith, C.W. (2009). Evaluation of adipose-derived stromal vascular fraction or bone marrow-derived mesenchymal stem cells for treatment of osteoarthritis. J Orthop Res *27*, 1675-1680.

Fukuchi, Y., Nakajima, H., Sugiyama, D., Hirose, I., Kitamura, T., and Tsuji, K. (2004). Human placenta-derived cells have mesenchymal stem/progenitor cell potential. Stem Cells *22*, 649-658.

Furness, S.G., and McNagny, K. (2006). Beyond mere markers: functions for CD34 family of sialomucins in hematopoiesis. Immunol Res *34*, 13-32.

Galli, S.J., and Tsai, M. (2010). Mast cells in allergy and infection: versatile effector and regulatory cells in innate and adaptive immunity. Eur J Immunol *40*, 1843-1851.

Gazzerro, E., and Canalis, E. (2006). Bone morphogenetic proteins and their antagonists. Rev Endocr Metab Disord *7*, 51-65.

Gilbert, S.F. (2010). Developmental biology, 9th edn (Sunderland, Mass., Sinauer Associates).

Gobert, R.P., Joubert, L., Curchod, M.L., Salvat, C., Foucault, I., Jorand-Lebrun, C., Lamarine, M., Peixoto, H., Vignaud, C., Fremaux, C.*, et al.* (2009). Convergent functional genomics of oligodendrocyte differentiation identifies multiple autoinhibitory signaling circuits. Mol Cell Biol *29*, 1538-1553.

Gregory, C.A., Singh, H., Perry, A.S., and Prockop, D.J. (2003). The Wnt signaling inhibitor dickkopf-1 is required for reentry into the cell cycle of human adult stem cells from bone marrow. J Biol Chem *278*, 28067-28078.

Gronthos, S., Franklin, D.M., Leddy, H.A., Robey, P.G., Storms, R.W., and Gimble, J.M. (2001). Surface protein characterization of human adipose tissue-derived stromal cells. J Cell Physiol *189*, 54-63.

Guo, B., Rooney, P., Slevin, M., Li, C., Parameshwar, S., Liu, D., Kumar, P., Bernabeu, C., and Kumar, S. (2004). Overexpression of CD105 in rat myoblasts: role of CD105 in cell attachment, spreading and survival. Int J Oncol *25*, 285-291.

Gurdon, J.B. (1962). The developmental capacity of nuclei taken from intestinal epithelium cells of feeding tadpoles. J Embryol Exp Morphol *10*, 622-640.

Han, J., Xiao, Y., Lin, J., and Li, Y. (2006). PDGF-C controls proliferation and is down-regulated by retinoic acid in mouse embryonic palatal mesenchymal cells. Birth Defects Res B Dev Reprod Toxicol *77*, 438-444.

Hanafusa, H., Torii, S., Yasunaga, T., and Nishida, E. (2002). Sprouty1 and Sprouty2 provide a control mechanism for the Ras/MAPK signalling pathway. Nat Cell Biol *4*, 850-858.

Hauner, H., Entenmann, G., Wabitsch, M., Gaillard, D., Ailhaud, G., Negrel, R., and Pfeiffer, E.F. (1989). Promoting effect of glucocorticoids on the differentiation of human adipocyte precursor cells cultured in a chemically defined medium. J Clin Invest *84*, 1663-1670.

Hino, J., Miyazawa, T., Miyazato, M., and Kangawa, K. (2012). Bone morphogenetic protein-3b (BMP-3b) is expressed in adipocytes and inhibits adipogenesis as a unique complex. Int J Obes (Lond) *36*, 725-734.

Horwitz, E.M. (2004). Dkk-1-mediated expansion of adult stem cells. Trends Biotechnol *22*, 386-388.

Huang, N.F., Lam, A., Fang, Q., Sievers, R.E., Li, S., and Lee, R.J. (2009). Bone marrow-derived mesenchymal stem cells in fibrin augment angiogenesis in the chronically infarcted myocardium. Regen Med *4*, 527-538.

Huard, B., Schneider, P., Mauri, D., Tschopp, J., and French, L.E. (2001). T cell costimulation by the TNF ligand BAFF. J Immunol *167*, 6225-6231.

Im, G.I., Shin, Y.W., and Lee, K.B. (2005). Do adipose tissue-derived mesenchymal stem cells have the same osteogenic and chondrogenic potential as bone marrow-derived cells? Osteoarthritis Cartilage *13*, 845-853.

Jones, D.L., and Wagers, A.J. (2008). No place like home: anatomy and function of the stem cell niche. Nat Rev Mol Cell Biol *9*, 11-21.

Jones, E.A., Kinsey, S.E., English, A., Jones, R.A., Straszynski, L., Meredith, D.M., Markham, A.F., Jack, A., Emery, P., and McGonagle, D. (2002). Isolation and characterization of bone marrow multipotential mesenchymal progenitor cells. Arthritis Rheum *46*, 3349-3360.

Kasper, G., Dankert, N., Tuischer, J., Hoeft, M., Gaber, T., Glaeser, J.D., Zander, D., Tschirschmann, M., Thompson, M., Matziolis, G.*, et al.* (2007). Mesenchymal stem cells regulate angiogenesis according to their mechanical environment. Stem Cells *25*, 903-910.

Kern, S., Eichler, H., Stoeve, J., Kluter, H., and Bieback, K. (2006). Comparative analysis of mesenchymal stem cells from bone marrow, umbilical cord blood, or adipose tissue. Stem Cells *24*, 1294-1301.

Kim, H.J., and Im, G.I. (2009a). Chondrogenic differentiation of adipose tissue-derived mesenchymal stem cells: greater doses of growth factor are necessary. J Orthop Res *27*, 612-619.

Kim, H.J., and Im, G.I. (2009b). Combination of transforming growth factor-beta2 and bone morphogenetic protein 7 enhances chondrogenesis from adipose tissue-derived mesenchymal stem cells. Tissue Eng Part A *15*, 1543-1551.

Kim, J.D., Kim, H., Ekram, M.B., Yu, S., Faulk, C., and Kim, J. (2011). Rex1/Zfp42 as an epigenetic regulator for genomic imprinting. Hum Mol Genet *20*, 1353-1362.

Kim, M., Yoon, S., Lee, S., Ha, S.A., Kim, H.K., Kim, J.W., and Chung, J. (2012). Gremlin-1 induces BMP-independent tumor cell proliferation, migration, and invasion. PLoS One *7*, e35100.

Kirfel, J., Magin, T.M., and Reichelt, J. (2003). Keratins: a structural scaffold with emerging functions. Cell Mol Life Sci *60*, 56-71.

Koc, O.N., Day, J., Nieder, M., Gerson, S.L., Lazarus, H.M., and Krivit, W. (2002). Allogeneic mesenchymal stem cell infusion for treatment of metachromatic leukodystrophy (MLD) and Hurler syndrome (MPS-IH). Bone Marrow Transplant *30*, 215-222.

Koc, O.N., Gerson, S.L., Cooper, B.W., Dyhouse, S.M., Haynesworth, S.E., Caplan, A.I., and Lazarus, H.M. (2000). Rapid hematopoietic recovery after coinfusion of autologous-blood stem cells and culture-expanded marrow mesenchymal stem cells in advanced breast cancer patients receiving high-dose chemotherapy. J Clin Oncol *18*, 307-316.

Kolf, C.M., Cho, E., and Tuan, R.S. (2007). Mesenchymal stromal cells. Biology of adult mesenchymal stem cells: regulation of niche, self-renewal and differentiation. Arthritis Res Ther *9*, 204.

Kopf, J., Petersen, A., Duda, G.N., and Knaus, P. (2012). BMP2 and mechanical loading cooperatively regulate immediate early signalling events in the BMP pathway. BMC Biol *10*, 37.

Krause, D.S., Fackler, M.J., Civin, C.I., and May, W.S. (1996). CD34: structure, biology, and clinical utility. Blood *87*, 1-13.

Krautler, N.J., Kana, V., Kranich, J., Tian, Y., Perera, D., Lemm, D., Schwarz, P., Armulik, A., Browning, J.L., Tallquist, M.*, et al.* (2012). Follicular dendritic cells emerge from ubiquitous perivascular precursors. Cell *150*, 194-206.

Kuznetsov, S.A., Friedenstein, A.J., and Robey, P.G. (1997). Factors required for bone marrow stromal fibroblast colony formation in vitro. Br J Haematol *97*, 561-570.

Lander, A.D., Kimble, J., Clevers, H., Fuchs, E., Montarras, D., Buckingham, M., Calof, A.L., Trumpp, A., and Oskarsson, T. (2012). What does the concept of the stem cell niche really mean today? BMC Biol *10*, 19.

Lanza, R.P. (2006). Essentials of stem cell biology (Amsterdam ; Boston, Elsevier/Academic Press).

Laoukili, J., Kooistra, M.R., Bras, A., Kauw, J., Kerkhoven, R.M., Morrison, A., Clevers, H., and Medema, R.H. (2005). FoxM1 is required for execution of the mitotic programme and chromosome stability. Nat Cell Biol *7*, 126-136.

Larson, B.L., Ylostalo, J., and Prockop, D.J. (2008). Human multipotent stromal cells undergo sharp transition from division to development in culture. Stem Cells *26*, 193-201.

Le Blanc, K., Rasmusson, I., Sundberg, B., Gotherstrom, C., Hassan, M., Uzunel, M., and Ringden, O. (2004). Treatment of severe acute graft-versus-host disease with third party haploidentical mesenchymal stem cells. Lancet *363*, 1439-1441.

Le Blanc, K., Tammik, L., Sundberg, B., Haynesworth, S.E., and Ringden, O. (2003). Mesenchymal stem cells inhibit and stimulate mixed lymphocyte cultures and mitogenic responses independently of the major histocompatibility complex. Scand J Immunol *57*, 11-20.

Lee, J., Han, D.J., and Kim, S.C. (2008). In vitro differentiation of human adipose tissue-derived stem cells into cells with pancreatic phenotype by regenerating pancreas extract. Biochem Biophys Res Commun *375*, 547-551.

Lee, K.F., Bachman, K., Landis, S., and Jaenisch, R. (1994). Dependence on p75 for innervation of some sympathetic targets. Science *263*, 1447-1449.

Lee, K.F., Li, E., Huber, L.J., Landis, S.C., Sharpe, A.H., Chao, M.V., and Jaenisch, R. (1992). Targeted mutation of the gene encoding the low affinity NGF receptor p75 leads to deficits in the peripheral sensory nervous system. Cell *69*, 737-749.

Lee, S., Bui Nguyen, T.M., Kovalenko, D., Adhikari, N., Grindle, S., Polster, S.P., Friesel, R., Ramakrishnan, S., and Hall, J.L. (2010). Sprouty1 inhibits angiogenesis in association with up-regulation of p21 and p27. Mol Cell Biochem *338*, 255-261.

Lepperdinger, G. (2011). Inflammation and mesenchymal stem cell aging. Curr Opin Immunol *23*, 518-524.

Li, C., Hampson, I.N., Hampson, L., Kumar, P., Bernabeu, C., and Kumar, S. (2000). CD105 antagonizes the inhibitory signaling of transforming growth factor beta1 on human vascular endothelial cells. FASEB J *14*, 55-64.

Li, C.D., Zhang, W.Y., Li, H.L., Jiang, X.X., Zhang, Y., Tang, P.H., and Mao, N. (2005). Mesenchymal stem cells derived from human placenta suppress allogeneic umbilical cord blood lymphocyte proliferation. Cell Res *15*, 539-547.

Liang, Q., De Windt, L.J., Witt, S.A., Kimball, T.R., Markham, B.E., and Molkentin, J.D. (2001). The transcription factors GATA4 and GATA6 regulate cardiomyocyte hypertrophy in vitro and in vivo. J Biol Chem *276*, 30245-30253.

Lin, G., Garcia, M., Ning, H., Banie, L., Guo, Y.L., Lue, T.F., and Lin, C.S. (2008). Defining stem and progenitor cells within adipose tissue. Stem Cells Dev *17*, 1053-1063.

Lo Celso, C., and Scadden, D.T. (2011). The haematopoietic stem cell niche at a glance. J Cell Sci *124*, 3529-3535.

Mackay, A.M., Beck, S.C., Murphy, J.M., Barry, F.P., Chichester, C.O., and Pittenger, M.F. (1998). Chondrogenic differentiation of cultured human mesenchymal stem cells from marrow. Tissue Eng *4*, 415-428.

Madonna, R., Renna, F.V., Cellini, C., Cotellese, R., Picardi, N., Francomano, F., Innocenti, P., and De Caterina, R. (2011). Age-dependent impairment of number and angiogenic potential of adipose tissue-derived progenitor cells. Eur J Clin Invest *41*, 126-133.

Magin, T.M., Vijayaraj, P., and Leube, R.E. (2007). Structural and regulatory functions of keratins. Exp Cell Res *313*, 2021-2032.

Malanchi, I., Peinado, H., Kassen, D., Hussenet, T., Metzger, D., Chambon, P., Huber, M., Hohl, D., Cano, A., Birchmeier, W.*, et al.* (2008). Cutaneous cancer stem cell maintenance is dependent on beta-catenin signalling. Nature *452*, 650-653.

Malumbres, M., and Barbacid, M. (2009). Cell cycle, CDKs and cancer: a changing paradigm. Nat Rev Cancer *9*, 153-166.

Mani, S.A., Guo, W., Liao, M.J., Eaton, E.N., Ayyanan, A., Zhou, A.Y., Brooks, M., Reinhard, F., Zhang, C.C., Shipitsin, M.*, et al.* (2008). The epithelial-mesenchymal transition generates cells with properties of stem cells. Cell *133*, 704-715.

Masui, S., Ohtsuka, S., Yagi, R., Takahashi, K., Ko, M.S., and Niwa, H. (2008). Rex1/Zfp42 is dispensable for pluripotency in mouse ES cells. BMC Dev Biol *8*, 45.

Maumus, M., Peyrafitte, J.A., D'Angelo, R., Fournier-Wirth, C., Bouloumie, A., Casteilla, L., Sengenes, C., and Bourin, P. (2011). Native human adipose stromal cells: localization, morphology and phenotype. Int J Obes (Lond) *35*, 1141-1153.

McDonald, J.A., Kelley, D.G., and Broekelmann, T.J. (1982). Role of fibronectin in collagen deposition: Fab' to the gelatin-binding domain of fibronectin inhibits both fibronectin and collagen organization in fibroblast extracellular matrix. J Cell Biol *92*, 485-492.

Medici, D., Shore, E.M., Lounev, V.Y., Kaplan, F.S., Kalluri, R., and Olsen, B.R. (2010). Conversion of vascular endothelial cells into multipotent stem-like cells. Nat Med *16*, 1400-1406.

Mehlhorn, A.T., Niemeyer, P., Kaschte, K., Muller, L., Finkenzeller, G., Hartl, D., Sudkamp, N.P., and Schmal, H. (2007). Differential effects of BMP-2 and TGF-beta1 on chondrogenic differentiation of adipose derived stem cells. Cell Prolif *40*, 809-823.

Midgley, V.C., and Khachigian, L.M. (2004). Fibroblast growth factor-2 induction of platelet-derived growth factor-C chain transcription in vascular smooth muscle cells is ERK-

dependent but not JNK-dependent and mediated by Egr-1. J Biol Chem *279*, 40289-40295.

Morrisey, E.E. (2000). GATA-6: the proliferation stops here: cell proliferation in glomerular mesangial and vascular smooth muscle cells. Circ Res *87*, 638-640.

Mulvihill, M.S., Kwon, Y.W., Lee, S., Fang, L.T., Choi, H., Ray, R., Kang, H.C., Mao, J.H., Jablons, D., and Kim, I.J. (2012). Gremlin is overexpressed in lung adenocarcinoma and increases cell growth and proliferation in normal lung cells. PLoS One *7*, e42264.

Munoz-Fernandez, R., Blanco, F.J., Frecha, C., Martin, F., Kimatrai, M., Abadia-Molina, A.C., Garcia-Pacheco, J.M., and Olivares, E.G. (2006). Follicular dendritic cells are related to bone marrow stromal cell progenitors and to myofibroblasts. J Immunol *177*, 280-289.

Muthuswamy, R., Mueller-Berghaus, J., Haberkorn, U., Reinhart, T.A., Schadendorf, D., and Kalinski, P. (2010). PGE(2) transiently enhances DC expression of CCR7 but inhibits the ability of DCs to produce CCL19 and attract naive T cells. Blood *116*, 1454-1459.

Nakae, J., Kitamura, T., Kitamura, Y., Biggs, W.H., 3rd, Arden, K.C., and Accili, D. (2003). The forkhead transcription factor Foxo1 regulates adipocyte differentiation. Dev Cell *4*, 119-129.

Namkoong, H., Shin, S.M., Kim, H.K., Ha, S.A., Cho, G.W., Hur, S.Y., Kim, T.E., and Kim, J.W. (2006). The bone morphogenetic protein antagonist gremlin 1 is overexpressed in human cancers and interacts with YWHAH protein. BMC Cancer *6*, 74.

Nassiri, F., Cusimano, M.D., Scheithauer, B.W., Rotondo, F., Fazio, A., Yousef, G.M., Syro, L.V., Kovacs, K., and Lloyd, R.V. (2011). Endoglin (CD105): a review of its role in angiogenesis and tumor diagnosis, progression and therapy. Anticancer Res *31*, 2283-2290.

Nauta, A.J., and Fibbe, W.E. (2007). Immunomodulatory properties of mesenchymal stromal cells. Blood *110*, 3499-3506.

Neuss, S., Schneider, R.K., Tietze, L., Knuchel, R., and Jahnen-Dechent, W. (2010). Secretion of fibrinolytic enzymes facilitates human mesenchymal stem cell invasion into fibrin clots. Cells Tissues Organs *191*, 36-46.

Nickoloff, B.J. (1991). The human progenitor cell antigen (CD34) is localized on endothelial cells, dermal dendritic cells, and perifollicular cells in formalin-fixed normal skin, and on proliferating endothelial cells and stromal spindle-shaped cells in Kaposi's sarcoma. Arch Dermatol *127*, 523-529.

Nishihira, S., Okubo, N., Takahashi, N., Ishisaki, A., Sugiyama, Y., and Chosa, N. (2011). High-cell density-induced VCAM1 expression inhibits the migratory ability of mesenchymal stem cells. Cell Biol Int *35*, 475-481.

Nombela-Arrieta, C., Ritz, J., and Silberstein, L.E. (2011). The elusive nature and function of mesenchymal stem cells. Nat Rev Mol Cell Biol *12*, 126-131.

Ohtani, H., Jin, Z., Takegawa, S., Nakayama, T., and Yoshie, O. (2009). Abundant expression of CXCL9 (MIG) by stromal cells that include dendritic cells and accumulation of CXCR3+ T cells in lymphocyte-rich gastric carcinoma. J Pathol *217*, 21-31.

Okada, S., Nakauchi, H., Nagayoshi, K., Nishikawa, S., Miura, Y., and Suda, T. (1991). Enrichment and characterization of murine hematopoietic stem cells that express c-kit molecule. Blood *78*, 1706-1712.

Oshimori, N., and Fuchs, E. (2012). Paracrine TGF-beta signaling counterbalances BMP-mediated repression in hair follicle stem cell activation. Cell Stem Cell *10*, 63-75.

Ouyang, H.W., Cao, T., Zou, X.H., Heng, B.C., Wang, L.L., Song, X.H., and Huang, H.F. (2006). Mesenchymal stem cell sheets revitalize nonviable dense grafts: implications for repair of large-bone and tendon defects. Transplantation *82*, 170-174.

Padovan, E., Spagnoli, G.C., Ferrantini, M., and Heberer, M. (2002). IFN-alpha2a induces IP-10/CXCL10 and MIG/CXCL9 production in monocyte-derived dendritic cells and enhances their capacity to attract and stimulate CD8+ effector T cells. J Leukoc Biol *71*, 669-676.

Paul, G., Ozen, I., Christophersen, N.S., Reinbothe, T., Bengzon, J., Visse, E., Jansson, K., Dannaeus, K., Henriques-Oliveira, C., Roybon, L.*, et al.* (2012). The adult human brain harbors multipotent perivascular mesenchymal stem cells. PLoS One *7*, e35577.

Pittenger, M.F., Mackay, A.M., Beck, S.C., Jaiswal, R.K., Douglas, R., Mosca, J.D., Moorman, M.A., Simonetti, D.W., Craig, S., and Marshak, D.R. (1999). Multilineage potential of adult human mesenchymal stem cells. Science *284*, 143-147.

Potenta, S., Zeisberg, E., and Kalluri, R. (2008). The role of endothelial-to-mesenchymal transition in cancer progression. Br J Cancer *99*, 1375-1379.

Prather, W.R., Toren, A., Meiron, M., Ofir, R., Tschope, C., and Horwitz, E.M. (2009). The role of placental-derived adherent stromal cell (PLX-PAD) in the treatment of critical limb ischemia. Cytotherapy *11*, 427-434.

Quirici, N., Scavullo, C., de Girolamo, L., Lopa, S., Arrigoni, E., Deliliers, G.L., and Brini, A.T. (2010). Anti-L-NGFR and -CD34 monoclonal antibodies identify multipotent mesenchymal stem cells in human adipose tissue. Stem Cells Dev *19*, 915-925.

Quirici, N., Soligo, D., Bossolasco, P., Servida, F., Lumini, C., and Deliliers, G.L. (2002). Isolation of bone marrow mesenchymal stem cells by anti-nerve growth factor receptor antibodies. Exp Hematol *30*, 783-791.

Raff, M. (2003). Adult stem cell plasticity: fact or artifact? Annu Rev Cell Dev Biol *19*, 1-22.

Ramasamy, R., Tong, C.K., Seow, H.F., Vidyadaran, S., and Dazzi, F. (2008). The immunosuppressive effects of human bone marrow-derived mesenchymal stem cells target T cell proliferation but not its effector function. Cell Immunol *251*, 131-136.

Rasmusson, I., Uhlin, M., Le Blanc, K., and Levitsky, V. (2007). Mesenchymal stem cells fail to trigger effector functions of cytotoxic T lymphocytes. J Leukoc Biol *82*, 887-893.

Reya, T., and Clevers, H. (2005). Wnt signalling in stem cells and cancer. Nature *434*, 843-850.

Ritt, M.G., Mayor, J., Wojcieszyn, J., Smith, R., Barton, C.L., and Modiano, J.F. (2000). Sustained nuclear localization of p21/WAF-1 upon growth arrest induced by contact inhibition. Cancer Lett *158*, 73-84.

Romieu-Mourez, R., Francois, M., Boivin, M.N., Stagg, J., and Galipeau, J. (2007). Regulation of MHC class II expression and antigen processing in murine and human mesenchymal stromal cells by IFN-gamma, TGF-beta, and cell density. J Immunol *179*, 1549-1558.

Roobrouck, V.D., Vanuytsel, K., and Verfaillie, C.M. (2011). Concise review: culture mediated changes in fate and/or potency of stem cells. Stem Cells *29*, 583-589.

Ross, E.A., Freeman, S., Zhao, Y., Dhanjal, T.S., Ross, E.J., Lax, S., Ahmed, Z., Hou, T.Z., Kalia, N., Egginton, S.*, et al.* (2008). A novel role for PECAM-1 (CD31) in regulating haematopoietic progenitor cell compartmentalization between the peripheral blood and bone marrow. PLoS One *3*, e2338.

Rotondi, M., Lazzeri, E., Romagnani, P., and Serio, M. (2003). Role for interferon-gamma inducible chemokines in endocrine autoimmunity: an expanding field. J Endocrinol Invest *26*, 177-180.

Sacchetti, B., Funari, A., Michienzi, S., Di Cesare, S., Piersanti, S., Saggio, I., Tagliafico, E., Ferrari, S., Robey, P.G., Riminucci, M.*, et al.* (2007). Self-renewing osteoprogenitors in bone marrow sinusoids can organize a hematopoietic microenvironment. Cell *131*, 324-336.

Sachsenmaier, C., Sadowski, H.B., and Cooper, J.A. (1999). STAT activation by the PDGF receptor requires juxtamembrane phosphorylation sites but not Src tyrosine kinase activation. Oncogene *18*, 3583-3592.

Samavarchi-Tehrani, P., Golipour, A., David, L., Sung, H.K., Beyer, T.A., Datti, A., Woltjen, K., Nagy, A., and Wrana, J.L. (2010). Functional genomics reveals a BMP-driven mesenchymal-to-epithelial transition in the initiation of somatic cell reprogramming. Cell Stem Cell *7*, 64-77.

Schneider, P., MacKay, F., Steiner, V., Hofmann, K., Bodmer, J.L., Holler, N., Ambrose, C., Lawton, P., Bixler, S., Acha-Orbea, H.*, et al.* (1999). BAFF, a novel ligand of the tumor necrosis factor family, stimulates B cell growth. J Exp Med *189*, 1747-1756.

Schriever, F., Freedman, A.S., Freeman, G., Messner, E., Lee, G., Daley, J., and Nadler, L.M. (1989). Isolated human follicular dendritic cells display a unique antigenic phenotype. J Exp Med *169*, 2043-2058.

Scotland, K.B., Chen, S., Sylvester, R., and Gudas, L.J. (2009). Analysis of Rex1 (zfp42) function in embryonic stem cell differentiation. Dev Dyn *238*, 1863-1877.

Sekiya, I., Larson, B.L., Vuoristo, J.T., Cui, J.G., and Prockop, D.J. (2004). Adipogenic differentiation of human adult stem cells from bone marrow stroma (MSCs). J Bone Miner Res *19*, 256-264.

Shea, K.L., Xiang, W., LaPorta, V.S., Licht, J.D., Keller, C., Basson, M.A., and Brack, A.S. (2009). Sprouty1 regulates reversible quiescence of a self-renewing adult muscle stem cell pool during regeneration. Cell Stem Cell *6*, 117-129.

Shi, Y., and Massague, J. (2003). Mechanisms of TGF-beta signaling from cell membrane to the nucleus. Cell *113*, 685-700.

Shin, S.Y., Nam, J.S., Lim, Y., and Lee, Y.H. (2010). TNFalpha-exposed bone marrow-derived mesenchymal stem cells promote locomotion of MDA-MB-231 breast cancer cells through transcriptional activation of CXCR3 ligand chemokines. J Biol Chem *285*, 30731-30740.

Song, L., and Tuan, R.S. (2004). Transdifferentiation potential of human mesenchymal stem cells derived from bone marrow. FASEB J *18*, 980-982.

Steed, E., Balda, M.S., and Matter, K. (2010). Dynamics and functions of tight junctions. Trends Cell Biol *20*, 142-149.

Steele, J.G., Johnson, G., and Underwood, P.A. (1992). Role of serum vitronectin and fibronectin in adhesion of fibroblasts following seeding onto tissue culture polystyrene. J Biomed Mater Res *26*, 861-884.

Subramanian, A., Tamayo, P., Mootha, V.K., Mukherjee, S., Ebert, B.L., Gillette, M.A., Paulovich, A., Pomeroy, S.L., Golub, T.R., Lander, E.S.*, et al.* (2005). Gene set enrichment analysis: a knowledge-based approach for interpreting genome-wide expression profiles. Proc Natl Acad Sci U S A *102*, 15545-15550.

Suga, H., Matsumoto, D., Eto, H., Inoue, K., Aoi, N., Kato, H., Araki, J., and Yoshimura, K. (2009). Functional implications of CD34 expression in human adipose-derived stem/progenitor cells. Stem Cells Dev *18*, 1201-1210.

Takahashi, K., and Yamanaka, S. (2006). Induction of pluripotent stem cells from mouse embryonic and adult fibroblast cultures by defined factors. Cell *126*, 663-676.

Tallone, T., Realini, C., Bohmler, A., Kornfeld, C., Vassalli, G., Moccetti, T., Bardelli, S., and Soldati, G. (2011). Adult human adipose tissue contains several types of multipotent cells. J Cardiovasc Transl Res *4*, 200-210.

Tamama, K., and Barbeau, D.J. (2013). Early growth response genes signaling supports strong paracrine capability of mesenchymal stem cells. Stem Cells Int *2012*, 428403.

Tang, W., Zeve, D., Suh, J.M., Bosnakovski, D., Kyba, M., Hammer, R.E., Tallquist, M.D., and Graff, J.M. (2008). White fat progenitor cells reside in the adipose vasculature. Science *322*, 583-586.

Tang, Z., Wang, A., Yuan, F., Yan, Z., Liu, B., Chu, J.S., Helms, J.A., and Li, S. (2012). Differentiation of multipotent vascular stem cells contributes to vascular diseases. Nat Commun *3*, 875.

Tavazoie, M., Van der Veken, L., Silva-Vargas, V., Louissaint, M., Colonna, L., Zaidi, B., Garcia-Verdugo, J.M., and Doetsch, F. (2008). A specialized vascular niche for adult neural stem cells. Cell Stem Cell *3*, 279-288.

Thiery, J.P., and Sleeman, J.P. (2006). Complex networks orchestrate epithelial-mesenchymal transitions. Nat Rev Mol Cell Biol *7*, 131-142.

Tormin, A., Li, O., Brune, J.C., Walsh, S., Schutz, B., Ehinger, M., Ditzel, N., Kassem, M., and Scheding, S. (2011). CD146 expression on primary nonhematopoietic bone marrow stem cells is correlated with in situ localization. Blood *117*, 5067-5077.

Traktuev, D.O., Merfeld-Clauss, S., Li, J., Kolonin, M., Arap, W., Pasqualini, R., Johnstone, B.H., and March, K.L. (2008). A population of multipotent CD34-positive adipose stromal cells share pericyte and mesenchymal surface markers, reside in a periendothelial location, and stabilize endothelial networks. Circ Res *102*, 77-85.

Tsutsumi, S., Shimazu, A., Miyazaki, K., Pan, H., Koike, C., Yoshida, E., Takagishi, K., and Kato, Y. (2001). Retention of multilineage differentiation potential of mesenchymal cells during proliferation in response to FGF. Biochem Biophys Res Commun *288*, 413-419.

Uezumi, A., Fukada, S., Yamamoto, N., Takeda, S., and Tsuchida, K. (2010). Mesenchymal progenitors distinct from satellite cells contribute to ectopic fat cell formation in skeletal muscle. Nat Cell Biol *12*, 143-152.

Upadhyay, G., Yin, Y., Yuan, H., Li, X., Derynck, R., and Glazer, R.I. (2011). Stem cell antigen-1 enhances tumorigenicity by disruption of growth differentiation factor-10 (GDF10)-dependent TGF-beta signaling. Proc Natl Acad Sci U S A *108*, 7820-7825.

van Eys, G.J., Voller, M.C., Timmer, E.D., Wehrens, X.H., Small, J.V., Schalken, J.A., Ramaekers, F.C., and van der Loop, F.T. (1997). Smoothelin expression characteristics: development of a smooth muscle cell in vitro system and identification of a vascular variant. Cell Struct Funct *22*, 65-72.

Veevers-Lowe, J., Ball, S.G., Shuttleworth, A., and Kielty, C.M. (2011). Mesenchymal stem cell migration is regulated by fibronectin through alpha5beta1-integrin-mediated activation of PDGFR-beta and potentiation of growth factor signals. J Cell Sci *124*, 1288-1300.

Wade, A., Thomas, C., Kalmar, B., Terenzio, M., Garin, J., Greensmith, L., and Schiavo, G. (2012). Activated leukocyte cell adhesion molecule modulates neurotrophin signaling. J Neurochem *121*, 575-586.

Wang, H., Chen, T., Ding, T., Zhu, P., Xu, X., Yu, L., and Xie, Y. (2011). Adipogenic differentiation alters the immunoregulatory property of mesenchymal stem cells through BAFF secretion. Hematology *16*, 313-323.

Wang, H.S., Hung, S.C., Peng, S.T., Huang, C.C., Wei, H.M., Guo, Y.J., Fu, Y.S., Lai, M.C., and Chen, C.C. (2004). Mesenchymal stem cells in the Wharton's jelly of the human umbilical cord. Stem Cells *22*, 1330-1337.

Watt, S.M., Karhi, K., Gatter, K., Furley, A.J., Katz, F.E., Healy, L.E., Altass, L.J., Bradley, N.J., Sutherland, D.R., Levinsky, R.*, et al.* (1987). Distribution and epitope analysis of the cell membrane glycoprotein (HPCA-1) associated with human hemopoietic progenitor cells. Leukemia *1*, 417-426.

Webb, R.C. (2003). Smooth muscle contraction and relaxation. Adv Physiol Educ *27*, 201-206.

Weidle, U.H., Eggle, D., Klostermann, S., and Swart, G.W. (2010). ALCAM/CD166: cancer-related issues. Cancer Genomics Proteomics *7*, 231-243.

Widberg, C.H., Newell, F.S., Bachmann, A.W., Ramnoruth, S.N., Spelta, M.C., Whitehead, J.P., Hutley, L.J., and Prins, J.B. (2009). Fibroblast growth factor receptor 1 is a key regulator of early adipogenic events in human preadipocytes. Am J Physiol Endocrinol Metab *296*, E121-131.

Wilke, M.M., Nydam, D.V., and Nixon, A.J. (2007). Enhanced early chondrogenesis in articular defects following arthroscopic mesenchymal stem cell implantation in an equine model. J Orthop Res *25*, 913-925.

Winkler, T., von Roth, P., Schuman, M.R., Sieland, K., Stoltenburg-Didinger, G., Taupitz, M., Perka, C., Duda, G.N., and Matziolis, G. (2008). In vivo visualization of locally transplanted mesenchymal stem cells in the severely injured muscle in rats. Tissue Eng Part A *14*, 1149-1160.

Xu, L.L., Warren, M.K., Rose, W.L., Gong, W., and Wang, J.M. (1996). Human recombinant monocyte chemotactic protein and other C-C chemokines bind and induce directional migration of dendritic cells in vitro. J Leukoc Biol *60*, 365-371.

Yamazaki, S., Iwama, A., Takayanagi, S., Eto, K., Ema, H., and Nakauchi, H. (2009). TGF-beta as a candidate bone marrow niche signal to induce hematopoietic stem cell hibernation. Blood *113*, 1250-1256.

Zeisberg, M., and Neilson, E.G. (2009). Biomarkers for epithelial-mesenchymal transitions. J Clin Invest *119*, 1429-1437.

Zeng, G.F., Cai, S.X., and Wu, G.J. (2011). Up-regulation of METCAM/MUC18 promotes motility, invasion, and tumorigenesis of human breast cancer cells. BMC Cancer *11*, 113.

Zhang, W., Ge, W., Li, C., You, S., Liao, L., Han, Q., Deng, W., and Zhao, R.C. (2004). Effects of mesenchymal stem cells on differentiation, maturation, and function of human monocyte-derived dendritic cells. Stem Cells Dev *13*, 263-271.

Zheng, Q., Safina, A., and Bakin, A.V. (2008). Role of high-molecular weight tropomyosins in TGF-beta-mediated control of cell motility. Int J Cancer *122*, 78-90.

Zhong, Y., Wang, Z., Fu, B., Pan, F., Yachida, S., Dhara, M., Albesiano, E., Li, L., Naito, Y., Vilardell, F.*, et al.* (2011). GATA6 activates Wnt signaling in pancreatic cancer by negatively regulating the Wnt antagonist Dickkopf-1. PLoS One *6*, e22129.

Zimmerlin, L., Donnenberg, V.S., Pfeifer, M.E., Meyer, E.M., Peault, B., Rubin, J.P., and Donnenberg, A.D. (2010). Stromal vascular progenitors in adult human adipose tissue. Cytometry A *77*, 22-30.

Zuk, P.A., Zhu, M., Ashjian, P., De Ugarte, D.A., Huang, J.I., Mizuno, H., Alfonso, Z.C., Fraser, J.K., Benhaim, P., and Hedrick, M.H. (2002). Human adipose tissue is a source of multipotent stem cells. Mol Biol Cell *13*, 4279-4295.

7. Appendix

Erklärung

Berlin, den 08.05.2013

Ich, Julian Braun, erkläre an Eides Statt, dass die vorliegende Dissertation in allen Teilen von mir selbständig angefertigt wurde und die benutzen Hilfsmittel vollständig angegeben worden sind.

Veröffentlichungen von irgendwelchen Teilen der vorliegenden Dissertation sind von mir wie folgt vorgenommen worden.

Peer-reviewed Publication:

Braun J, Kurtz A, Barutcu N, Bodo J, Thiel A, Dong J
"Concerted Regulation of CD34 and CD105 accompanies MSC Derivation from Human Adventitial Stromal Cells."
Stem Cells and Development. 2013 March; 22(5): 815-827.

Conference Poster:

Braun J, Bodo J, Kurtz A, Thiel A, Dong J
"'Birth' of an MSC: analysis of the early culture phase of AT-MSC progenitors"
at Keystone Conference "Life of a Stem Cell: From Birth to Death"
Squaw Valley, CA, USA in March 2012

Weiter erkläre ich, daß ich nicht schon anderweitig einmal die Promotionsabsicht angemeldet oder ein Promotionseröffnungsverfahren beantragt habe.

Julian Braun

8. Danksagung

Hiermit möchte ich allen danken, die mich während meiner gesamten Promotionszeit unterstützt, motiviert und an mich geglaubt haben.

Zu allererst danke ich meinen Betreuern Jun Dong, Andreas Kurtz und Andreas Thiel, die mich stets in allen Belangen unterstützt haben. Desweiteren danke ich Andreas Kurtz und Roland Lauster, die sich bereit erklärt haben, diese Arbeit zu begutachten.

Ein sehr größer Dank gilt Frau Dr. Juliane Bodo und Frau Neslihan Barutcu, die mich während unserer langjährigen Kooperation stets mit frischem Fettgewebe versorgt haben.

Allen Kollegen in der AG Thiel danke ich für die immer verfügbare wissenschaftliche Hilfe, die vielen Kuchen, den großen Spaß und die wunderbare Atmosphäre. Ohne euch hätte ich bestimmt irgendwann aufgegeben.
Mein Dank gilt auch meinen BSRT-Genossen, mit denen ich einige schöne Abende und tolle Retreats mit vielen lustige Erinnerungen erlebt habe. Ausserdem danke ich allen Mitarbeitern, Diplomanden und Doktoranden im BCRT für die angenehme, kollegiale Arbeitsatmosphäre.

Für Korrekturen und Anmerkungen danke ich Jun Dong, Karolina Tykwinska, Katrin Warstat, Regina Stark, Sibel Durlanik, Ulrik Stervbo-Kristensen, Andreas Thiel und Andreas Kurtz.

Auch möchte ich mich bei meinen Eltern bedanken, ohne deren Unterstützung ich nie soweit gekommen wäre.
Zu guter letzt gilt mein größter Dank meiner Katrin, die es sehr gut vermochte mich von meinen Sorgen abzulenken, mir den Rücken freizuhalten und mich in schweren Zeiten zu ermuntern.